Synchronization in Heterogeneous Networks of Hippocampal Interneurons

by

Hojjat Bazzazi

A thesis
presented to the University of Waterloo
in fulfilment of the
thesis requirement for the degree of
Master of Mathematics
in
Applied Mathematics

Waterloo, Ontario, Canada, 2005

AUTHOR'S DECLARATION FOR ELECTRONIC SUBMISSION OF A THESIS

I hereby declare that I am the sole author of this thesis. This is a true copy of the thesis, including any required final revision, as accepted by my examiners.

I understand that my thesis may be made electronically available to the public.

Abstract

The hippocampus is one of the most intensely studied brain structures and the oscillatory activity of the hippocampal neurons is believed to be involved in learning and memory consolidation. Therefore, studying rhythm generation and modulation in this structure is an important step in understanding its function. In this thesis, these phenomena are studied via mathematical models of networks of hippocampal interneurons. The two types of neural networks considered here are homogenous and heterogenous networks. In homogenous networks, the input current to each neuron is equal, while in heterogenous networks, this assumption is relaxed and there is a specified degree of heterogeneity in the input stimuli. A phase reduction technique is applied to the neural network model of the hippocampal interneurons and attempts are made to understand the implications of heterogeneity to the existence and stability of the synchronized oscillations. The Existence of a critical level of heterogeneity above which the synchronized rhythms are not stable is established, and linear analysis is applied to derive expressions for estimating the perturbations in the network frequency and timing of the neural spikes. The mathematical techniques developed in this thesis are general enough to be applied to models describing other types of neurons not considered here. Possible biological implications include the application of high frequency local stimulation to alleviate the synchronous neural oscillations in pathological conditions such as epilepsy and Parkinson's disease and the possible role of heterogeneity in controlling the rhythm frequency and switching between various cognitive states.

Acknowledgments

I acknowledge the support provided by my supervisors Dr. Sue Ann Campbell and Dr. Brian Ingalls and their tireless reading of the various versions of this thesis. Their encouragement and supervision were essential for the successful completion of this project. I also acknowledge the partial financial support provided by the Department of Applied Mathematics through the graduate teaching assistantships.

Dedication

This thesis is dedicated to the following individuals: My father Vahid Bazzazi and mother Parisima Charehsaz, for all their selfless sacrifices throughout my life, and to my aunt Ms. Gilan Bazzazi who is a role model of faith and spiritual strength and a continual source of inspiration.

Contents

List of Figures

List of Tables

Chapter 1

Introduction

A neuron is the basic functional unit of the brain involved in information storage, transmission, and processing. Figure 1.1 presents a schematic representation of a single neuron with the important structures labeled and below is the description of the parts labeled in the figure.

1. The axon terminal is the end of the axon where the neuron meets other neighboring neurons and communicates with them.

2. The axons are long protein coated structures that conduct (transmit) signals.

3. The cell body, called the soma, contains the nucleus and other cellular organelles.

4. The nucleus is where all the cellular functions are programmed.

5. The dendrites receive signals from other nerve cells and direct them to the cell body for processing.

Large population of neurons (neural networks) in the brain are connected via synapses (described later) and function in concert to perform a desired function such as recognizing a sound, understanding an image, or retrieving a past memory ([35], [16]). Information in the brain is encoded by carefully timed trains of pulse-like changes in the neural membrane potential, called action potentials or spikes. The mechanisms responsible for the generation of these membrane potential

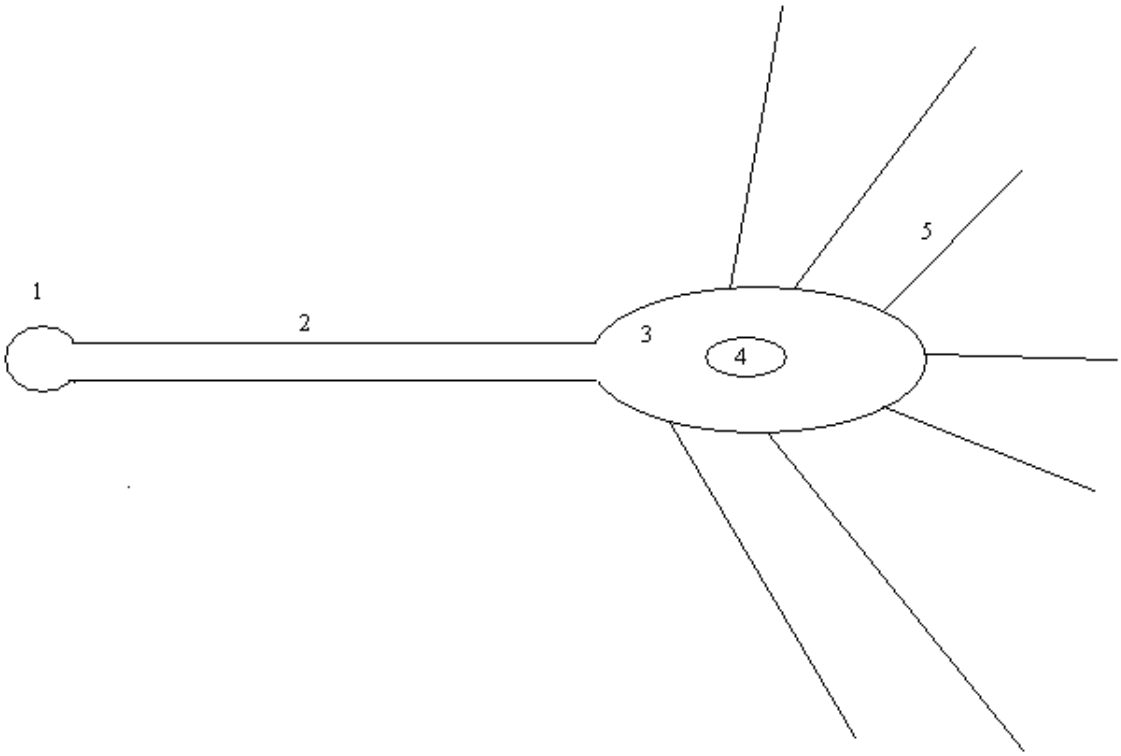

Figure 1.1: Schematics representation of the basic neural structures.

spikes will be described in greater detail in the next chapter as we present a detailed overview of the basic neuron electrophysiology. The neural networks in the brain can be either homogenous or heterogeneous. In homogenous networks, properties of all neurons and their connectivity are exactly the same and are homogenous throughout the population. On the other hand, in heterogenous networks, the external input to each neuron is different and the neural connectivity properties are also heterogeneous throughout the population. For example, if the coupling between neurons are through resistive pathways (e.g. gap junctions), the resistivity property is heterogeneous for different regions of the network. In this thesis, heterogeneity is characterized by differences in external input (or external stimuli) to neurons and the connectivity properties are assumed to be the same for all cells in the network.

1.1 Hippocampus and inhibitory interneuronal networks

Hippocampus is located within the temporal lobe of the brain and is the most widely studied structure which is believed to be involved in memory formation and learning [32, pp. 191-193]. Figure 1.2 shows a schematic view of the brain with the temporal lobe labeled. Interneurons or inhibitory GABAergic cells in the hippocampus make up about $10 - 20\%$ of the total neuronal population. Their biochemical content, morphology, and electrophysiological characteristics are very diverse [29]. Networks of inhibitory cells have been found to be responsible for the generation and control of rhythmic brain activities ([6], [7])and several experimental studies support that population (network) rhythms arise from coherent activities in interneurons ([40], [47], [48]). According to the recent findings ([5], [6]), oscillatory activity in the hippocampus in the theta (8-12Hz) and gamma (20-80Hz) frequency bands occur during memory consolidation and spatial navigation and a type of inhibitory interneurons called the parvalbumium-containing basket cells are responsible for generating these rhythms [13].
It was in 1992 that modelling studies showed the possibility of obtaining synchronous output from purely inhibitory networks [44]. Since then, several research groups have performed modelling and theoretical studies of homogenous inhibitory networks ([42] and [38]). Some of the studies focused in particular on the hippocampal interneuronal networks ([39], [31]). In later studies, the inclusion of heterogenous inputs to inhibitory networks were considered ([1], [2], [41], [43], [45], and [37]). Some authors also carried out analytical studies of the of heterogenous neural couplings ([28]) assuming homogenous inputs. Since the focus of this thesis, is only on the effects of heterogeneous inputs, we exclude the works that involve internal heterogeneities (heterogeneity in the coupling strength and properties). From these studies, it is clear that input heterogeneity is an import factor that strongly affects the ability of inhibitory networks to synchronize. For example, inhibitory networks can tolerate a specific level of heterogeneity above which synchronous solutions

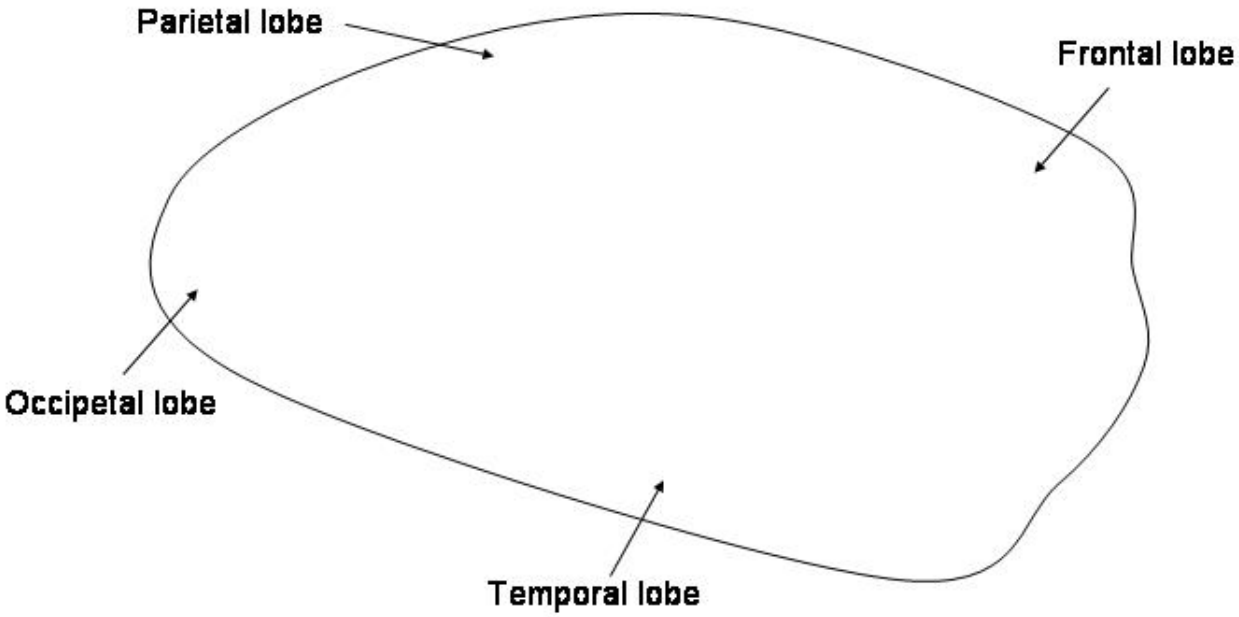

Figure 1.2: Schematic view of the brain lobes

do not exist ([8], [37], [36]). Since the modeling studies ([1], [2], and [43])were performed using large (100-cell)networks along with consideration of other issues (such as amount of connectivity and electrical coupling), it is difficult to determine the underlying mechanisms that give rise to different network characteristics such as frequency. However, it was shown that [45] studying smaller networks (2-cell)is helpful in understanding larger network dynamics. Later studies using two cells ([37], [36]) showed that there are optimal values of the biophysical parameters for tolerating the largest level of heterogeneity and further the stability characteristics of the synchronous solutions of the two cell system are retained in larger networks.

Most of the results on heterogeneous networks are obtained by computer simulations (e.g. [41], [43], [45], [15], [37], [36]) and some groups ([37], [36]) have performed bifurcation analysis of the two cell network and observed that there is a strong correlation between range of the parameters for the loss of synchrony in the 2-cell and that of the corresponding N-cell network. We have taken a middle path in this thesis and combined numerical simulations with analytical approaches based on the phase reduction of the recently developed model of hippocampal interneurons [43]. The advantage of using the phase reduction is that one can readily make connections between the effect of biophysical parameters defining the network (e.g. coupling strength, and time constants) and the network properties such as frequency and synchronization.

1.2 Outline of the thesis

Structure of this thesis is as follows: Second chapter presents a detailed review of the basic concepts in neuron electrophysiology such as communication between neurons. The first mathematical model of a neuron developed in 1950s by Alan Hodgkin and Andrew Huxley [19], and in particular the recent model of the hippocampal interneurons [43] are then discussed in detail. The third chapter, discusses phase reduction which is the approach taken in this thesis for simplifying the hippocampal interneuron model. In the fourth chapter, we begin by presenting general results for homogenous networks such as conditions for the stability of synchronous solutions and the possibility of bi-stability between various rhythmic equilibrium solutions (the notion of rhythmic equilibrium solutions will later be made more precise). The later part of chapter four is devoted to the heterogeneous networks, beginning by presenting two analytical approaches for estimating the maximum level of heterogeneity that can be tolerated by a network consisting of N neurons. We then apply linear approximations to obtain analytical expressions quantifying the amount of perturbation in the homogenous solutions resulting from the heterogeneous inputs. An expression for the network frequency will also be derived and it will be shown that to the first order approximation, it depends on the interneuronal coupling strength , time constant of signal transduction

between neurons and the mean input to the neurons. The analytical results are then compared with numerical simulations of networks consisting of three and four cell networks. It is found that there is a very good correlation between the analytical and numerical results.

Chapter 2

The Hodgkin-Huxley Model and Basic Neuron Electrophysiology

In this chapter, a detailed introduction to fundamental ideas of the neuron electrophysiology culminating in the Hodgkin-Huxley model of squid giant axon is presented. Following discussion, is based closely on the presentation by Hille in his classic book on ion channels [18, pp. 1-58].

2.1 Ion Channels

Before proceeding into details, we need to make precise of what it means for a membrane to be excitable. A working definition is that a membrane is excitable when small perturbations in membrane potential cause a direct return to steady-state, while above threshold perturbations cause large excursion before returning to the steady-state. This idea is illustrated in Figure 2.1. The large excursion in the membrane potential in response to an above threshold stimulus is called an action potential. To describe the mechanistic reason behind this phenomena, it it crucial to have a basic understanding of ion channels, which are the fundamental elements of excitable membranes. They are macromolecular pores that regulate ion movement through the cell membrane. The greatest technical progress in this study was the development of an experimental technique to resolve the activity of individual channels. This technique lead to the discovery that the rate of ion passage through a pore is often as high as 10^6 ions per seconds.

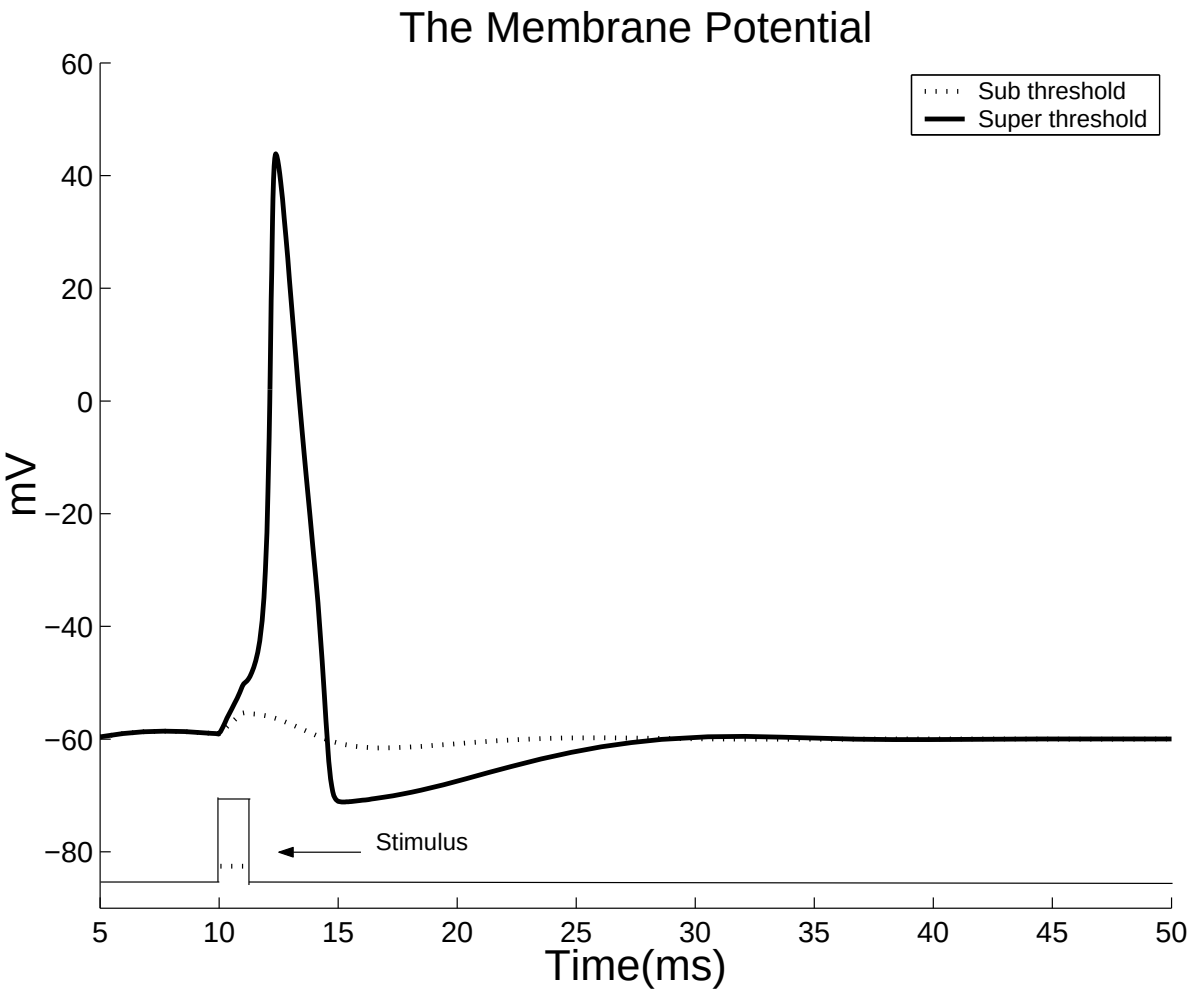

Figure 2.1: Consequences of a super and sub threshold stimulus current pulse.

2.1.1 The importance of ions and ion channels for excitability

It has long been observed that ions are central in excitability of neurons and muscle cells. In the 1880s, Sidney Ringer showed that sodium and potassium salts and calcium must be mixed in a definite proportion in the medium perfusing frog heart in order for the heart to continue beating. Walther Nernst's work (also in the 1880s), on electrical potentials arising from electrolyte diffusion in a solution paved the way for a basic understanding of the generation of bioelectrical potentials. For instance, it was conjectured that the inside of the cell should be negative relative to the outside, because the tissue makes acid in the process of metabolism and protons (positively charged) can diffuse to the extracellular space more easily than other larger negatively charged molecules. Julius Bernstein (1902,1912) proposed that membrane potential is more permeable to the potassium ions (K^+) at rest and that during excitation the membrane permeability to other ions increases. Bernstein explained the resting membrane potential in neurons, as the tendency of positively charged ions to diffuse from their high concentration in the cytoplasm (inside of the cell) to the extracellular solution while other ions are blocked. Following ground breaking ideas of Bernestein, further studies by various investigators including Alan Hodgkin and Andrew Huxley determined that the major ion channels involved in excitability are $Na,^+$, $K,^+$ and Ca^{2+}.

The type of channels that are involved in the Hodgkin-Huxley model are sensitive to the changes in the membrane potential and open or close as a result of perturbations in the membrane potential. This opening and closing in response to external stimuli is called **gating**.

2.1.2 Electric circuit model of the membrane

Because the membrane separates charges and also allows for the flow of ionic currents through specific pathways (channels), it can be thought of as a capacitor along with a resistor as shown in Figure 2.2. The capacitor discharges through the resistor shown in the figure and the the current flow through the resistor and the capacitor determines the membrane potential.
For a parallel plate capacitor, the formula relating the membrane potential to the excess charges Q on each plate is

$$V = \frac{Q}{C}. \tag{2.1}$$

Differentiating both sides of the equation 2.1 yields

$$\frac{dV}{dt} = \frac{I_C}{C}, \tag{2.2}$$

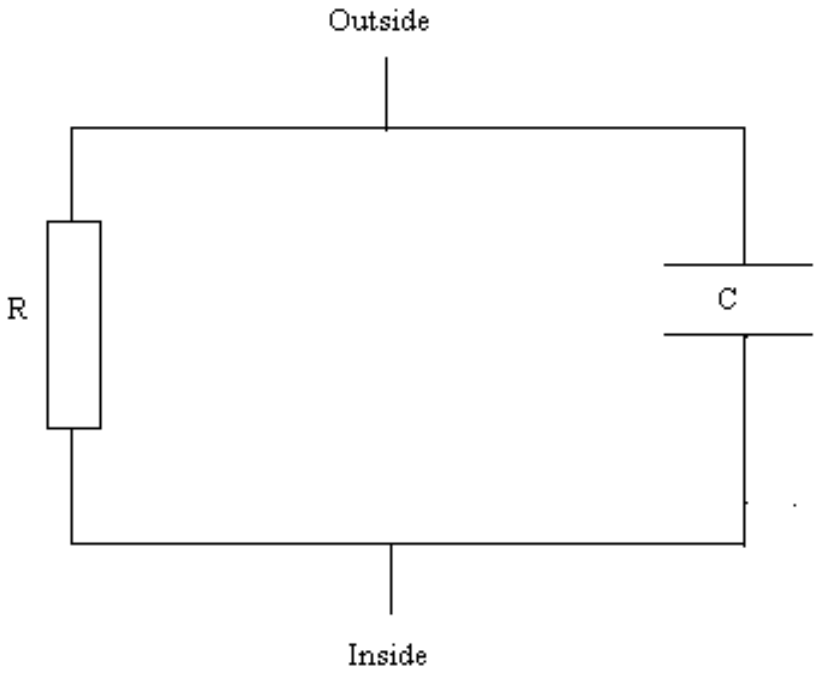

Figure 2.2: The cell membrane electrical circuit model.

where, $I_C = \frac{dQ}{dt}$ is the current generated by the capacitor discharge which flows through the resistor in Figure 2.2.
Recall the Ohm's law :

$$V = -RI = -I/g, \tag{2.3}$$

where V is the voltage (in volts), R is the resistance (in Ohms), I is the current flowing through the resistor (in amperes), and $g = 1/R$ is the conductance (in siemens). Substituting Ohm's law $E = -RI_C$ into equation (2.2) yields

$$\frac{dV}{dt} = -\frac{V}{RC}. \tag{2.4}$$

The constant $\tau_m = RC$ is called the **membrane time constant**. In practice, the resistor in Figure 2.1 is divided into several parallel resistors representing the specific ionic currents flowing through the membrane. For instance, Figure 2.3 shows the circuit representation of the Hodgkin-Huxley model of the squid giant axon, where the prominent ionic players are sodium and potassium. In this figure there is also a leak current which represents the flow of other ions. From Kirchhoff's law, the current resulting from the capacitor discharge is equal to sum of the currents flowing through each resistor but in the opposite direction

$$I_C = -I_{\mathrm{K}^+} - I_{\mathrm{Na}^+} - I_{Leak}. \tag{2.5}$$

Recall that

$$I_C = C\frac{dV}{dt},$$

Thus

$$-C\frac{dV}{dt} = I_{\mathrm{K}^+} + I_{\mathrm{Na}^+} + I_{Leak}, \tag{2.6}$$

The Hodgkin-Huxley model was formulated by determining the dependence on voltage and time of the currents on the right hand side of equation (2.6).

2.1.3 Introducing The Nernst equation

To understand the mechanism by which the equilibrium (or resting) membrane potential is generated in cells, consider Figure 2.4 which shows two compartments separated by a semi-permeable membrane. The two compartments contains the salt, NaCl at a different concentrations. The semi-permeable membrane is permeable to Na^+ but not to Cl^-. Suppose that sodium concentrations in compartments A and B are $[\mathrm{Na}^+]_A$ and $[\mathrm{Na}^+]_B$ respectively, such that $[\mathrm{Na}^+]_A > [\mathrm{Na}^+]_B$.

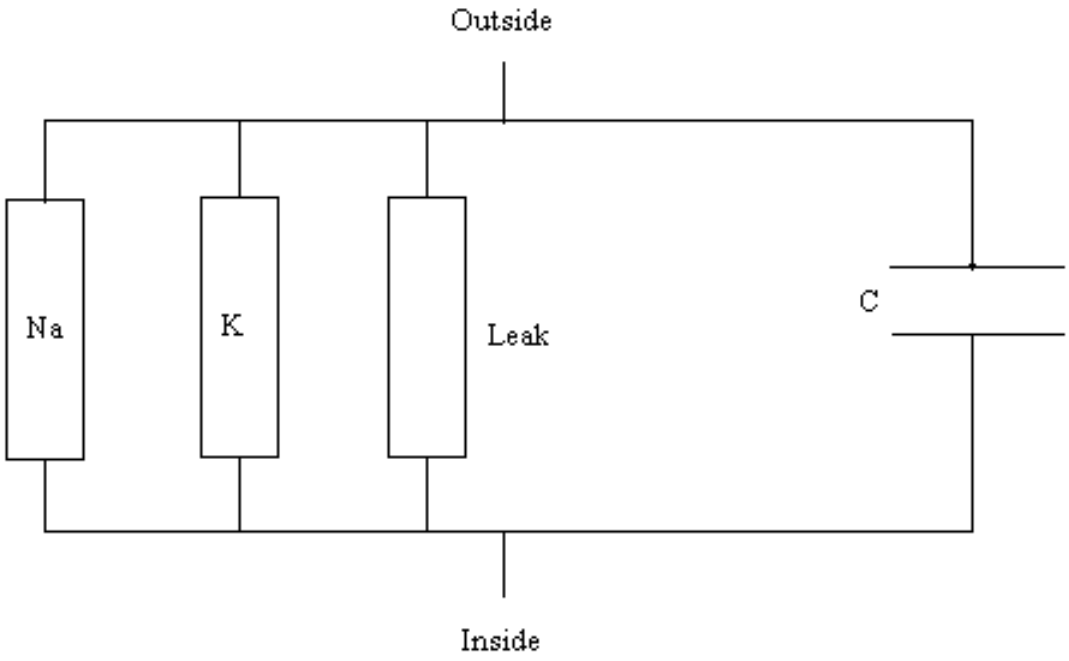

Figure 2.3: The cell membrane electrical circuit model for the Hodgkin-Huxley model of the squid giant axon.

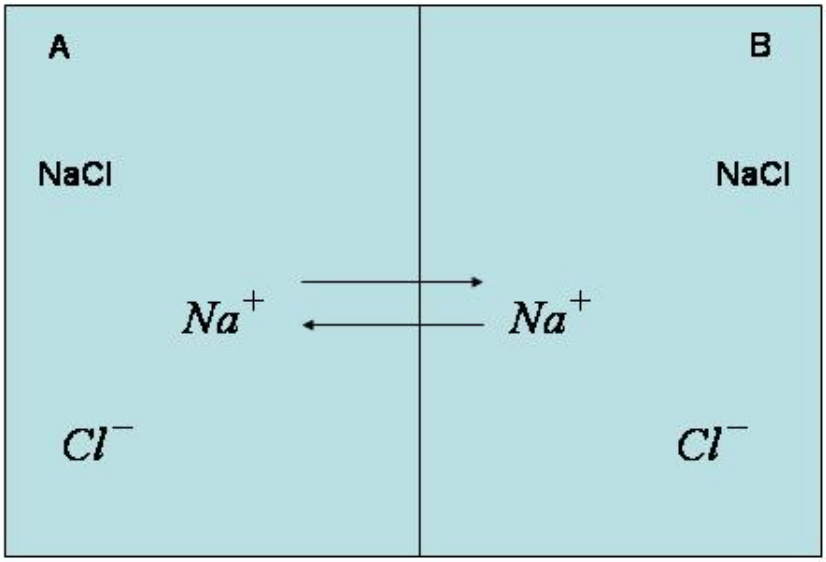

Figure 2.4: The two compartments each containing a salt and separated by a membrane permeable to Na^+ but not Cl^-.

Na^+ ions will therefore diffuse down their chemical gradient from A to B. This movement sets up an excess of Na^+ ions in compartment B and generates an electric potential that opposes further diffusion of the Na^+ ions. At the equilibrium, the resultant electric force balances the thermal force causing diffusion. The Nernst equation gives the resultant equilibrium potential between the two compartments A and B. Since we are interested in the generation of the resting membrane potential in cells, let us denote compartment A as the intracellular matrix and B, the extracellular matrix and let $[\mathrm{Na}]_i$ and $[\mathrm{Na}]_e$ be sodium concentrations in the intracellular and extracellular matrices, respectively. The Nernst potential is then given by the following formula

$$V_{\mathrm{Na}} = \frac{RT}{zF} \ln\left(\frac{[\mathrm{Na}]_e}{[\mathrm{Na}]_i}\right), \tag{2.7}$$

where $R = 8.3145$ J mol^{-1} K^{-1} is the gas constant, T, in Kelvins, is the temperature, F is the Faraday constant and z is the valance of the charged ions. For example, $z = 1$, and $z = 2$ for the sodium and the calcium ions respectively.

2.1.4 The Channel current-voltage relationship

There are different forms for the relationship between the current flow through the membrane ion channels and the membrane potential. One form which is based on the Ohm's law assumes a linear current-voltage relationship. For example, in this form the potassium current is given by:

$$I_K = g_{\mathrm{K}}(V - E_{\mathrm{K}}), \tag{2.8}$$

where g_{K} is the conductance (in siemens) which is time and voltage dependent. The term $(V - E_K)$ is used to reflect the fact that at the potassium equilibrium potential ($V = E_K$), I_K vanishes and if $V > E_{\mathrm{K}}$ flow out of the cell. Similarly the sodium current is given by

$$I_{\mathrm{Na}} = g_{\mathrm{Na}}(V - E_K). \tag{2.9}$$

Based on the above linear current-voltage relationships, we can calculate the equilibrium membrane potential in the Hodgkin-Huxley model (Recall that in this model, the main currents are the potassium, sodium and the leak current). Thus at the steady state we have

$$I_{\mathrm{Total}} \doteq I_{\mathrm{Na}} + I_{\mathrm{K}} + I_{\mathrm{Leak}} = 0,$$

That is

$$g_{\mathrm{Na}}(V_{\mathrm{eq}} - E_{\mathrm{Na}}) + g_{\mathrm{K}}(V_{\mathrm{eq}} - E_K) + g_{\mathrm{Leak}}(V_{\mathrm{eq}} - E_{Leak}) = 0,$$

so the equilibrium membrane potential is given by

$$V_{\text{eq}} = \frac{g_{\text{Na}} E_{\text{Na}} + g_{\text{K}} E_{\text{K}} + g_{\text{Leak}} E_{\text{Leak}}}{g_{\text{Na}} + g_{\text{K}} + g_{\text{Leak}}}. \tag{2.10}$$

As mentioned earlier, this linear current-voltage relationship is only one form which is used in formulating membrane models such as the original Hodgkin-Huxley model. Another formalism which is used is the Goldman-Hodgkin-Katz (GHK) equation (see [23] for more details and the derivation). For an ion S with valence z the GHK current equation is (in units of the current per area of the membrane):

$$I_s = P_s \frac{z^2 F^2}{RT} V \frac{c_i - c_e \exp\left(-\frac{zFV}{RT}\right)}{1 - \exp\left(-\frac{zFV}{RT}\right)}, \tag{2.11}$$

where P_s is the permeability of the membrane to S,and c_i and c_e are the intracellular and extracellular ionic concentrations respectively. It is instructive to notice that the flow is zero ($I_s = 0$) if :

$$V = V_S = \frac{RT}{zF} \ln\left(\frac{c_e}{c_i}\right). \tag{2.12}$$

which is the Nernst equilibrium potential for S. We emphasize that the Hodgkin-Huxley model assumes the linear current-voltage relationship.

2.2 Biophysics of The Squid Giant Axon

This section is based on a review written by M. Guevara [17] describing basic mechanisms behind the Hodgkin-Huxley model of the squid giant axon.

2.2.1 Ionic basis of the action potential generation

Figure 2.5 shows a typical action potential simulated by the Hodgkin-Huxley equations. This model consists of four coupled nonlinear ordinary differential equations. The sodium current is responsible for generating the rapid upstroke of the action potential, while the potassium current repolarizes (pushes the voltage down towards its resting value) the membrane. It is important to remember that other types of neurons can have many more currents than the three involved in the original Hodgkin-Huxley model.

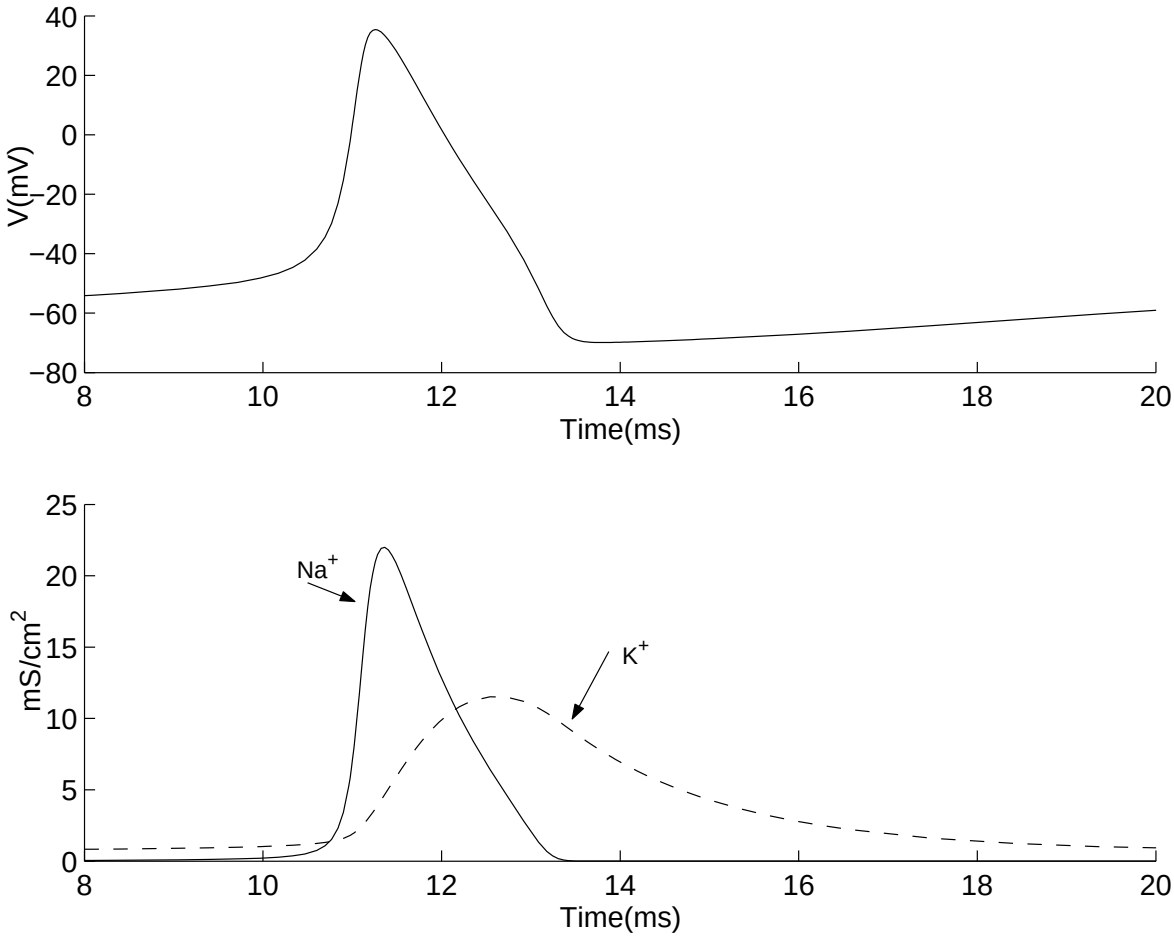

Figure 2.5: The action potential and the ionic conductances in the Hodgkin-Huxley model.

Single-channel recording

The most direct evidence for the existence of single channels on the cell membrane comes from the path-clamp technique. In 1991, Neher and Sakmann were awarded the Nobel prize in Physiology or Medicine for inventing this widely used technique. In this technique, a glass microelectrode with tip diameter on the order of $1\mu m$ is brought in contact with the cell membrane. It is hoped that the membrane patch subtended by the electrode rim contains only one channel. If this is the case, one can capture experimentally the stochastic opening and closing of the single channel. Channel openings cause current flow with amplitude of a few picoamps [34] that are then recorded over a range of time.

Voltage-clamp technique

Although the large size of the squid axon was invaluable in measurement of the transmembrane potential, it was the invention of a technique called voltage-clamp that revolutionized the field of excitable membrane electrophysiology. This technique was pioneered by Cole, Curtis, Hodgkin, Huxley, Katz and Marmont. Two electrodes are placed in the internal medium: one to measure the membrane potential, and the other to inject current. The current is injected using a feedback circuitry in order to maintain a fixed voltage difference at a particular potential. The injected current is in fact equal to the ionic current flowing through the membrane at the clamped potential. Figure 2.6 shows a simulation of the voltage-clamp experiment obtained by solving the Hodgkin-Huxley equations. In this simulation, the membrane potential is held at -70 mV for 200 milliseconds, in order to provide sufficient time for all the variables to reach their steady-state values, and is then stepped to -10 mV for another 10 milliseconds. The Sodium and potassium currents through the membrane are shown for this virtual experiment. It can be observed from the figure that the potassium current turns on (activates) relatively slowly, while the sodium current turns on (activates) very quickly and unlike the potassium current, it turns off (inactivates).

Kinetics of the potassium currents

The equation describing the potassium current is

$$I_K = g_K(V - E_K), \tag{2.13}$$

where g_{K} is the potassium conductance which is time and voltage dependent. To device the model, it is assumed that potassium channels contain a number of voltage-sensitive sensors that move in response to membrane potential changes and plug or unplug the opening of the channel pore. It would then be natural to assume the following form for the potassium conductance:

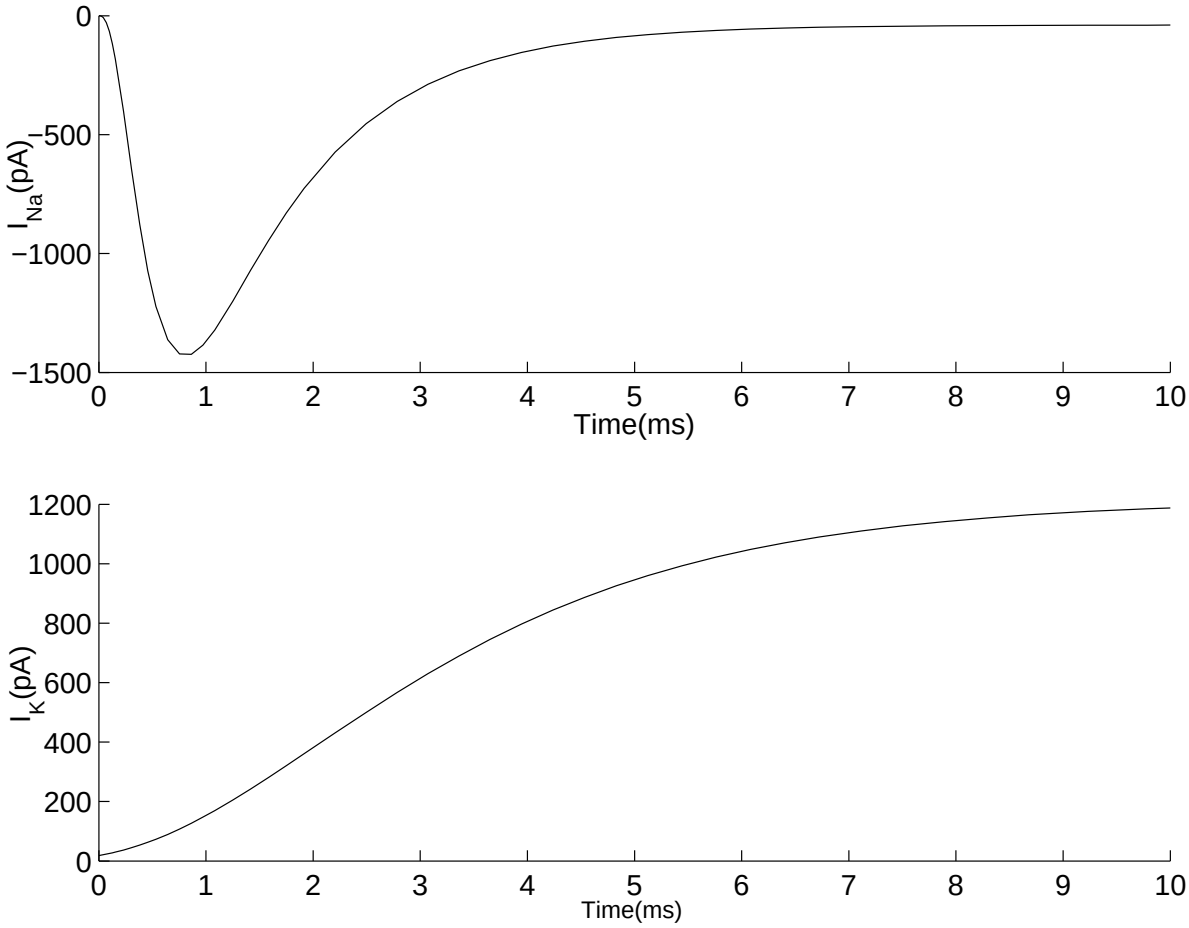

Figure 2.6: The sodium and potassium currents following a voltage-clamp step from a holding potential of -70mV to -10 mV.

$$g_{\mathrm{K}} = \overline{g}_{\mathrm{K}} O, \tag{2.14}$$

where O is the fraction of the channels that are open at a given instant of time and $\overline{g}_{\mathrm{K}}$ is the maximum potassium conductance. Assume that there are k types of sensors that can occupy two states with fractions n and $1-n$ respectively. It is assumed that the channel pore will open if all the sensors are in the state with fraction n. If the sensors move independent of each other, then the fraction of the potassium channels that are open is given by

$$O = n^k. \tag{2.15}$$

The movement of the sensor is assumed to follow the first order kinetic

$$\begin{aligned} 1 - n &\overset{\alpha_n}{\rightarrow} n \\ n &\overset{\beta_n}{\rightarrow} 1 - n, \end{aligned}$$

where α_n and β_n are the voltage-dependent functions. Hence

$$\frac{dn}{dt} = \alpha_n(1-n) - \beta_n n. \tag{2.16}$$

Hodgkin and Huxley observed that the best fit to their data was obtained by choosing $k = 4$. The equations for the potassium current are then:

$$I_{\mathrm{K}} = \overline{g}_{\mathrm{K}} n^4 (V - E_{\mathrm{K}}) \tag{2.17}$$

$$\frac{dn}{dt} = \alpha_n(1-n) - \beta_n n. \tag{2.18}$$

where α_n and β_n are fitted to the specific voltage-clamp experimental data (see [19] for details of the experiments) and are given by

$$\begin{aligned} \alpha_n &= \frac{0.01(V+50)}{1 - \exp\left(-\frac{V+50}{10}\right)} \\ \beta_n &= 0.125 \exp\left(-\frac{V+60}{80}\right). \end{aligned} \tag{2.19}$$

Figure 2.7 compares the trace of n and n^4 following a voltage-clamp step from a holding potential of -70 mV to 30 mV.

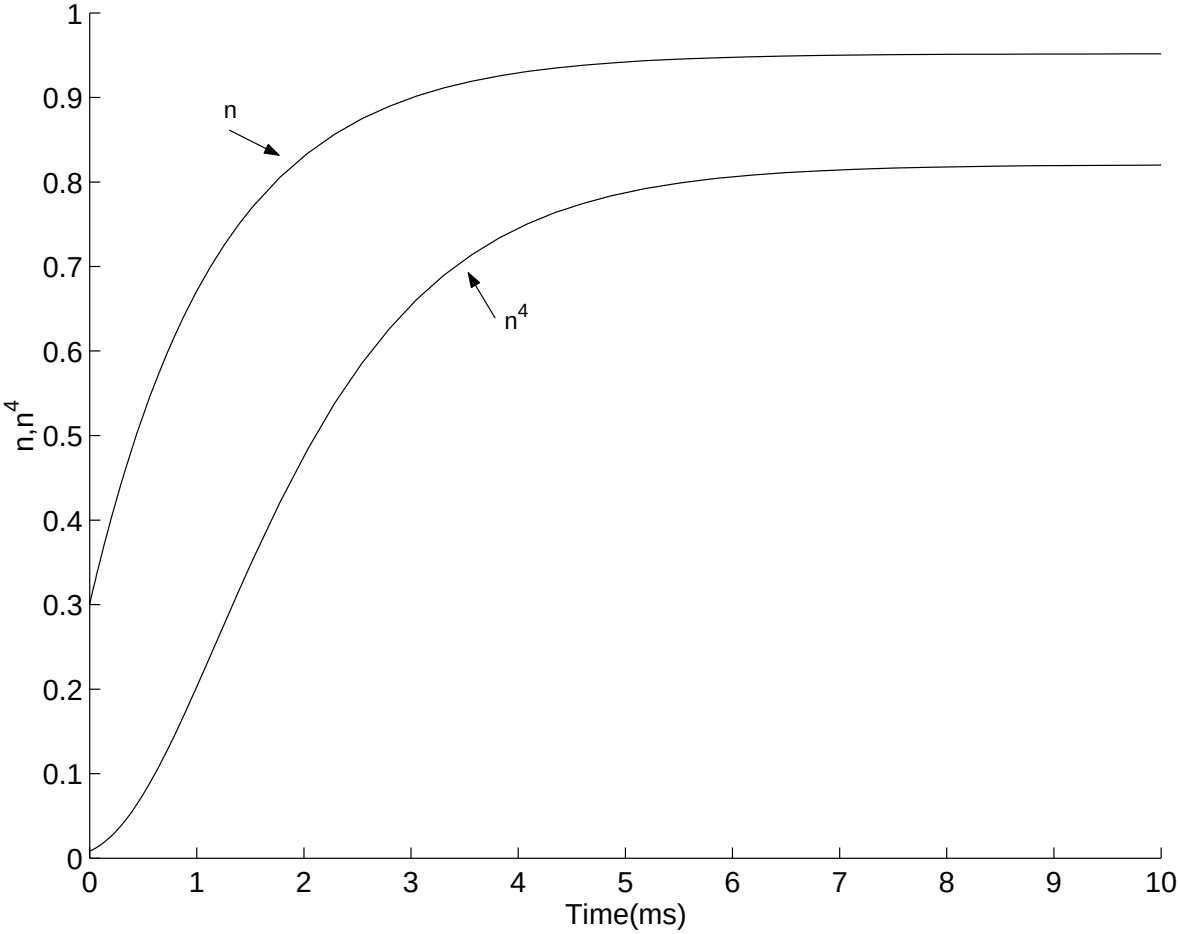

Figure 2.7: Comparing the first and fourth powers of the n gating variable following the voltage-clamp step from a holding potential of -70 mV to 30 mV.

Kinetics of the sodium currents

As in the previous section, fitting the macroscopic currents generated from voltage-clamp steps to different potentials led Hodgkin and Huxley to the following equation for sodium current

$$I_{Na} = g_{\mathrm{Na}}(V - E_{\mathrm{Na}}). \tag{2.20}$$

From Figure 2.6, it is clear that kinetics of the sodium current is more complicated. As for the potassium current, the sodium current activates and results in the opening of the channel; however, in contrast to the potassium current, the channel then inactivates and closes which results in the decline of the current as shown in Figure 2.6. As in the previous section, the conductance is given by the maximum conductance multiplied by the fraction of open channels O

$$g_{\mathrm{Na}} = \overline{g}_{\mathrm{Na}} O.$$

It is assumed that there are two categories of voltage sensors:

- Activating voltage-sensors, that can occupy two states with fractions m and $1 - m$.
- Inactivating voltage-sensors that can occupy two states with fractions h and $1 - h$.

Suppose that there are l types of activating sensors, and r types of inactivating sensors. The channel pore opens when all the activating sensor types are in the state with fraction m and all the inactivating sensor types are in the state with fraction h. Assuming independent movement of the sensors relative to each other, the fraction of the open channels is governed by

$$O = m^l h^r. \tag{2.21}$$

Additionally, it is assumed that the voltage sensors follow the first order kinetics

$$1 - m \overset{\alpha_m}{\rightarrow} m \tag{2.22}$$

$$m \overset{\beta_m}{\rightarrow} 1 - m. \tag{2.23}$$

Similarly for the inactivating sensor:

$$1 - h \overset{\alpha_h}{\rightarrow} h \tag{2.24}$$

$$h \overset{\beta_h}{\rightarrow} 1 - h. \tag{2.25}$$

Where all the rate constants are voltage-dependent functions. This leads to the following equations describing the the sensors dynamics

$$\frac{dm}{dt} = \alpha_m(1-m) - \beta_m m \tag{2.26}$$
$$\frac{dh}{dt} = \alpha_h(1-h) - \beta_h h. \tag{2.27}$$
$$\tag{2.28}$$

In the Hodgkin-Huxley model, there are three types of activating ($l = 3$) and one inactivating sensor ($r = 1$). These values were observed to best fit the experimental data (see [18] and [23], [19] for details). The sodium current dynamics is then governed by the following set of equations

$$\begin{aligned} I_{\mathrm{Na}} &= \overline{g}_{\mathrm{Na}} m^3 h (V - E_{\mathrm{Na}}) \\ \frac{dm}{dt} &= \alpha_m(1-m) - \beta_m m \\ \frac{dh}{dt} &= \alpha_h(1-h) - \beta_h h. \end{aligned} \tag{2.29}$$

where the rate-constants are given by

$$\begin{aligned} \alpha_m &= \frac{0.1(V+35)}{1 - \exp\left(-\frac{V+35}{10}\right)} \\ \beta_m &= 4\exp\left(-\frac{V+60}{18}\right) \\ \alpha_h &= 0.07\exp\left(-\frac{V+60}{20}\right) \\ \beta_h &= \frac{1}{1+\exp\left(-\frac{V+30}{10}\right)}. \end{aligned} \tag{2.30}$$

2.2.2 The Hodgkin-Huxley equations

Gathering together all of the previous equations for the sodium and potassium currents, one obtains the Hodgkin-Huxley equations that describe the membrane potential dynamics of the squid giant axon [19]. The model equations are as follows:

Table 2.1: Parameter values for the Hodgkin-Huxley model. The stimulus current is assumed to be $3\mu\text{A/cm}^2$ throughout this thesis and the physiological range is between 1 and 10 $\mu\text{A/cm}^2$.

Parameter	Unit	Parameter value
$\overline{g}_{\text{Na}}$	mS cm^{-2}	120
$\overline{g}_{\text{K}}$	mS cm^{-2}	36
$\overline{g}_L$	mS cm^{-2}	0.3
E_{Na}	mV	55
E_K	mV	-72
E_L	mV	-49.387
C	μF cm^{-2}	1

$$\begin{aligned}
\frac{dV}{dt} &= -\frac{1}{C}\left(\overline{g}_{Na}m^3h(V-E_{Na}) + \overline{g}_K n^4(V-E_K) + g_L(V-E_L) - I_{stim}\right) \\
\frac{dm}{dt} &= \alpha_m(1-m) - \beta_m m \\
\frac{dh}{dt} &= \alpha_h(1-h) - \beta_h h \\
\frac{dn}{dt} &= \alpha_n(1-n) - \beta_n n,
\end{aligned} \tag{2.31}$$

where I_{stim} is the total stimulus current to the neuron. Table 2.1 summarizes values of the parameters involved in the model.

I_{stim} is the total stimulus current to the neuron. The voltage dependent rate constants are described by

$$\begin{aligned}
\alpha_m &= \frac{0.1(V+35)}{1-\exp\left(-\frac{V+35}{10}\right)} \\
\beta_m &= 4\exp\left(-\frac{V+60}{18}\right) \\
\alpha_h &= 0.07\exp\left(-\frac{V+60}{20}\right) \\
\beta_h &= \frac{1}{1+\exp\left(-\frac{V+30}{10}\right)} \\
\alpha_n &= \frac{0.01(V+50)}{1-\exp\left(-\frac{V+50}{10}\right)} \\
\beta_n &= 0.125\exp\left(-\frac{V+60}{80}\right).
\end{aligned} \tag{2.32}$$

To summarize, Figure 2.8 shows all the gating variables during one action potential.

2.3 Model of the Hippocampal Interneurons

In this section, the Wang and Buszàki [43] model of the hippocampal interneurons is presented. The model is a modification of the Hodgkin-Huxley equations for the squid giant axon. The potassium and sodium currents are the main currents in this model as in the squid giant axon. The equations are as follows

$$\begin{aligned} C\frac{dV}{dt} &= I_{stim} - g_{\mathrm{Na}} m_\infty^3 h(V - E_{\mathrm{Na}}) - g_{\mathrm{K}} n^4 (V - E_{\mathrm{K}}) - g_{\mathrm{leak}}(V - E_{leak}) \\ \frac{dh}{dt} &= 5(\alpha_h(1-h) - \beta_h h) \\ \frac{dn}{dt} &= 5(\alpha_n(1-n) - \beta_n n) \\ m_\infty &= \frac{\alpha_m}{\alpha_m + \beta_m}. \end{aligned} \tag{2.33}$$

where the rate constants are given by

$$\begin{aligned} \alpha_m &= -\frac{0.1(V+35)}{\exp(-0.1(V+35)) - 1} \\ \beta_m &= 4\exp(-\frac{V+60}{18}) \\ \alpha_h &= 0.07\exp(-\frac{V+58}{20}) \\ \beta_h &= \frac{1}{\exp(-0.1(V+28))} \\ \alpha_n &= -\frac{0.01\exp(-(V+34))}{\exp(-0.1(V+34)) - 1} \\ \beta_n &= 0.25\exp(-\frac{V+44}{80}) \end{aligned} \tag{2.34}$$

and the model parameters are summarized in Table 2.2.

All currents are in units of $\mu\mathrm{A/cm}^2$. Notice that the activating variable m is assumed to be at the steady-state. This assumption is valid since the kinetics of the sodium channel activation is much more rapid than its inactivation. This implies that

$$\frac{dm}{dt} = \alpha_m(1-m) - \beta_m m \approx 0$$

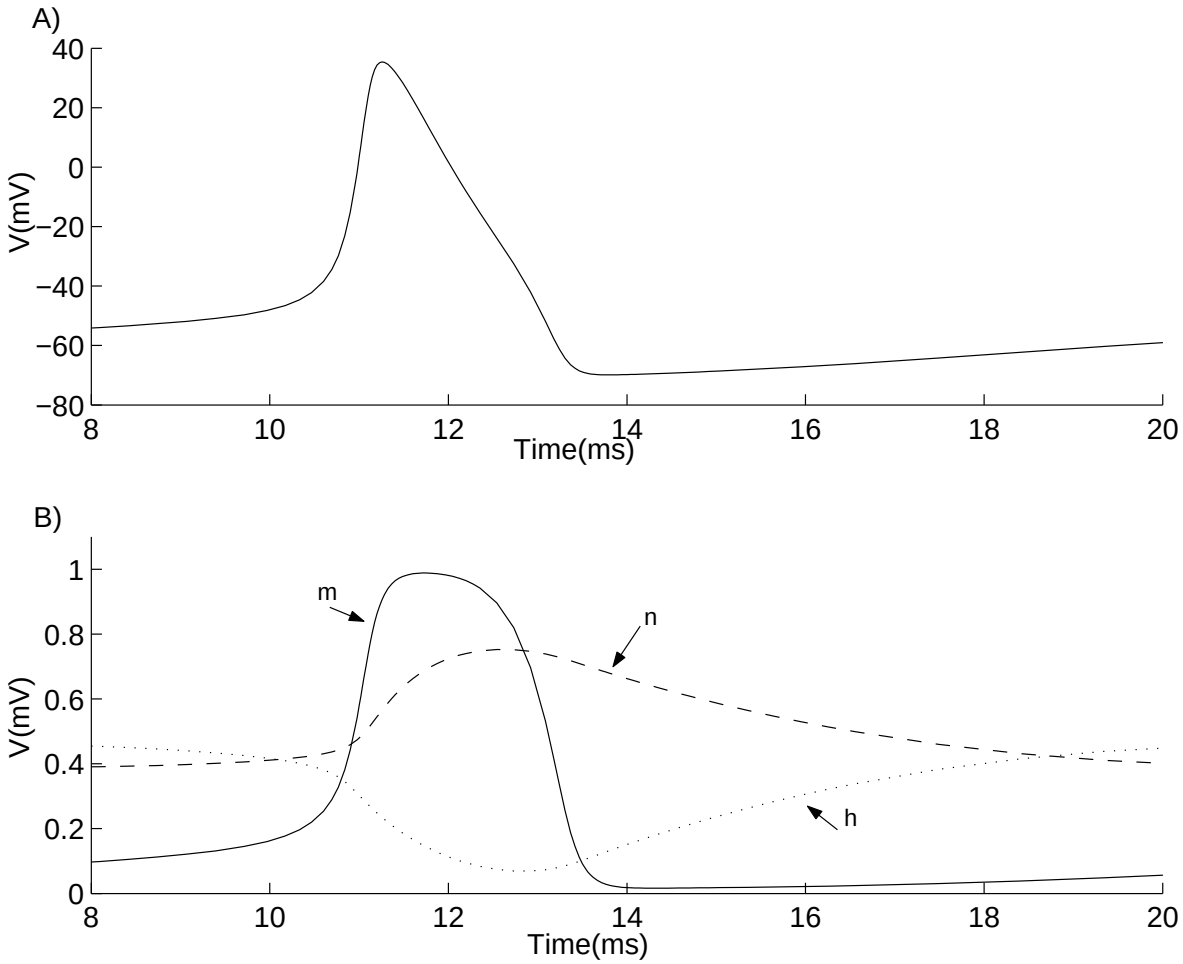

Figure 2.8: The gating variables and the action potential in the Hodgkin-Huxley model.

Table 2.2: Values of the parameters for the mathematical model of hippocampal interneurons.

Parameter	Unit	Parameter value
g_{Na}	$\mathrm{mS/cm^2}$	35
g_{K}	$\mathrm{mS/cm^2}$	9
g_{leak}	$\mathrm{mS/cm^2}$	0.1
E_{Na}	mV	55
E_{K}	mV	-90
V_{leak}	mV	-65
C	$\mu\mathrm{F/cm^2}$	1

and the voltage-dependent steady-state activating variable (denoted by m_∞) is

$$\frac{\alpha_m}{\alpha_m + \beta_m}.$$

Figure 2.9 presents a series of action potentials generated by numerically integrating system (2.33). For later convenience denote the total ionic current, I_{ionic}, as

$$I_{ionic}(V, n, h) = g_{\mathrm{Na}} m_\infty^3 h(V - E_{\mathrm{Na}}) + g_{\mathrm{K}} n^4 (V - E_{\mathrm{K}}) + g_{\mathrm{leak}}(V - E_{leak}). \tag{2.35}$$

For completeness, we emphasize that the single neuron exhibits oscillatory behavior for a specific range of the values of the stimulus current. As the stimulus current is increased from 0 to a sufficiently large value, the neuron enters oscillatory phase via a saddle-node bifurcation [37]. Throughout this thesis, it is assumed that the stimulus current is large enough so that the neurons exhibit oscillatory behavior. See [22] for an in depth discussion of the single neuron dynamics and the corresponding bifurcation diagrams.

2.4 Synaptic Coupling Between Neurons

In this section a brief introduction will be given to synaptic communication between neurons (see [23], and [3] for more details). Communication in the nervous systems is achieved mainly via what is called a chemical synapse. The chemical synapse has two sides: presynaptic and postsynaptic. The presynaptic cell is the neuron that sends the signal and the postsynaptic neuron is the receiving side. There are several specialized structures that work in concert for regulating synaptic communication. Figure 2.10 shows a schematic diagram of the synapse between two neurons and the following is a description of the structures labeled in Figure 2.10:

1. Axon of the presynaptic neuron.
2. The axon terminal containing vesicles.
3. Membrane vesicles that contain special chemicals called neurotransmitters. When an action potential reaches the axon terminal (see item 2), these vesicles move towards and fuse with the terminal membrane and release their contents into the synaptic cleft (item 4). The transmitter molecules then diffuse in the synaptic cleft and are received at specialized receptors on the membrane of the postsynaptic neuron.
4. The space between the axon terminal of the presynaptic neuron and dendrites of the postsynaptic neuron.
5. The dendrite of the postsynaptic neuron. This has special ion channels on its membrane which open in response to the neurotransmitter molecules released from the vesicles.

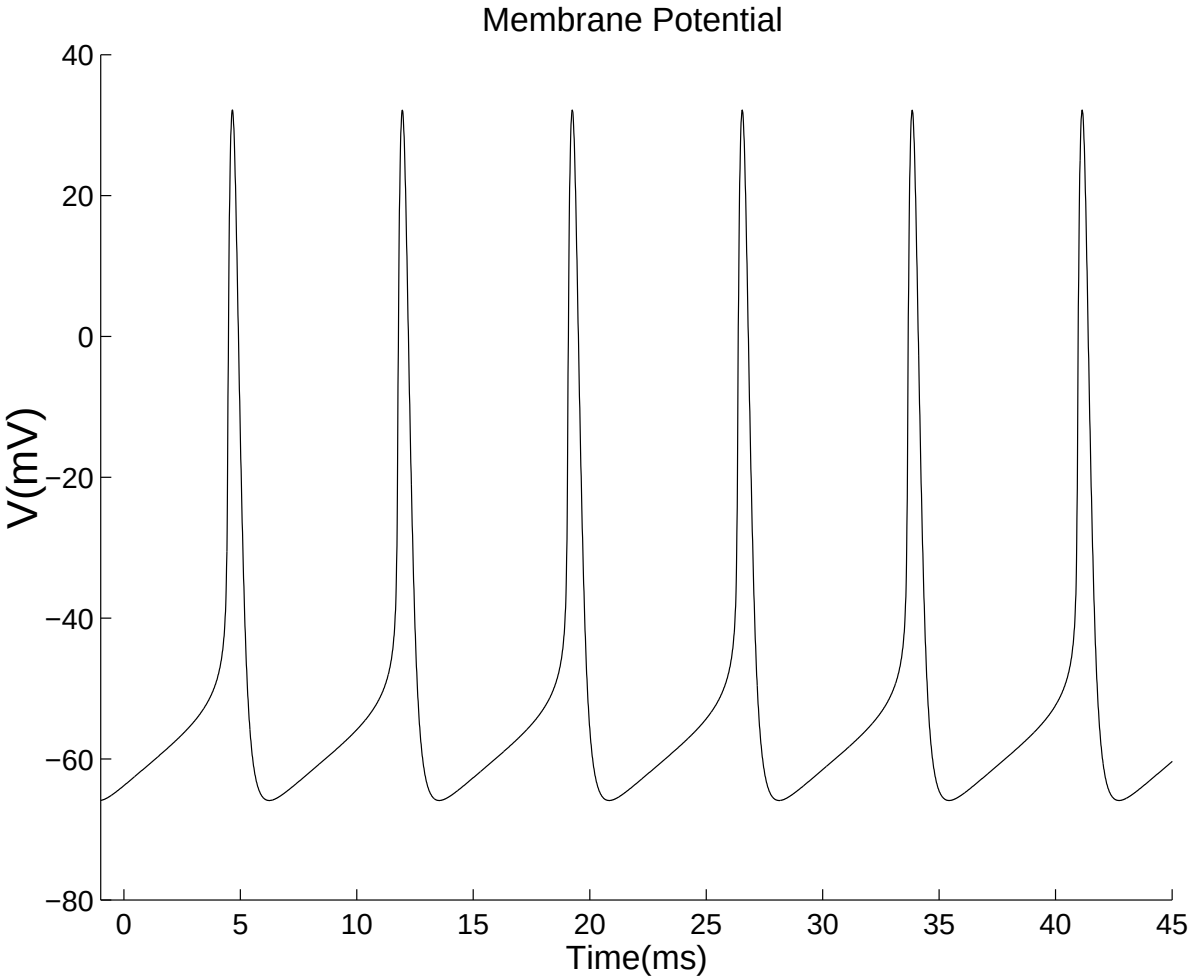

Figure 2.9: The action potentials in Wang-Buszàki model of the hippocampal interneurons.

The axon terminal (Figure 1.1) contains vesicles that store chemicals called neurotransmitters (also called synaptic transmitters). When an action potential reaches the terminal, these vesicles release their contents into the region between the terminal and the postsynaptic neuron (this space is called the synaptic cleft). There are different types of synaptic transmitters depending on their effects on the postsynaptic membrane. For example, acetylcholine(ACh) binds to ACh receptors on the postsynaptic cell, which act as cation (positively charged ion) channels. When ACh binds to the ACh receptors it opens these channels and causes the flow of positive ions into the postsynaptic membrane and therefore results in depolarization (moving the voltage to more positive values) of the membrane potential in the postsynaptic neuron. The communication between hippocampal interneurons is regulated by gamma-butiric acid (GABA) [43] which opens anion (negatively charged ion) channels allowing flow of negatively charged ions through the postsynaptic membrane and therefore hyperpolarizes (moves the voltage to more negative values) the postsynaptic membrane potential. Synapses that cause depolarization of the postsynaptic membrane are called excitatory, while the ones that result in hyperpolarization are called inhibitory. The synapses between hippocampal interneurons are therefore inhibitory in nature.

2.4.1 Simple model for the chemical synapse

A simple model [33] for the current generated in the postsynaptic neuron membrane will be given in this section and will be used throughout our study of the coupled hippocampal interneurons. We assume that binding of the transmitter molecules to the channels on the postsynaptic membrane causes opening of the channel. A simple reaction scheme can be assumed as follows

$$C + T \xrightarrow{\alpha} O$$
$$O \xrightarrow{\beta} C + T.$$

Where:

- C: Closed channel state
- T: Transmitter molecules
- O: Open channel state

Let s and $1 - s$ be the fraction of channels in the open and closed states respectively and let $[T]$ be the transmitter concentration in the vicinity of the postsynaptic membrane channel (in the

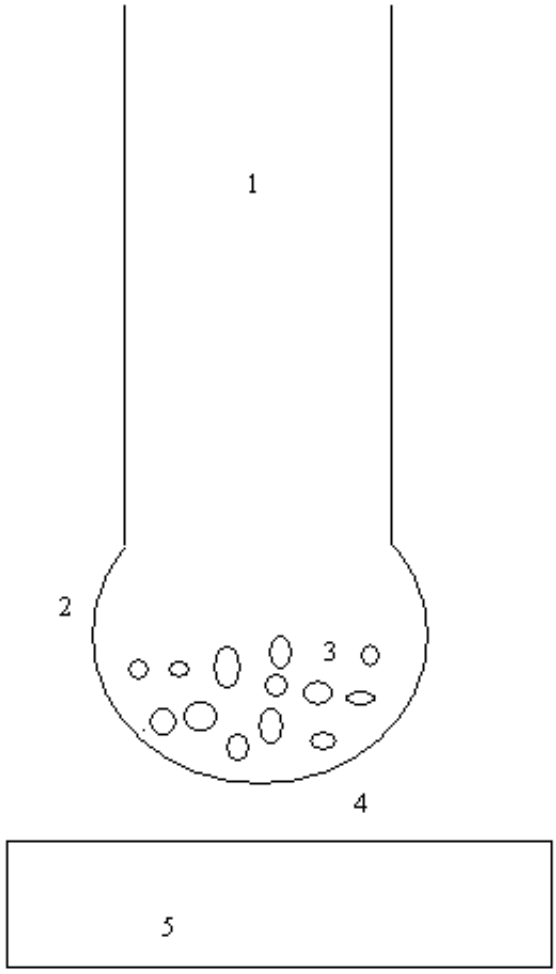

Figure 2.10: Schematic view of the chemical synapse between two neurons.

synaptic cleft). Then from the above reaction scheme we have

$$\frac{ds}{dt} = \alpha(1-s)[T] - \beta s. \tag{2.36}$$

It only remains to specify the time course of the transmitter concentration $[T]$. It is assumed that $[T]$ depends on the membrane potential of the presynaptic neuron and the usual functional form is taken to be sigmoidal to reflect switching effect of the transmitter concentration in turning the postsynaptic channels on or off

$$[T] = \frac{1}{1+\exp(-(V_{pres}-\theta)/k_{syn})}. \tag{2.37}$$

where V_{pres} is the membrane potential of the presynaptic neuron and θ and k_{syn} are the shape parameters of the sigmoidal function. For the hippocampal interneurons model [43], $\theta = 0$ and $k_{syn} = 2$. Thus, equation 2.36 becomes

$$\frac{ds}{dt} = \alpha s \frac{1}{1+\exp(-V_{pres}/2)} - \beta(1-s). \tag{2.38}$$

Let the maximum conductance through the postsynaptic membrane be g_{syn}, the fraction of the open channels is s, and the current through the postsynaptic membrane has the form

$$I_{syn} = g_{syn} s(V - V_{syn}). \tag{2.39}$$

where V_{syn} is the equilibrium potential for the ions flowing through the postsynaptic membrane (note that when $V = V_{syn}$ no synaptic current flows) and depends on the concentration differences for the ion species that flow through the open receptor channels.

We mentioned that there are excitatory or inhibitory synapses depending on whether the synaptic current is depolarizing or hyperpolarizing respectively. These two distinct synaptic couplings can be modeled by choosing the appropriate V_{syn}. If V_{syn} is lower than the threshold for action potential generation, the synapse is called inhibitory (the resulting current hyperpolarizes the membrane since $V - V_{syn} > 0$ and $-I_{syn} < 0$), and if it is larger than the threshold, the synapse is called excitatory. For the hippocampal model with inhibitory synapses, $V_{syn} = -75$ mV. To recapitulate what we have so far, the dynamics of the two hippocampal interneurons coupled via chemical synapses is described by the following system:

$$
\begin{aligned}
C\frac{dV_1}{dt} &= I_{stim_1} - I_{ionic}(V_1, n_1, h_1) - g_{syn}s_{21}(V_1 - V_{syn}) \\
\frac{dh_1}{dt} &= 5(\alpha_{h_1}(1-h_1) - \beta_{h_1}h_1) \\
\frac{dn_1}{dt} &= 5(\alpha_{n_1}(1-n_1) - \beta_{n_1}n_1) \\
\frac{ds_{21}}{dt} &= \alpha\frac{1}{1+\exp(-V_2/2)}s_{21} - (1-s_{21})/\tau_{syn} \\
C\frac{dV_2}{dt} &= I_{stim_2} - I_{ionic}(V_2, n_2, h_2) - g_{syn}s_{12}(V_2 - V_{syn}) \\
\frac{dh_2}{dt} &= 5(\alpha_{h_2}(1-h_2) - \beta_{h_2}h_2) \\
\frac{dn_2}{dt} &= 5(\alpha_{n_2}(1-n_2) - \beta_{n_2}n_2) \\
\frac{ds_{12}}{dt} &= \alpha\frac{1}{1+\exp(-V_1/2)}s_{12} - (1-s_{12})/\tau_{syn},
\end{aligned}
$$

where $\alpha = 6.25$ ms^{-1} [36] and synaptic time constant is defined by $\tau_{syn} = 1/\beta$ with biological relevant values between 1 to 10 ms. The maximum conductance is estimated to be $g_{syn} = 0.25$ mS/cm^2 [36].
Single cell total ionic currents, $I_{ionic}(V_1, n_1, h_1)$ and $I_{ionic}(V_2, n_2, h_2)$, were described as in equation (2.35). Figure 2.11 shows schematic diagram of two neurons interacting via inhibitory synapses. Throughout this thesis it is assumed that neurons reciprocally inhibit each other as shown.

In this thesis, we will be working with networks consisting of N neurons where the general biophysical model of the interneuronal network is as follows

$$
\begin{aligned}
C\frac{dV_k}{dt} &= I_{stim} - I_{ionic}(V_k) - \frac{g_{syn}}{N-1}(V_k - E_{syn})\sum_{\substack{j=1 \\ j\neq k}}^{N} s_{jk} \\
\frac{ds_{jk}}{dt} &= \alpha\frac{1}{1+\exp(-V_j/2)}s_{jk} - \frac{(1-s_{jk})}{\tau_{syn}}, \quad k, j = 1, \ldots, N.
\end{aligned} \tag{2.40}
$$

where the effective synaptic coupling is denoted by $\frac{g_{syn}}{N-1}$ to account for the interaction of each neuron with $N-1$ other neurons. This model will be used to study action potential pattern in networks consisting of two, three and four neurons and the results will be compared with predictions of the phase coupled oscillator model which will be discussed in the next chapter.

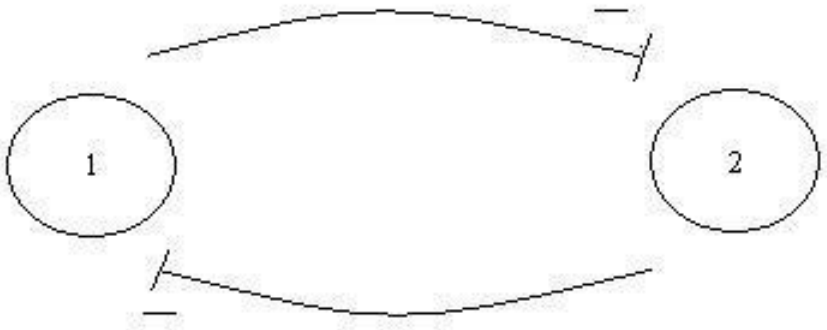

Figure 2.11: Schematic representation of two neurons reciprocally inhibiting each other.

Chapter 3

System of Coupled Oscillators

System of coupled oscillators are ubiquitous in biological systems. Hippocampal interneurons coupled via inhibitory synapses are an example of coupled oscillators that are being studied in this thesis. The following section presents an overview of the coupled oscillator concepts and techniques for simplifying general coupled dynamical systems having stable limit cycle solutions.

3.1 Basic definitions

We begin by introducing the notions of phase, synchronization and phase locking based on the discussion in Hoppensteadt and Izhikevich [20].

Phase

Suppose that we are given an oscillator, that is a dynamical system

$$\frac{dX}{dt} = F(X), \quad X \in R^m \tag{3.1}$$

having a limit cycle attractor $\gamma \subset R^m$. Let T and $\Omega = \frac{2\pi}{T}$ be the period and frequency of the limit cycle, respectively. Let $x(t) \in R^m$ be a T-periodic solution starting from $x(0) = x_0 \in \gamma$. For each point $y \in \gamma$ there is a unique $t \in [0, T)$ such that $y = x(t)$. We can assign a phase (θ) to each point on the limit cycle such that as x goes around a limit cycle from $x(0)$ to $x(T)$, the phase makes one rotation around the unit circle by going from $\theta(0) = 0$ to $\theta = 2\pi$ (Figure 3.1). In the other words, this parametrization is a transformation which deforms the limit cycle into a circle (S^1) by assigning an angle value to each point on the limit cycle. $\theta(t)$ defined in this way is

called the *natural phase* of the point $x(t) \in \gamma$. In case of a single oscillator, the phase, $\theta(t) \in S^1$, is the solution to the phase equation

$$\frac{d\theta}{dt} = \Omega = \frac{2\pi}{T}, \tag{3.2}$$

such that $\theta(0) = 0$. For N uncoupled oscillators, the dynamical system is

$$\frac{dX_j}{dt} = F_j(X_j), \quad X_j \in R^m \quad j = 1, \ldots, N \tag{3.3}$$

where each ODE in the above system has a stable limit cycle attractor γ_j. The phase equations in this case are

$$\frac{d\theta_j}{dt} = \Omega_j, \quad \theta_j \in S^1, \quad j = 1, \ldots, N, \tag{3.4}$$

where θ_j is coordinate of the jth oscillator on the torus $T^N = S^1 \times \ldots \times S^1$. For coupled oscillators the dynamical system becomes

$$\frac{dX_j}{dt} = F_j(X_j) + \epsilon G_j(X), \quad j = 1, \ldots, N. \tag{3.5}$$

The functions $G_j(X_1, \ldots, X_N)$ describe the state dependent coupling between the oscillators and ϵ is the coupling parameter. In this thesis we shall assume that, the parameter ϵ is sufficiently small such that the oscillators do not leave the torus defined by the uncoupled system (3.4). As we will see later, the assumption of sufficiently weak coupling, leads to the reduction of the dynamical system (3.5) to a system describing the phase dynamics

$$\frac{d\theta_j}{dt} = \Omega_j + \epsilon g_j(\theta_1, \ldots, \theta_N), \quad \theta_j \in S^1, \quad j = 1, \ldots, N. \tag{3.6}$$

The functions $g_j(\theta_1, \ldots, \theta_N)$ describe the influence of the coupling on the oscillator phases. The original system containing $m \times N$ ODES (m for each of the limit cycle oscillator and N for the number of oscillators in the system) is reduced to a system containing N equations. Phase models are powerful tools for analyzing phenomena such as synchronization which would be impossible to address with the full model (3.5).

Synchronization and phase locking

Suppose we are given two neural oscillators with the phases $\theta_1(t)$ and $\theta_2(t)$ which are coupled weakly via some mechanism. Also assume that each oscillator oscillates with the same natural frequency, Ω. Let $\phi_1 = \theta_1 - \theta_2$, be the phase-difference between the oscillators. We say that the two-oscillator system is *phase locked* if $\frac{d\phi_1}{dt} = 0$. The system of two neural oscillators is said to be *synchronized* if the following conditions hold

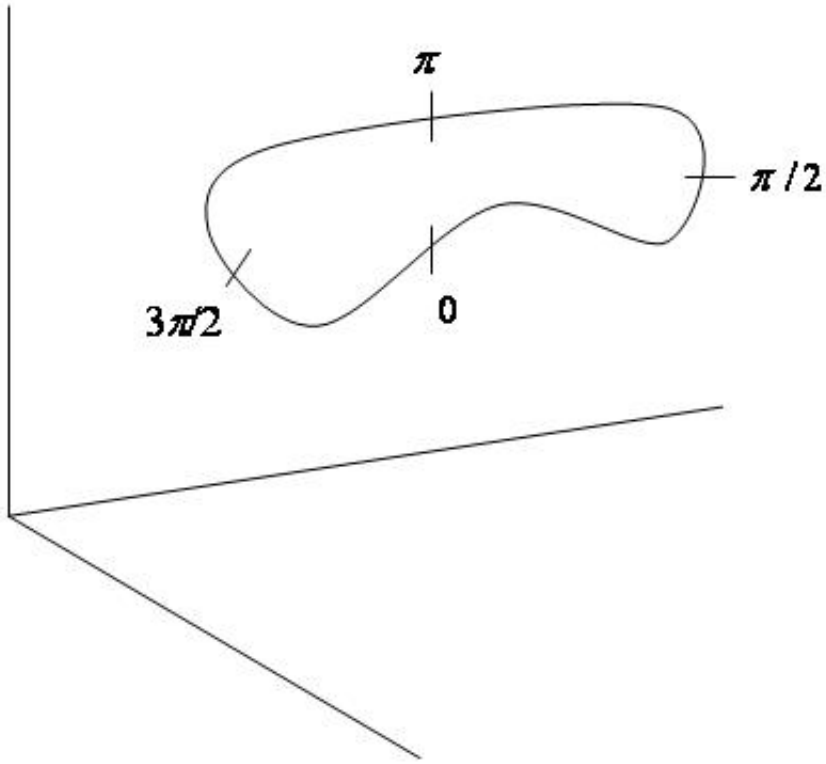

Figure 3.1: Phase parametrization of the limit cycle.

1. $\frac{d\phi_1}{dt} = 0$.

2. $\phi_1 = 0$.

These conditions guarantee concurrent oscillations of the two neurons. In study of the oscillator networks, it is often instructive to study the case of *antiphase* oscillations. We say that the two-neuron system exhibits *antiphase* oscillations, if $\frac{d\phi_1}{dt} = 0$ and $\phi_1 \equiv \theta_1 - \theta_2 \equiv \pi$, which implies that the two neural oscillators are a half-cycle apart.
The above definitions can be extended to a network of N neurons. Let $\theta_1, \theta_2, \ldots, \theta_N$ be the phases of the corresponding oscillators and take θ_1 as the reference point from which all other phases are measured. Suppose that the natural frequency of each oscillator is Ω and set $\phi_j = \theta_j - \theta_{j+1}, \quad j = 1, \ldots, N-1$ as the phase-difference between the jth and $(j+1)$st neuron. The network is said to be phase locked if

$$\frac{d\phi_j}{dt} = 0, \quad j = 1, \ldots, N-1. \tag{3.7}$$

This implies that ϕ_j, $j = 1, \ldots, N-1$ remain constant (not necessarily equal) over time. For synchronization we further require the phase differences be zero.

$$\phi_j \equiv 0, \quad j = 1, \ldots, N-1. \tag{3.8}$$

Additionally, in a synchronized network of N neurons the phases are given by

$$\frac{d\theta_j}{dt} = \Lambda t, \quad j = 1, \ldots, N. \tag{3.9}$$

Λ is called the *network frequency* which is in general different from the natural frequency, Ω. For the anti-phase oscillations, with an appropriate choice of indexing, the following pattern is retained for all times in the network

$$\begin{aligned}
&\theta_1 = \Lambda t + 0 \\
&\theta_2 = \Lambda t + \pi \\
&\theta_3 = \Lambda t + 0 \\
&\vdots \\
&\theta_k = \Lambda t + \pi \text{ for even } k \\
&\theta_k = \Lambda t \text{ for odd } k.
\end{aligned}$$

Equivalently, we may write:

$$\theta_j = \Lambda t + \frac{1+(-1)^j}{2}\pi, \quad j = 1, \ldots, N. \tag{3.10}$$

and

$$\phi_j = \theta_j - \theta_{j+1} = (-1)^j \pi, \quad j = 1, \ldots, N-1. \tag{3.11}$$

An alternative definition of phase locking, which is used by some authors [10] and will be used in some situations in this thesis, is a definition that puts constraints on the phases of the oscillators (θ_j). Suppose that we have a network of neural oscillators having phases $\theta_1, \ldots, \theta_N$. The oscillators are said to be phase-locked if

$$\frac{d\theta_j}{dt} = \Lambda, \quad j = 1, \ldots, N. \tag{3.12}$$

Physically this means that all of the neurons in the network are oscillating with the same frequency. Integrating equation (3.12) shows that in a phase-locked network the phases have the form

$$\theta_j = \Lambda t + \beta_j, \quad j = 1, \ldots, N. \tag{3.13}$$

for some constants β_j. Notice that for synchronous oscillations $\beta_k = 0$ and for the anti-phase oscillations $\beta_k = \frac{1+(-1)^k}{2}\pi$. Additionally, the relationship between this definition and the previous one can be established by noting that
$\phi_k \equiv \theta_k - \theta_{k+1} = \beta_k - \beta_{k+1}$ and $\frac{d\phi_k}{dt} = \frac{d\beta_k}{dt} - \frac{d\beta_{k+1}}{dt} = 0$.
It is also instructive to discussed the concept of *phase deviation* which will be important in the next section and understanding some of the related work on coupled oscillators ([21], [22] and [20]). The phases are sometimes written in the following form

$$\theta_j(t) = \Omega_j t + \varphi_j(t), \tag{3.14}$$

where Ω_j are the natural frequencies and the variables $\varphi_j \in S^1$ are the *phase deviations*. They describes deviation of the phases θ_j from the natural oscillations $\Omega_j t$.

Following this overview, the next section presents an account of the phase reduction technique, which greatly simplifies the analysis of the weakly coupled oscillatory networks. Our discussion is based on Hoppensteadt and Izhikevich [20] and Izhikevich [22].

3.2 Phase equations

Suppose that we have a network consisting of N neural oscillators. Recall from the previous section that each oscillator in the system is a dynamical system

$$\frac{dX_j}{dt} = F_j(X_j, \lambda) \quad X_j \in R^m \quad j = 1, \ldots, N. \tag{3.15}$$

having an attracting limit cycle $\gamma_j \in R^m, \quad j = 1, \ldots, N$. λ is a parameter which will be associated with the variation of the natural frequencies of the uncoupled oscillators. Based on the discussion in the previous section, each limit cycle can be parametrized by the phases $\theta_j(t)$, and the above system is reduced to the following

$$\frac{d\theta_j}{dt} = \Omega_j(\lambda), \quad \theta_j \in S^1, \quad j = 1, \ldots, N. \tag{3.16}$$

We next suppose that the oscillators are coupled via some nonlinear functions with coupling strength ϵ. The dynamical system describing the coupled network is then

$$\frac{dX_j}{dt} = F_j(X_j, \lambda) + \epsilon G_j(X) \quad X_j \in R^m \quad j = 1, \ldots, N. \tag{3.17}$$

The functions $G_j(X)$ describe the interactions between the oscillators.
We are now in a position to state an important theorem regarding the reduction of the dynamical system of the form (3.16) to a lower dimensional system.

Theorem 3.2.1 (Phase Equations For Oscillatory Neural Networks)
Consider a family of coupled systems

$$\frac{dX_j}{dt} = F_j(X_j, \lambda) + \epsilon G_j(X, \epsilon), \quad j = 1, \ldots, N \tag{3.18}$$

such that each equation in the uncoupled system ($\epsilon = 0$) has an exponentially stable limit cycle attractor $\gamma_j \subset R^m$ having natural frequency $\Omega_j(\lambda) \neq 0$. Then, there exists $\epsilon_0 > 0$ such that for $|\epsilon| < \epsilon_0$ there exists an open neighborhood W of $M = \gamma_1 \times \ldots \times \gamma_N \subset R^{nm}$ and a continuous function $h : W \to T^n$, that maps solutions of (3.18) to those of

$$\frac{d\theta_j}{dt} = \Omega_j + \epsilon g_j(\theta_1, \ldots, \theta_N), \quad \theta_j \in S^1, \quad j = 1, \ldots, N. \tag{3.19}$$

defined on the torus $T^n = S^1 \times \ldots \times S^1$.

The next theorem, due to Malkin ([20] and [21]), presents an approximate formula for the interaction functions $g_j(\theta_1, \ldots, \theta_N)$, and phase deviations described earlier.

Theorem 3.2.2 (Malkin's Theorem for Weakly Connected Oscillators)
Consider a coupled system of the form

$$\frac{dX_j}{dt} = F_j(X_j, \lambda) + \epsilon G_j(X), \quad X_j \in R^m, \tag{3.20}$$

such that each equation in the uncoupled system

$$\frac{dX_j}{dt} = F_j(X_j, \lambda) \tag{3.21}$$

has an exponentially stable T-periodic solution $\gamma_j(t) \in R^m$. Let $\tau = \epsilon t$, and let $\varphi_j(\tau) \in S^1$ be the phase deviations of the solution of the coupled system (2.20) from the uncoupled oscillations $\gamma_j(t)$.

Then, the vector of the phase deviations $\varphi = (\varphi_1, \ldots, \varphi_N)^T$ is a solution to

$$\frac{d\varphi_j}{d\tau} = H_j(\varphi - \varphi_j) + O(\epsilon). \tag{3.22}$$

Here $(\varphi - \varphi_j) = (\varphi_1 - \varphi_j, \ldots, \varphi_N - \varphi_j)^T$, and

$$H_j(\varphi - \varphi_j) = \frac{1}{T}\int_0^T Q_j(t)^T G_j(\gamma(t + \varphi - \varphi_j))dt, \tag{3.23}$$

where

$$\gamma(t + \varphi - \varphi_j) \equiv (\gamma_1(t + \varphi_1 - \varphi_j), \gamma_2(t + \varphi_2 - \varphi_j), \ldots, \gamma_N(t + \varphi_N - \varphi_j))$$

and $Q_j(t)$ is the unique nontrivial T-periodic solution to the adjoint system

$$\frac{dQ_j}{dt} = -DF_j(\gamma_j(t))^T Q_j, \tag{3.24}$$

satisfying the normalization condition

$$Q_j(0)^T F_j(\gamma_j(0)) = 1. \tag{3.25}$$

It follows that the phase deviations are governed by

$$\frac{d\varphi_j}{dt} = \epsilon H_j(\varphi - \varphi_j) + O(\epsilon^2). \tag{3.26}$$

Suppose that we choose the parameter λ such that the natural frequencies $\Omega_1, \ldots, \Omega_N$ are ϵ close to each other, $|\Omega_i - \Omega_j| = O(\epsilon)$ for all i, j. It can be shown that [20] the equations for describing the phase dynamics for an oscillator network with heterogeneity in the oscillator frequencies are:

$$\frac{d\theta_j}{dt} = \Omega_j + \epsilon H_j(\theta - \theta_j) + O(\epsilon^2), \quad j = 1, \ldots, N. \tag{3.27}$$

and for a homogenous network (all the natural frequencies are the same) the phase equations become

$$\frac{d\theta_j}{dt} = \Omega + \epsilon H_j(\theta - \theta_j) + O(\epsilon^2), \quad j = 1, \ldots, N. \tag{3.28}$$

For cells coupled via chemical synapses, the interaction function depends only on the state of the mutually coupled cells. In other words, interaction between cell i and cell j in the population is a function of state variables of i and j only. According to Theorem (3.2.1), the general phase model of an oscillator network (dropping the $O(\epsilon^2)$) has the following form

$$\frac{d\theta_j}{dt} = \Omega_j + g_j(\theta_1, \ldots, \theta_N)$$

Take cell j in the population and exclude self-interaction, then function g_j has the following additive form

$$g_j(\theta_1, \ldots, \theta_N) = \sum_{\substack{i=1 \\ i \neq j}}^{N} g_j(\theta_i, \theta_j) \tag{3.29}$$

By application of the Malkin's theorem, the interaction function for the cell j is given by $\epsilon H_j(\theta_1 - \theta_j, \ldots, \theta_N - \theta_j)$, and for a neural network with chemical synapses, the interaction function takes the form

$$\epsilon H_j(\theta_1 - \theta_j, \ldots, \theta_N - \theta_j) = \epsilon \sum_{\substack{i=1 \\ i \neq j}}^{N} H_j(\theta_i - \theta_j) \tag{3.30}$$

Therefore, the phase model in terms of the phase deviation (3.22) can be written as

$$\frac{d\varphi_j}{dt} = \epsilon \sum_{k=1}^{N} H(\varphi_k - \varphi_j) \tag{3.31}$$

and in terms of the phases (3.27), it becomes

$$\frac{d\theta_j}{dt} = \Omega_j + \epsilon \sum_{\substack{k=1 \\ k \neq j}}^{N} H_j(\theta_k - \theta_j) \tag{3.32}$$

Equation (3.32) describes a general situation where the cells are not identical (and hence the interaction function is different for each interacting pair). For network of identical cells which are being considered in this thesis, all the interaction functions are identical and hence

$$H_j(\theta_k - \theta_j) = H(\theta_k - \theta_j), \quad j = 1, \ldots, N. \tag{3.33}$$

The phase dynamics is then governed by

$$\frac{d\theta_j}{dt} = \Omega_j + \epsilon \sum_{\substack{k=1 \\ k \neq j}}^{N} H(\theta_k - \theta_j). \tag{3.34}$$

In a network of identically coupled neurons, we only need to compute the interaction function for a pair of neurons and the only difficulty in using Malkin's Theorem lies in finding the periodic solution of the adjoint system

$$\frac{dQ_j}{dt} = -DF_j(\gamma_j(t))^T Q_j,$$

satisfying the normalization condition

$$Q_j(0)^T F_j(\gamma_j(0)) = 1.$$

Williams and Bowetell [46] (see also [12]) devised a simple way to compute $Q_j(t)$ for a stable limit cycle:
start with random initial conditions and integrate

$$\frac{dQ_j}{dt} = -DF_j(\gamma_j(t))^T Q_j$$

backwards. Since all the Floquet multipliers (eigenvalues of the Poincaré map) are outside the unit circle (except for a multiplier of 1), backward integration will converge to the periodic solution of the adjoint system. The software XPPAUT [11] developed by G.B.Ermentrout, usee this method to numerically compute the interaction functions. Furthermore, since the interaction function is periodic, one can then expand the function in the Fourier series and use an appropriate truncation of the series for further analysis:

$$H(x) \approx a_0 + \sum_{n=1}^{M} \left(a_n \cos(nx) + b_n \sin(x)\right). \tag{3.35}$$

The software XPPAUT contains a subroutine for computing the Fourier coefficients and throughout this thesis, where an explicit interaction function is needed, it will be used to numerically compute the Fourier coefficients.

The next chapter is devoted to studying the existence and stability of the phase-locked solutions with a particular emphasis on the synchronous oscillations. We will observe that in the case of

a weakly coupled system, the phase equations provide a convenient mean of obtaining important insights into the mechanisms responsible for modulating the network rhythms.

Chapter 4

Synchronization in Neural Networks

This chapter presents the main results of this thesis on the existence and stability of the synchronized solutions. We begin by considering homogenous neural networks (i.e. networks where the intrinsic (natural) frequencies of the neurons are equal). The effect of adding small perturbations to the intrinsic frequencies will be considered after analyzing the homogenous case. The stability of the synchronous and phase-locked solutions is investigated. For the first part of this chapter, we will work with a general interaction function H, and do not assume a specific form. However, later on we will use XPPAUT [11] to compute the interaction function for the hippocampal interneurons coupled through inhibitory synapses. This specific form of the interaction function will be then used to compare the analytical results with the numerical simulations.

4.1 Homogenous Neural Networks

We begin by analyzing the phase-locked solutions of a network consisting of just two neurons. An interesting finding is that the condition for the stability of the phase-locked solutions in N-neural network is exactly the same as that for the two-neuron case.

4.2 Two Neuron System

Suppose that two neurons are mutually coupled and that θ_1 and θ_2 are their respective phases. Let Ω be the intrinsic frequency of each neuron. The equations (see equation (3.32)) describing the phase dynamics are

$$\begin{aligned} \frac{d\theta_1}{dt} &= \Omega + \epsilon H(\theta_2 - \theta_1) \\ \frac{d\theta_2}{dt} &= \Omega + \epsilon H(\theta_1 - \theta_2). \end{aligned} \tag{4.1}$$

Let $\phi_1 = \theta_1 - \theta_2$ denote the phase difference. Then the above system yields

$$\begin{aligned} \frac{d\phi_1}{dt} &= \epsilon(H(\theta_2 - \theta_1) - H(\theta_1 - \theta_2)) = \\ &\epsilon(H(-\phi_1) - H(\phi_1)) = -2\epsilon H_{odd}(\phi_1), \end{aligned} \tag{4.2}$$

where, $H_{odd}(.)$ is the odd part of the function $H(.)$.

To study phase-locking, we look for values of ϕ_1 such that, $\frac{d\phi_1}{dt} = 0$. Thus the phase-locked oscillations are characterized by the following algebraic equation

$$H_{odd}(\phi_1) = 0. \tag{4.3}$$

As an example, let H be a simple sinusoidal function:

$$H(x) = A\sin(x), \quad A > 0.$$

as is the case with the Kuramoto phase model ([25], [26]). The zeros in $[0, 2\pi)$ are 0 and π implying the existence of synchronous and anti-phase oscillations respectively. The stability can be studied by considering the sign of $-2\epsilon H'_{odd}$ at the equilibrium points. The condition for the stability is therefore

$$H_{odd}(\phi_1^*) > 0. \tag{4.4}$$

Notice that for the synchronous solution, $H'_{odd}(0) = A > 0$ and for the anti-phase solution $\phi_1^* = \pi$, $H'_{odd}(\pi) = -A < 0$, implying that the synchronous solution is stable while the anti-phase solution is unstable for this particular choice of the interaction function.
The next section considers general network of all-to-all coupled neural oscillators and establishes conditions that guarantee the stability of the synchronous and anti-phase solutions.

4.3 Network of N Neural Oscillations

Recall the biophysically detailed equation for a network consisting of N neural oscillators coupled via chemical synapses (2.40)

$$C\frac{dV_k}{dt} = I_{stim} - I_{ionic}(V_k) - \frac{g_{syn}}{N-1}(V_k - E_{syn})\sum_{\substack{j=1\\ j\neq k}}^{N} s_{jk}$$
$$\frac{ds_{jk}}{dt} = \alpha\frac{1}{1+\exp(-V_j/2)}s_{jk} - \frac{(1-s_{jk})}{\tau_{syn}}, \quad k,j = 1,\ldots,N. \tag{4.5}$$

Each cell in the population is coupled to $N-1$ other cells and therefore the coupling strength ϵ is defined by the maximum synaptical coupling conductance, g_{syn}, normalized by $N-1$ to reflect the effective interaction surface area between the two mutually coupled cells.

$$\epsilon = \frac{g_{syn}}{N-1}. \tag{4.6}$$

For the rest of this thesis, we will assume this form of the coupling strength, ϵ ([19], [36], [37]).

Consider a network consisting of N neurons where each neuron is coupled to all other neurons in the population (all-to-all coupled network). Let $\theta_1,\ldots,\theta_N$ be the phases, and Ω the intrinsic frequency. The phase equations are then given by (3.32)

$$\frac{d\theta_k}{dt} = \Omega + \epsilon\sum_{\substack{j=1\\ j\neq k}}^{N} H(\theta_j - \theta_k), \quad k = 1,\ldots,N. \tag{4.7}$$

In terms of the pairwise phase differences, $\phi_k = \theta_k - \theta_{k+1}$, the above system is transformed to

$$\frac{d\phi_k}{dt} = \epsilon\sum_{j=1}^{N}\left(H(\theta_j - \theta_k) - H(\theta_j - \theta_{k+1})\right). \tag{4.8}$$

It is also convenient for the later analysis to define a new function, f_k

$$f_k = \epsilon\sum_{j=1}^{N}\left(H(\theta_j - \theta_k) - H(\theta_j - \theta_{k+1})\right) \tag{4.9}$$

the zeros of which characterize the phase locked solutions. Taking the first cell as the reference

point and writing the phases as a function of the pairwise phase differences

$$\begin{aligned}\theta_2 &= \theta_1 - \phi_1 \\ \theta_3 &= \theta_1 - (\phi_1 + \phi_2) \\ &\vdots \\ \theta_k &= \theta_1 - \sum_{j=1}^{k-1} \phi_j \end{aligned} \tag{4.10}$$

Elements of the Jacobian matrix for (4.8) can then be calculated by the following

$$a_{kl} = \frac{\partial f_k}{\partial \phi_l}(\phi_1^*, \ldots, \phi_N^*), \quad k, l = 1, \ldots, N. \tag{4.11}$$

where $\phi_1 *, \ldots, \phi_N^*$ are the phase locked pairwise phase differences. Recall that under phase locking, all the neurons are oscillating with the same frequency and the phases are given by

$$\theta_k = \Lambda t + \beta_k, \quad k = 1, \ldots, N. \tag{4.12}$$

thus

$$a_{kl} = \epsilon \sum_{j=1}^{N} \left[H'(\beta_j - \beta_k) \left(\frac{\partial \theta_j}{\partial \phi_l} - \frac{\partial \theta_k}{\partial \phi_l} \right) - H'(\beta_j - \beta_{k+1}) \left(\frac{\partial \theta_j}{\partial \phi_l} - \frac{\partial \theta_{k+1}}{\partial \phi_l} \right) \right] \tag{4.13}$$

Based on equation (4.10)

$$\begin{aligned} \frac{d\theta_j}{d\phi_l} &= 0, \quad \text{for } j \leq l. \\ \frac{d\theta_j}{d\phi_l} &= -1, \quad \text{for } j > l. \end{aligned} \tag{4.14}$$

We therefore separate the sums for $j = 1, \ldots, l \quad$ and $j = l+1, \ldots, N$

$$\begin{aligned} a_{kl} = \epsilon \sum_{j=1}^{l} \left[H'(\beta_j - \beta_{k+1}) \frac{\partial \theta_{k+1}}{\partial \phi_l} - H'(\beta_j - \beta_k) \frac{\partial \theta_k}{\partial \phi_l} \right] + \\ \epsilon \sum_{j=l+1}^{N} \left[H'(\beta_j - \beta_{k+1})(1 + \frac{\partial \theta_{k+1}}{\partial \phi_l}) - H'(\beta_j - \beta_k)(1 + \frac{\partial \theta_k}{\partial \phi_l}) \right] \end{aligned} \tag{4.15}$$

There are three cases to consider, namely $l < k$, $l = k$ and $l > l$:

1. $l < k$
   In this case,$\frac{\partial \theta_k}{\partial \phi_l} = -1$ and $\frac{\partial \theta_{k+1}}{\partial \phi_l} = -1$, so that the equation 4.15 becomes :

$$a_{kl} = \epsilon \sum_{j=1}^{l} \left[H'(\beta_j - \beta_k) - H'(\beta_j - \beta_{k+1}) \right]. \tag{4.16}$$

2. $l = k$
   Note that, $\frac{\partial \theta_k}{\partial \phi_k} = 0$ and $\frac{\partial \theta_{k+1}}{\partial \phi_{k+1}} = -1$ thus (4.15) becomes

$$a_{kk} = -\epsilon \left(\sum_{j=1}^{k} H'(\beta_j - \beta_{k+1}) + \sum_{j=k+1}^{N} H'(\beta_j - \beta_k) \right). \tag{4.17}$$

3. $l > k$
   In this case, $\frac{\partial \theta_k}{\partial \phi_l} = 0$, and $\frac{\partial \theta_{k+1}}{\partial \phi_l} = 0$, so that

$$a_{kl} = \epsilon \sum_{j=l+1}^{N} \left[H'(\beta_j - \beta_{k+1}) - H'(\beta_j - \beta_k) \right] \tag{4.18}$$

Stability of the synchronous and anti-phases solutions can be investigated by substituting the appropriate β_k, and looking for special structures in the Jacobian matrix. In particular, sufficient conditions may be obtained using the following theorem.

Theorem 4.3.1 Geršgorin's Theorem*[27, pp. 225-226]*
If A is an $N \times N$ matrix, and

$$R_k = \sum_{\substack{j=1 \\ j \neq k}}^{N} |a_{kj}|.$$

is the sum of the off diagonal elements in the kth row, then every eigenvalue of A lies in at least one of the disks

$$|z - a_{kk}| \leq R_k, \quad k = 1, \ldots, N. \tag{4.19}$$

in the complex z plane.
Furthermore, a set of m of these disks having no point in common with the remaining $N - m$ disks contains m and only m eigenvalues of A.

Stability is guaranteed if the real part of all the eigenvalues are negative, which is satisfied if the Geršgorin disks are all located in the left half of the complex plane. Therefore, if

1. $a_{kk} < 0$.

2. $|a_{kk}| > R_k$.

Then the equilibrium solution given by the vector $\beta = (\beta_1, \ldots, \beta_N)^T$ is stable. We will study the structure of the matrix for special cases of the synchronous and anti-phases oscillations and find conditions for the stability of these solutions.

4.3.1 Stability of the synchronous and anti-phase solution

Since the function H is periodic, it can be expanded in a Fourier series

$$H(x) = \sum_{n=0}^{\infty} \left[a_n \cos(nx) + b_n \sin(nx) \right]. \tag{4.20}$$

We will use this form of the interaction function in the analysis of the stability of the synchronous and anti-phase oscillations.
Recall that for the synchronous solution, $\beta_k = 0$ for all k, which implies that the off-diagonal elements (by equations (4.16) and (4.18)) are zero and the diagonal elements are given by

$$a_{kk} = -\epsilon \left(\sum_{j=1}^{k} H'(\beta_j - \beta_k) + \sum_{j=k+1}^{N} H'(\beta_j - \beta_k) \right) \tag{4.21}$$

$$= -\epsilon \left(\sum_{j=1}^{N} H'(0) + \sum_{j=k+1}^{N} H'(0) \right) = -\epsilon N H'(0). \tag{4.22}$$

Thus the stability of the synchronous solutions are guaranteed if and only if:

$$H'(0) > 0. \tag{4.23}$$

Note that

$$H'(x) = \sum_{n=1}^{\infty} n \left[b_n \cos(nx) - a_n \sin(nx) \right], \tag{4.24}$$

therefore

$$H'(0) = \sum_{n=1}^{\infty} n b_n = H'_{odd}(0).$$

Thus we see that the condition for the stability of the synchronous solution in the N-cell network is $H'_{odd}(0) > 0$, which is exactly the same condition as the two-cell case (equation (4.4)). Stability of the synchronous solution in the homogenous network of all-to-all coupled neural oscillators, is therefore determined by the odd part of the interaction function only. For the anti-phase solutions, $\beta_k = \frac{1+(-1)^k}{2}\pi$, and the population number, N, is assumed to be even for simplifying the calculations. Note that

$$H'(-\pi) = H'(\pi).$$

The following cases should be considered.

- $l < k$

$$\begin{aligned} a_{kl} &= \epsilon \sum_{j=1}^{l} \left[H'(\beta_j - \beta_k) - H'(\beta_j - \beta_{k+1}) \right] \\ &= \epsilon \sum_{j=1}^{l} \left[H'\left(\frac{(-1)^j - (-1)^k}{2}\pi \right) - H'\left(\frac{(-1)^j + (-1)^k}{2}\pi \right) \right]. \end{aligned}$$

There are two cases for even or odd k

1. Even k:

$$\begin{aligned} a_{kl} &= \epsilon \sum_{j=1}^{l} \left[H'(\frac{(-1)^j - 1}{2}\pi) - H'(\frac{(-1)^j + 1}{1}\pi) \right] \\ &= \epsilon n_{odd} \left(H'(-\pi) - H'(0) \right) + \epsilon n_{even} \left(H'(0) - H'(\pi) \right) \\ &= \epsilon (n_{odd} - n_{even}) H'(\pi) + \epsilon (n_{even} - n_{odd}) H'(0) \\ &= \epsilon (n_{even} - n_{odd}) (H'(0) - H'(\pi)). \end{aligned}$$

Where $n_{even} = \lfloor \frac{l}{2} \rfloor$ and $n_{odd} = \lceil \frac{l}{2} \rceil$ are the number of even and odd integers from

$j = 1$ to $j = l$.

- For odd l:

$$n_{even} - n_{odd} = -1,$$

therefore

$$a_{kl} = -\epsilon(H'(0) - H'(\pi)).$$

- For even l

$$n_{even} - n_{odd} = 0,$$

Which implies that

$$a_{kl} = 0.$$

2. Odd k:

$$\begin{aligned} a_{kl} &= \epsilon \sum_{j=1}^{l} \left[H'(\frac{(-1)^j + 1}{2}\pi) - H'(\frac{(-1)^j - 1}{2}\pi) \right] \\ &= \epsilon n_{odd} \left[H'(0) - H'(-\pi) \right] + \epsilon n_{even} \left[H'(\pi) - H'(0) \right] \\ &= -\epsilon(n_{even} - n_{odd})(H'(0) - H'(\pi)). \end{aligned}$$

Thus we have

- For odd l:

$$a_{kl} = \epsilon \left(H'(0) - H'(\pi) \right).$$

- For even l:

$$a_{kl} = 0.$$

- $l > k$

$$a_{kl} = \epsilon \sum_{j=l+1}^{N} \left[H'(\beta_j - \beta_{k+1}) - H'(\beta_j - \beta_k) \right],$$

$$
\begin{aligned}
a_{kl} &= \epsilon \sum_{j=l+1}^{N} \left[H'\left(\frac{(-1)^j + (-1)^k}{2}\pi \right) - H'(\frac{(-1)^j - (-1)^k}{2}\pi) \right] \\
&= \epsilon n_{odd} \left[H'\left(\frac{-1 + (-1)^k}{2}\pi \right) - H'(\frac{-1 - (-1)^k}{2}\pi) \right] + \\
&\epsilon n_{even} \left[H'(\frac{1 + (-1)^k}{2}\pi) - H'(\frac{1 - (-1)^k}{2}\pi) \right].
\end{aligned}
$$

The two cases are:

1. Even k:

$$
\begin{aligned}
a_{kl} &= \epsilon n_{odd} \left[H'(0) - H'(\pi) \right] + \epsilon n_{even} \left[H'(\pi) - H'(0) \right] \\
&= \epsilon (n_{odd} - n_{even}) \left(H'(0) - H'(\pi) \right),
\end{aligned}
$$

   Simplifying as in the previous case

   - For odd l:

$$
a_{kl} = -\epsilon \left(H'(0) - H'(\pi) \right).
$$

   - For even l:

$$
a_{kl} = 0.
$$

2. Odd k:

$$
\begin{aligned}
a_{kl} &= \epsilon n_{odd} \left(H'(-\pi) - H'(0) \right) + \epsilon n_{even} \left(H'(0) - H'(\pi) \right) \\
&= \epsilon (n_{even} - n_{odd}) \left(H'(0) - H'(\pi) \right).
\end{aligned}
$$

   - For odd l:

$$
a_{kl} = \epsilon \left(H'(0) - H'(\pi) \right).
$$

   - For even l:

$$a_{kl} = 0.$$

Thus in general for any $k \neq l$ we have

$$|a_{kl}| = \begin{cases} \epsilon|H'(0) - H'(\pi)| & \text{If } l \text{ is odd} \\ 0 & \text{If } l \text{ is even.} \end{cases} \tag{4.25}$$

This will be used later when we apply Geršgorin's theorem to establish sufficient conditions for stability.

- $l = k$

  There are two cases as before:

  1. Even k:

$$a_{kk} = -\epsilon \left(\sum_{j=1}^{k} H'(\beta_j - \beta_{k+1}) + \sum_{j=k+1}^{N} H'(\beta_j - \beta_k)) \right).$$

Now

$$\begin{aligned} \sum_{j=1}^{k} H'(\beta_j - \beta_{k+1}) &= \sum_{j=1}^{k} H'(\frac{(-1)^j + 1}{2}\pi) \\ &= \frac{k}{2}H'(0) + \frac{k}{2}H'(\pi). \end{aligned}$$

Further

$$\begin{aligned} \sum_{j=k+1}^{N} H'(\beta_j - \beta_k) &= \sum_{j=k+1}^{N} H'(\frac{(-1)^j - 1}{2}\pi) \\ &= \frac{N-k}{2}H'(0) + \frac{N-k}{2}H'(\pi), \end{aligned}$$

Therefore

$$a_{kk} = -\epsilon \frac{N}{2} \left(H'(0) + H'(\pi) \right).$$

2. Odd k:

$$\begin{aligned}
&\sum_{j=1}^{k} H'(\beta_j - \beta_{k+1}) \\
&\qquad = \sum_{j=1}^{k} H'(\frac{(-1)^j - 1}{2}\pi) \\
&\qquad = \frac{k+1}{2} H'(\pi) + \frac{k-1}{2} H'(0).
\end{aligned}$$

$$\begin{aligned}
\sum_{j=k+1}^{N} H'(\beta_j - \beta_k) &= \sum_{j=k+1}^{N} H' \left(\frac{(-1)^j - (-1^k)}{2}\pi \right) \\
&= \sum_{j=k+1}^{N} H' \left(\frac{(-1)^j + 1}{2}\pi \right) \\
&= \left(\frac{N}{2} - 1 \right) H'(0) + \left(\frac{N}{2} + 1 \right) H'(\pi).
\end{aligned}$$

$$a_{kk} = -\epsilon \left[\frac{N}{2} (H'(0) + H'(\pi)) + H'(\pi) - H'(0) \right].$$

and

$$|a_{kk}| = \begin{cases} \epsilon \frac{N}{2} |H'(0) + H'(\pi)| & \text{for even } k \\ \epsilon | \frac{N}{2} (H'(0) + H'(\pi)) + H'(\pi) - H'(0)| & \text{for odd } k. \end{cases} \tag{4.26}$$

Recall that according to the Geršgorin's Theorem, a condition for having all eigenvalues with negative real parts is $a_{kk} < 0$ and $|a_{kk}| > R_k$ for all k. According to the elements of the Jacobian matrix, if $H'(0) > 0$ and $H'(\pi) > 0$ then $a_{kk} < 0$ and we will show that this implies that the other inequality is automatically satisfied. There are two separate cases for even and odd row numbers which are going to be considered.

- Even k:

If $H'(0) > 0$ and $H'(\pi) > 0$,

$$\begin{aligned}
|a_{kk}| &= \epsilon\frac{N}{2}|H'(0) + H'(\pi)| > \epsilon\frac{N}{2}|H'(0) - H'(\pi)| \\
R_k &= \sum_{\substack{l=1 \\ l\neq k}}^{N-1} |a_{kl}| \\
&= n_{odd}\epsilon|H'(0) - H'(\pi)| + n_{even}(0) \\
&= \epsilon\frac{N}{2}|H'(0) - H'(\pi)|.
\end{aligned}$$

therefore

$$|a_{kk}| > R_k.$$

- Odd k:

$$\begin{aligned}
|a_{kk}| &= \epsilon|\frac{N}{2}(H'(0) + H'(\pi)) + H'(\pi) - H'(0)| \\
&= \epsilon|\left(\frac{N}{2} - 1\right)H'(0) + \left(\frac{N}{2} + 1\right)H'(\pi)| \\
&> |\left(\frac{N}{2} - 1\right)H'(0) + \left(\frac{N}{2} - 1\right)H'(\pi)| \quad \text{if } H'(\pi) > 0 \\
&> \left(\frac{N}{2} - 1\right)|H'(0) - H'(\pi)|.
\end{aligned}$$

and

$$\begin{aligned}
R_k &= \sum_{\substack{l=1 \\ l\neq k}}^{N-1} |a_{kl}| \\
&= n_{odd}\epsilon|H'(0) - H'(\pi)| = \left(\frac{N}{2} - 1\right)|H'(0) - H'(\pi)|.
\end{aligned}$$

therefore

$$|a_{kk}| > R_k \quad \text{if } H'(0) > 0 \text{ and } H'(\pi) > 0.$$

Thus if $H'(0) = H'_{odd}(0) > 0$ and $H'(\pi) = H'_{odd}(\pi) > 0$, then the anti-phase solutions are stable. This condition implies that bi-stability between the synchronous and anti-phase oscillations in the two-cell network which is guaranteed by the conditions $H'_{odd}(0) > 0$ and $H'_{odd}(\pi) > 0$, is preserved in the N-cell network.

The stability results for the synchronous and anti-phase oscillations are summarized as follows

- In an N-cell network the synchronous solution is stable if and only if $H'_{odd}(0) > 0$.
- Additionally, suppose that number of the cells N is even and π is a phase-locked solution to the two-cell network. If $H'_{odd}(\pi) > 0$, then the anti-phase solution is also stable which implies bi-stability between the two solutions and network can switch from one solution to another by appropriate change of a biophysically relevant parameter. The nature of this parameter will be made clear in later sections when we use the hippocampal interneuron model to compute the relevant form of the interaction functions.

4.3.2 Change in the network frequency for synchronous and anti-phase scenarios

The network frequency can be calculated as described below, it will in general be different from the intrinsic frequencies of the uncoupled neurons. Substituting the phase-locked solution, $\theta_k = \Lambda t + \beta_k$, into the phase equation of the kth neuron yields

$$\frac{d\theta_k}{dt} = \Omega + \sum_{j=1}^{N} H(\theta_j - \theta_k) - \epsilon H(0)$$
$$\Lambda = \Omega + \epsilon \sum_{j=1}^{N} H(\beta_j - \beta_k) - \epsilon H(0).$$

Thus, for the synchronized oscillations

$$\Lambda = \Omega + \epsilon(N-1)H(0) = \Omega + g_{syn}H(0). \tag{4.27}$$

where we have used $\epsilon = \frac{g_{syn}}{N-1}$.
Similarly, for the anti-phase oscillations:

$$\begin{aligned}\Lambda &= \Omega + \epsilon \sum_{j=1}^{N} H\left(\frac{(-1)^j - (-1)^k}{2}\pi\right) - \epsilon H(0) \\ &= \Omega + \epsilon\left(\frac{N}{2}H\left(\frac{-1-(-1)^k}{2}\pi\right) + \frac{N}{2}H\left(\frac{1-(-1)^k}{2}\pi\right)\right) - \epsilon H(0).\end{aligned}$$

There are two cases, even and odd k, corresponding to the two population clusters:

- Even k:

$$\Lambda = \Omega + \epsilon\frac{N}{2}\left(H(0) + H(\pi)\right) = \Omega + \frac{g_{syn}}{2}\frac{N}{N-1}\left(H(0) + H(\pi)\right).$$

- Odd k:

$$\Lambda = \Omega + \frac{g_{syn}}{2}\frac{N}{N-1}\left(H(0) + H(\pi)\right).$$

As expected, both population clusters are oscillating with the same frequency:

$$\Lambda = \Omega + \frac{g_{syn}}{2}\frac{N}{N-1}\left(H(0) + H(\pi)\right). \tag{4.28}$$

Note that for an odd interaction function, the network frequency will be the same as the intrinsic frequency (Because $H_{odd}(0) = H_{odd}(\pi) = 0$ when H is odd).

4.3.3 Concluding remarks and summary

The above calculations imply that if $H'_{odd}(0) > 0$ and $H'_{odd}(\pi) > 0$, then by changing an appropriate parameter (for instance the synaptic decay time constant, τ_{syn}) the network can spontaneously break into two population clusters each fully synchronized. Several authors have observed this phenomena through numerical and analytical studies. In particular, Okuda [30] found analytically that the eigenvalues determining the stability of the anti-phase solutions are given by

$$\lambda_1 = -\frac{g_{syn}}{2}(H'_{odd}(0) + H'_{odd}(\pi)) \quad (N-2) \text{ multiplicity}$$
$$\lambda_2 = -g_{syn}H'_{odd}(\pi).$$

Where λ_1 determines the stability of the phase difference between neurons within each cluster (intra-cluster phase differences), while λ_2 determines the stability of the phase differences between the clusters (inter-cluster phase differences). Thus, the anti-phase solution is stable if and only if

$$H'_{odd}(0) + H'_{odd}(\pi) > 0$$
$$H'_{odd}(\pi) > 0. \tag{4.29}$$

These conditions are more general and encompass our results obtained by applying the Geršgorin's theorem. In another study, Golomb and Rinzel [14] considered (numerically and analytically) a large network of inhibitory neurons and observed that the network converged into stable synchrony. Additionally, the network could spontaneously break into smaller population clusters each fully synchronized. In a more general study, Li [28] obtained conditions for stability and existence of the population clusters in network with oscillators coupled via asymmetrical and heterogeneous interaction functions (asymmetrical coupling implies that the coupling function for interaction of say, cell i and cell j is not the same as that of cell j to cell i and heterogenous interaction function implies that that form of the coupling function is not uniform in the network).

4.4 Heterogeneous networks

In this thesis, heterogenous networks are characterized by differences in the intrinsic frequencies of neurons (The stimulus (input) current to each neuron determines its intrinsic frequency) in the population. In a heterogeneous network the symmetry is broken and it is impossible to achieve complete synchrony (characterized by zero pairwise phase differences between neurons). In this case one considers near-synchrony which is characterized by different but still sufficiently small pairwise phase differences. A heterogeneous network can tolerate a specific degree of heterogeneity above which the near-synchronous solution is lost. Numerical Bifurcation analysis taking an appropriate parameter to represent heterogeneity (the applied currents to each neuron), can be used to establish this critical value for neural networks consisting of small number of neurons. In particular, it is found that, the near-synchronous solution is lost via a saddle-node bifurcation ([36], [37]). Although bifurcation analysis is not feasible for large networks, some authors (by performing large number of computer simulations starting from different initial conditions)

have described the lose of near-synchrony in sufficiently heterogeneous large neural networks (see [36], [43], [45], [41]) and linked the results from the two-cell to the N-cell network ([37], [36]) by observing that the pattern for the loss of the synchronous oscillations are retained for larger networks. They have also shown numerically that bi-stability between the synchronous and anti-phase oscillations is preserved in the larger size networks.

In the first part of this section, our goal will be to estimate the maximum value of the heterogeneity above which phase-locked solutions do not exist. Two different approaches are developed to be compared with the numerically obtained values for two,three and four cells. First, a special phase-locked pattern is assumed and maximum heterogeneity is calculated for this special case. Second, a network of N neurons is divided into two clusters with populations N_1 and $N_2 = N - N_1$, oscillating with frequencies Ω_1 and Ω_2, respectively. Assuming that the main interaction is between the two clusters, the maximum frequency difference $\max|\Omega_1 - \Omega_2|$ is calculated as for the two-cell network. Predictions are compared with the numerical simulations. In the last part of this section, linear expansion of the interaction function around the homogenous synchronous solution is carried out to estimate the perturbation of the phases as a result of the added heterogeneity in the network. Further, an expression for the network frequency is derived and a good correlation is shown to exist between the analytical results and numerical simulations.

4.4.1 Existence and stability of the phase-locked solutions in heterogeneous networks

In this section we cite a theorem from literature that establishes the existence and stability of phase-locked solutions in a heterogeneous network given that solutions exist for the homogenous case.
We will study perturbation of the homogenous synchronous oscillations as a result of the heterogeneity and this theorem guarantees that as long as the homogenous solutions are stable, the corresponding perturbed solutions will be stable.
Recall the phase equations for a network of oscillators

$$\frac{d\theta_k}{dt} = \Omega_j(\lambda) + \epsilon \sum_{j=1}^{N} H(\theta_j - \theta_k) - \epsilon H(0), \quad k = 1, \ldots, N.$$

where Ω_j is a continuous and differentiable function with respect to the parameter λ. For phase-locked solutions, $\frac{d\theta_k}{dt} = \Lambda$, where Λ is the constant network frequency. Thus

$$\Lambda = \Omega_j(\lambda) + \epsilon \sum_{j=1}^{N} H(\theta_j - \theta_k) - \epsilon H(0), \quad k = 1, \ldots, N. \tag{4.30}$$

The parameter λ describes the heterogeneity in the intrinsic frequencies, and $\lambda = 0$ characterizes the homogenous case when all the natural frequencies are equal.

Theorem 4.4.1 *[10] (*Existence and stability of the phase-locked solutions in a heterogenous network*)*
Suppose that (4.30) has a solution θ_k^0 for $\lambda = 0$ and suppose that $a_{jk} = H'(\theta_j^0 - \theta_k^0) \geq 0$. Then, there is a unique branch of solutions containing θ_k^0 for all $\lambda \in (0, \tilde{\lambda})$. Additionally, this solution is asymptotically stable.

The next section begins our study of the heterogenous networks by re-visiting the two-cell network and evaluating the insights obtained by the phase model.

4.4.2 Re-visiting the two-cell network

Recall the equations that govern the phase dynamics of the two-cell network

$$\begin{aligned} \frac{d\theta_1}{dt} &= \Omega_1 + \epsilon H(\theta_2 - \theta_1) \\ \frac{d\theta_2}{dt} &= \Omega_2 + \epsilon H(\theta_1 - \theta_2). \end{aligned}$$

This, the equation for the phase-difference $\phi = \theta_1 - \theta_2$, is

$$\frac{d\phi}{dt} = \Lambda_1 + \epsilon(H(-\phi) - H(\phi)) = \Lambda_1 - 2\epsilon H_{odd}(\phi). \tag{4.31}$$

The heterogeneity is characterized by $\Lambda_1 = \Omega_1 - \Omega_2$ and recall that (4.31) will be valid as long as $\Lambda_1 = O(\epsilon)$ and ϵ sufficiently small. The phase-locked solutions will be roots of

$$\Lambda_1 - 2\epsilon H_{odd}(\phi) = 0. \tag{4.32}$$

Figure 4.1 shows the graph of $2\epsilon H_{odd}(\phi)$ where, $2\epsilon H(x) = 0.25\sin(x)$. Notice that there are two solutions and there is a critical value of the heterogeneity above which there are no intersections and thus no phase-locked solutions. Additionally, if the frequency difference is considered as

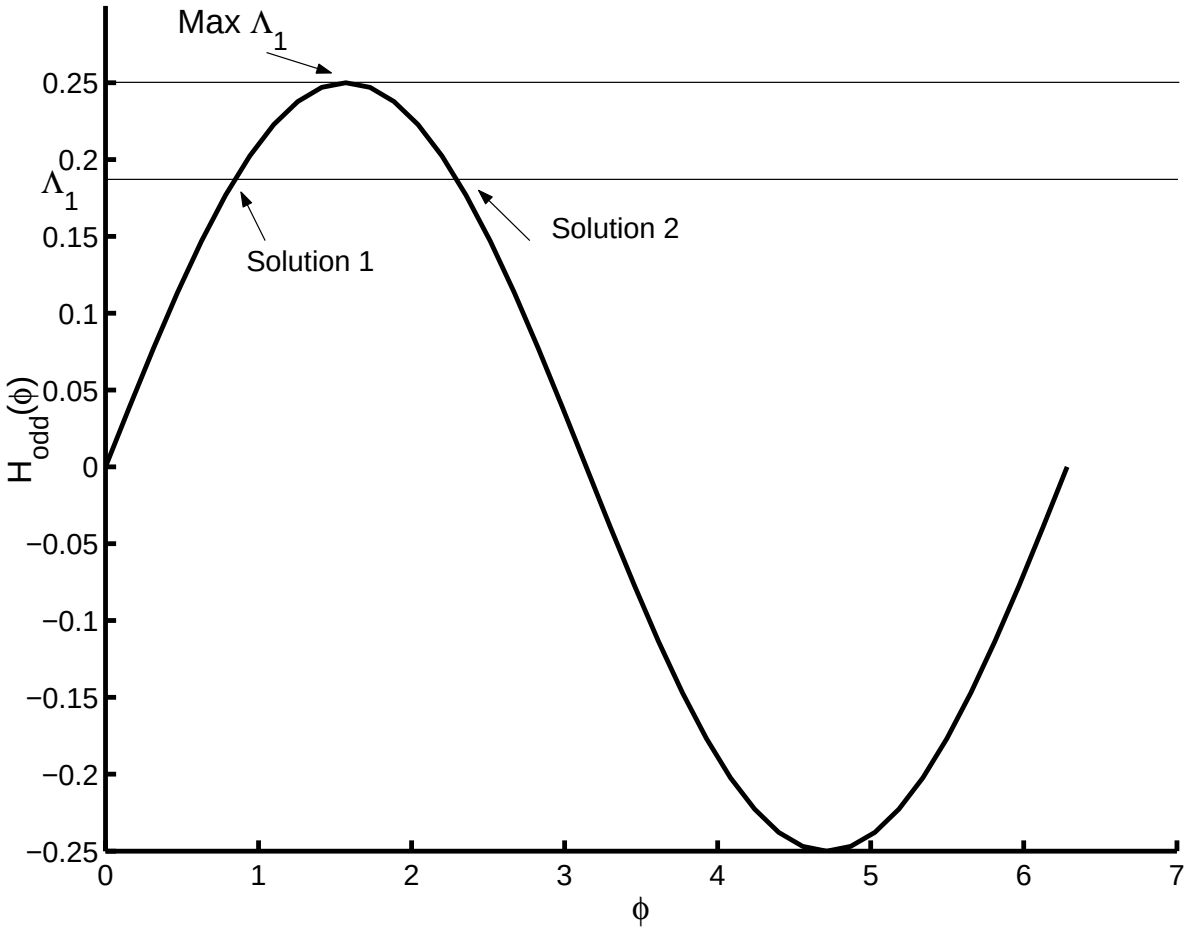

Figure 4.1: Phase-locked solutions of the two-cell network with a sinusoidal interaction function.

the bifurcation parameter, the phase-locked solutions are lost via saddle-node bifurcation as Λ_1 increases through the maximum value. This fact is confirmed later for the hippocampal neural model by numerical continuation using XPPAUT [11]. Below the critical level of the heterogeneity (shown in the figure), the solution closest to zero is stable because $H'_{odd}(.) > 0$ and while the other solution is unstable. This confirms Theorem (4.4.1) presented earlier for the existence and stability of the phase-locked solutions in the heterogeneous case. Our goal is to estimate the maximum value of the heterogeneity for the N-cell network under special simplifying hypothesis and test the estimations by numerical bifurcation analysis.

4.4.3 Calculation of the upper bound for equally separated phases:First approach

Consider the phase model for the N-cell network

$$\frac{d\theta_k}{dt} = \Omega_k + \epsilon \sum_{j=1}^{N} H(\theta_j - \theta_k) - \epsilon H(0), \quad k = 1, \ldots, N.$$

and in terms of the pairwise phase differences

$$\frac{d\phi_k}{dt} = \Gamma_k + \epsilon \sum_{j=1}^{N} \left(H(\theta_j - \theta_k) - H(\theta_j - \theta_{k+1}) \right), \quad k = 1, \ldots, N-1.$$

$\Gamma_k = \Omega_k - \Omega_{k+1}$ indicates the heterogeneity in the network. For the phase-locked solutions we require

$$\Gamma_k = \epsilon \sum_{j=1}^{N} \left(H(\theta_j - \theta_{k+1}) - H(\theta_j - \theta_k) \right), \quad k = 1, \ldots, N-1. \tag{4.33}$$

Summing both sides of (4.33) yields

$$\begin{aligned} \sum_{k=1}^{N-1} \Gamma_k &= \sum_{k=1}^{N-1} (\Omega_k - \Omega_{k+1}) = \Omega_1 - \Omega_N \\ &= \epsilon \sum_{j=1}^{N} \sum_{k=1}^{N-1} \left(H(\theta_j - \theta_{k+1}) - H(\theta_j - \theta_k) \right) \\ &= \epsilon \sum_{j=1}^{N} \left(H(\theta_j - \theta_N) - H(\theta_j - \theta_1) \right). \end{aligned} \tag{4.34}$$

We next assume a specific phase-locking where the phases are equally separated and distributed between 0 and 2π. In this situation the phases are characterized by the following

$$\theta_k = \Lambda t + (k-1)\zeta, \quad k = 1, \ldots, N, \quad 0 \leq \zeta \leq \frac{2\pi}{N}.$$

and

$$\beta_k = (k-1)\zeta, \quad k = 1, \ldots, N.$$

Thus the pairwise phase difference is fixed at

$$\phi_k = \beta_k - \beta_{k+1} = -\zeta, \quad k = 1, \ldots, N. \tag{4.35}$$

Substituting this into the equation (4.34) gives

$$\begin{aligned}\frac{\Omega_1 - \Omega_N}{\epsilon} &= \sum_{j=1}^{N} \left(H\left(\beta_j - \beta_N\right) - H\left(\beta_j\right)\right) \\ &= \sum_{j=1}^{N} H\left(\zeta(j-N)\right) - H\left(\zeta j - \zeta\right).\end{aligned}$$

Using the truncated Fourier expansion for $H(.)$, this becomes

$$\begin{aligned}\frac{\Omega_1 - \Omega_N}{\epsilon} &= \sum_{j=1}^{N} \left(H(\zeta(j-N) - H(\zeta j - \zeta))\right) \\ &= \sum_{j=1}^{N}\sum_{n=1}^{M} a_n(\cos(n\zeta(j-N)) - \cos(nj\zeta - n\zeta)) + b_n(\sin(n\zeta(j-N)) - \sin(n\zeta j - n\zeta)) \\ &= \sum_{n=1}^{M}\sum_{j=1}^{N} a_n(\cos(n\zeta(j-N)) - \cos(nj\zeta - n\zeta)) + b_n(\sin(n\zeta(j-N)) - \sin(n\zeta j - n\zeta)) \\ &= \sum_{n=1}^{M} \left[a_n \cos(n\zeta N) - b_n \sin(n\zeta N) - a_n \cos(n\zeta) + b_n \sin(n\zeta)\right] \sum_{j=1}^{N} \cos(n\zeta j) \\ &+ \sum_{n=1}^{M} \left[a_n \sin(n\zeta N) + b_n \cos(n\zeta N) - a_n \sin(n\zeta) - b_n \cos(n\zeta)\right] \sum_{j=1}^{N} \sin(n\zeta j).\end{aligned}$$

where we have used the following identities for simplifying the expressions

$$\begin{aligned}\cos(A \pm B) &= \cos(A)\cos(B) \mp \sin(A)\sin(B) \\ \sin(A \pm B) &= \sin(A)\cos(B) \pm \sin(B)\cos(A).\end{aligned}$$

We need to evaluate sums of the form $\sum_{j=1}^{N} \cos(n\zeta j)$ and $\sum_{j=1}^{N} \sin(n\zeta j)$. Notice that

$$\exp(inj\zeta) = \cos(nj\zeta) + i\sin(nj\zeta),$$

and

$$\begin{aligned}\sum_{j=1}^{N} \exp(inj\zeta) &= \sum_{j=1}^{N} (\exp(in\zeta))^j \\ &= \sum_{j=1}^{N} \cos(nj\zeta) + i\sum_{j=1}^{N} \sin(nj\zeta),\end{aligned}$$

Therefore

$$Re\left(\sum_{j=1}^{N} (\exp(in\zeta))^j\right) = \sum_{j=1}^{N} \cos(nj\zeta) \tag{4.36}$$

$$Im\left(\sum_{j=1}^{N} (\exp(in\zeta))^j\right) = \sum_{j=1}^{N} \sin(nj\zeta). \tag{4.37}$$

Notice that the sums in the left hand side are geometric and can be evaluated easily using the formula

$$\sum_{j=1}^{N} r^j = r\frac{r^N - 1}{r - 1}, \tag{4.38}$$

which implies that

$$\sum_{j=1}^{N} (\exp(in\zeta))^j = \exp(in\zeta)\frac{\exp(inN\zeta) - 1}{\exp(in\zeta) - 1}. \tag{4.39}$$

So the sums of interest can be easily evaluated from (4.36)

$$\sum_{j=1}^{N} \cos(jn\zeta)$$
$$= \mathrm{Re}\left(\exp(in\zeta)\frac{\exp(inN\zeta)-1}{\exp(in\zeta)-1}\right)$$
$$= \frac{\cos(nN\zeta)-\cos(n\zeta(N+1))+\cos(n\zeta)-1}{2(1-\cos(n\zeta))}.$$

and similarly

$$\sum_{j=1}^{N} \sin(jn\zeta)$$
$$= \mathrm{Im}\left(\exp(in\zeta)\frac{\exp(inN\zeta)-1}{\exp(in\zeta)-1}\right) \tag{4.40}$$
$$= \frac{\sin(nN\zeta)-\sin(n\zeta(1+N))+\sin(n\zeta)}{2(1-\cos(n\zeta))}.$$

Define a new function $U_N(\zeta), \quad 0 \le \zeta \le \frac{2\pi}{N}$ as follows

$$\frac{\Omega_1-\Omega_N}{\epsilon} = U_N(\zeta)$$
$$= \sum_{n=1}^{M} R_N \frac{\cos(nN\zeta)-\cos(n(1+N)\zeta)+\cos(n\zeta)-1}{2(1-\cos(n\zeta))}$$
$$+ \sum_{n=1}^{M} L_N \frac{\sin(nN\zeta)-\sin(n(1+N)\zeta)+\sin(n\zeta)}{2(1-\cos(n\zeta))}. \tag{4.41}$$

where

$$R_N = a_n\cos(nN\zeta) - b_n\sin(nN\zeta) - a_n\cos(n\zeta) + b_n\sin(n\zeta)$$
$$L_N = a_n\sin(nN\zeta) + b_n\cos(nN\zeta) - a_n\sin(n\zeta) - b_n\cos(n\zeta),$$

as this is a simpler formula to work with. There will be no phase-locked solutions if the following condition for the pairwise frequency differences is satisfied

$$|\Omega_1 - \Omega_N| > \frac{g_{syn}}{N-1}\text{Max}|U_N(\zeta)|. \tag{4.42}$$

Recall that the coupling strength is $\epsilon = \frac{g_{syn}}{N-1}$. Figure 4.2 shows an example of the plot of $\frac{|U_N(\zeta)|}{N-1}$ for $M = 1, a_1 = b_1 = 1$ and four different population numbers ($N = 10, 100, 1000, 10000$). Notice that for sufficiently large N, the maximum value is independent of N and approaches 1.5. Thus there will be no phase-locked solutions if the pairwise intrinsic frequency difference is greater than $1.5g_{syn}$. Values of the Fourier coefficients a_n and b_n will be determined more precisely for the hippocampal interneurons in the next section.

4.4.4 Estimating the upper bound on the natural frequencies: Second approach

Consider an initially synchronous neural network. Distribute the applied currents such that N_1 of the neurons have natural frequency Ω_1, while the other $N_2 = N - N_1$ neurons have frequency Ω_2. The units for the neural frequencies are in ms^{-1} or kHz throughout. Assume that neurons in each cluster are in synchrony and that the difference between the two natural frequencies, $\Omega_2 - \Omega_1$, is small enough such that the whole network is near-synchronous. Our aim is to find the maximum value of $\Omega_2 - \Omega_1$ below which the stability of the near-synchronous oscillations is retained and compare the results with the maximum heterogeneity obtained by numerical bifurcation analysis. If the interactions inside a cluster are assumed to be negligible, the problem will be shown to be equivalent to a two-neuron system.

Let $\theta_1, \ldots, \theta_{N_1}$, be the phases of the neurons oscillating with intrinsic frequency Ω_1, and $\theta_{N_1+1}, \ldots, \theta_N$, be the phases for the neurons oscillating with frequency Ω_2. The phase equations are then given by

$$\frac{d\theta_k}{dt} = \Omega_1 + \epsilon \sum_{j=1}^{N} H(\theta_j - \theta_k) - \epsilon H(0), \quad k = 1, \ldots, N_1. \tag{4.43}$$

$$\frac{d\theta_k}{dt} = \Omega_2 + \epsilon \sum_{j=1}^{N} H(\theta_j - \theta_k) - \epsilon H(0), \quad k = N_1 + 1, \ldots, N. \tag{4.44}$$

Since the phases in each population are constant, the sums simplify as follows. Let $\tilde{\theta_1}$ and $\tilde{\theta_2}$ describe the phases in populations 1 and 2, respectively. So the equations become

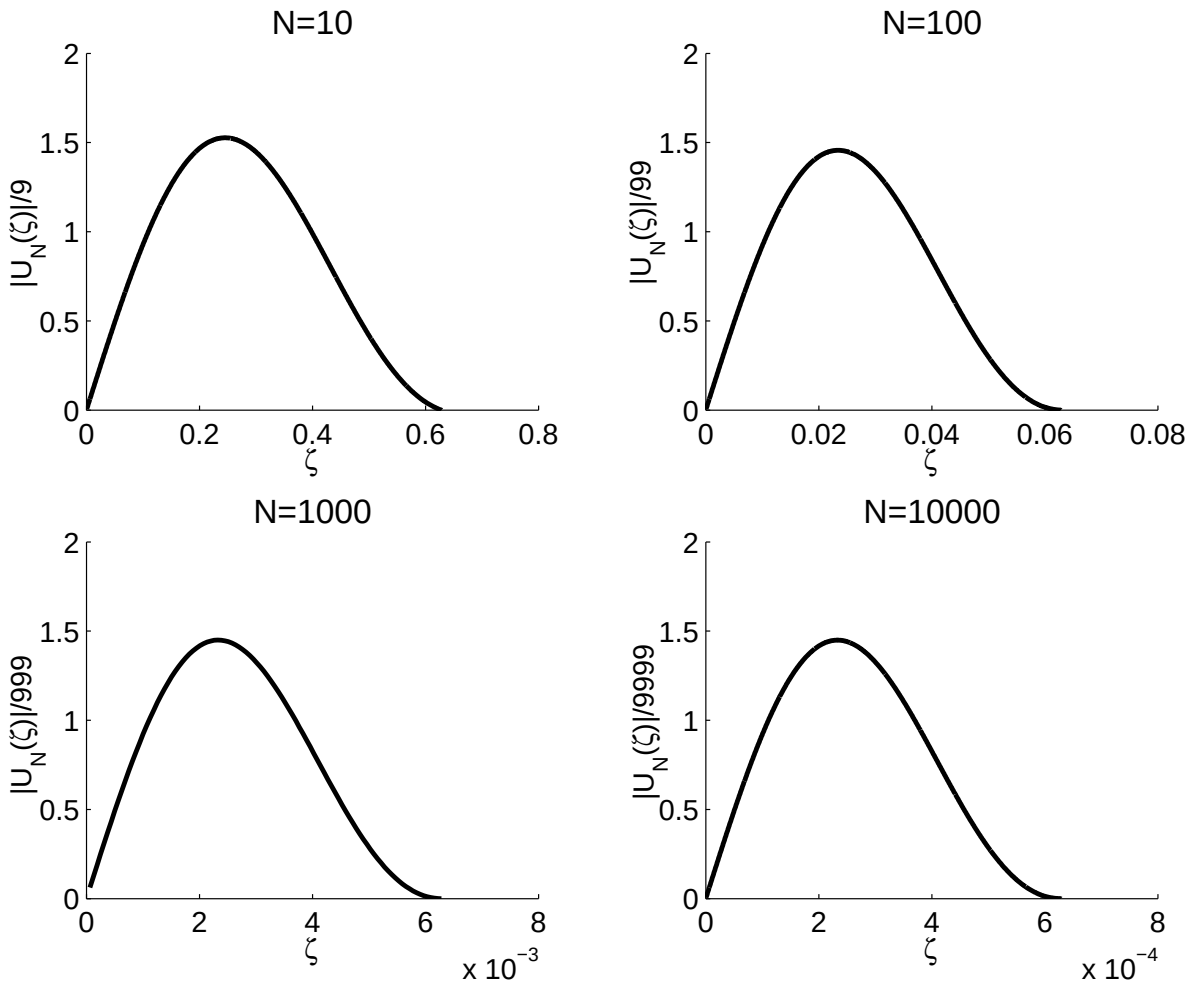

Figure 4.2: Plot of the function $\frac{|U_N(\zeta)|}{N-1}$.

$$\begin{aligned}\frac{d\theta_k}{dt} &= \Omega_1 + \epsilon \sum_{j=1}^{N} H(\theta_j - \theta_k) - \epsilon H(0) \\ &= \Omega_1 + \epsilon \sum_{j=1}^{N_1} H(\theta_j - \theta_k) + \epsilon \sum_{j=N_1+1}^{N} H(\theta_j - \theta_k) - \epsilon H(0) \\ &= \Omega_1 + \epsilon N_1 H(0) + \epsilon N_2 H(\tilde{\theta_2} - \tilde{\theta_1}) - \epsilon H(0), \quad k = 1, \ldots, N_1.\end{aligned}$$

$$\begin{aligned}\frac{d\theta_{k'}}{dt} &= \Omega_2 + \epsilon \sum_{j=1}^{N} H(\theta_j - \theta_{k'}) - \epsilon H(0) \\ &= \Omega_2 + \epsilon \sum_{j=1}^{N_1} H(\theta_j - \theta_{k'}) + \epsilon \sum_{j=N_1+1}^{N} H(\theta_j - \theta_{k'}) - \epsilon H(0) \\ &= \Omega_2 + \epsilon N_1 H(\tilde{\theta_1} - \tilde{\theta_2}) + \epsilon N_2 H(0) - \epsilon H(0), \quad k' = N_1 + 1, \ldots, N_2.\end{aligned}$$

Thus the final equations for the cluster phases, $\tilde{\theta_1}$ and $\tilde{\theta_2}$, become

$$\frac{d\tilde{\theta_1}}{dt} = \Omega_1 + \epsilon N_1 H(0) + \epsilon N_2 H(\tilde{\theta_2} - \tilde{\theta_1}) - \epsilon H(0) \tag{4.45}$$

$$\frac{d\tilde{\theta_2}}{dt} = \Omega_2 + \epsilon N_2 H(0) + \epsilon N_1 H(\tilde{\theta_1} - \tilde{\theta_2}) - \epsilon H(0). \tag{4.46}$$

Let $\phi = \tilde{\theta_1} - \tilde{\theta_2}$, then

$$\frac{d\phi}{dt} = \Omega_1 - \Omega_2 + \epsilon(N_1 - N_2)H(0) + \epsilon N_2 H(-\phi) - \epsilon N_1 H(\phi). \tag{4.47}$$

The phase-locked solution are given by roots of the following equation

$$\frac{\Omega_1 - \Omega_2}{\epsilon} = N_1 H(\phi) - N_2 H(-\phi) - (N_1 - N_2)H(0). \tag{4.48}$$

Define the function $f(\phi)$ as the right hand side of (4.48)

$$f(\phi) = N_1 H(\phi) - N_2 H(-\phi) - (N_1 - N_2)H(0). \tag{4.49}$$

Recall the truncated Fourier series expansion of the interaction function

$$H(\phi) = a_0 + \sum_{n=1}^{M} [a_n \cos(n\phi) + b_n \sin(n\phi)]$$
$$H(-\phi) = a_0 + \sum_{n=1}^{M} [a_n \cos(n\phi) - b_n \sin(n\phi)],$$

and

$$\begin{aligned} f(\phi) &= N_1 H(\phi) - N_2 H(-\phi) - (N_1 - N_2) H(0) \\ &= N_1 a_0 + \sum_{n=1}^{M} [N_1 a_n \cos(n\phi) + N_1 b_n \sin(n\phi)] \\ &\quad - N_2 a_0 - \sum_{n=1}^{M} [N_2 a_n \cos(n\phi) + N_2 b_n \sin(n\phi)] \\ &\quad - (N_1 - N_2) a_0 - (N_1 - N_2) \sum_{n=1}^{M} a_n \\ &= (N_2 - N_1) \sum_{n=1}^{M} a_n (1 - \cos(n\phi)) + (N_1 + N_2) \sum_{n=1}^{M} b_n \sin(n\phi). \end{aligned}$$

Thus, after using the identity $1 - \cos(x) = 2\sin\left(\frac{x}{2}\right)^2$, the final expression becomes

$$f(\phi) = 2(N_2 - N_1) \sum_{n=1}^{M} a_n \sin\left(\frac{n\phi}{2}\right)^2 + (N_1 + N_2) H_{odd}(\phi). \tag{4.50}$$

As for the two-cell scenario, $f(\phi)$ is plotted and the phase-locked solutions are the intersections of this curve with the line $y = \Omega_1 - \Omega_2$ (the solutions can also be obtained by using other softwares with capabilities to solve non-linear algebraic equations). Saddle-node bifurcation occurs at the intersection point where the slope of the line is zero. Figure 4.3 presents the method for a specific choice of the function, $\epsilon H(\phi) = 0.25\sin(\phi) + 0.05\cos(\phi)$ and population numbers, $N_1 = 10$, and $N_2 = 15$.

So far we have worked with the general form of the interaction function. In the next section, we compute the specific form of the interaction functions for the hippocampal interneurons model. We will see that the shape of the function is modulated by the synaptic decay time constant, τ_{syn} (ms).

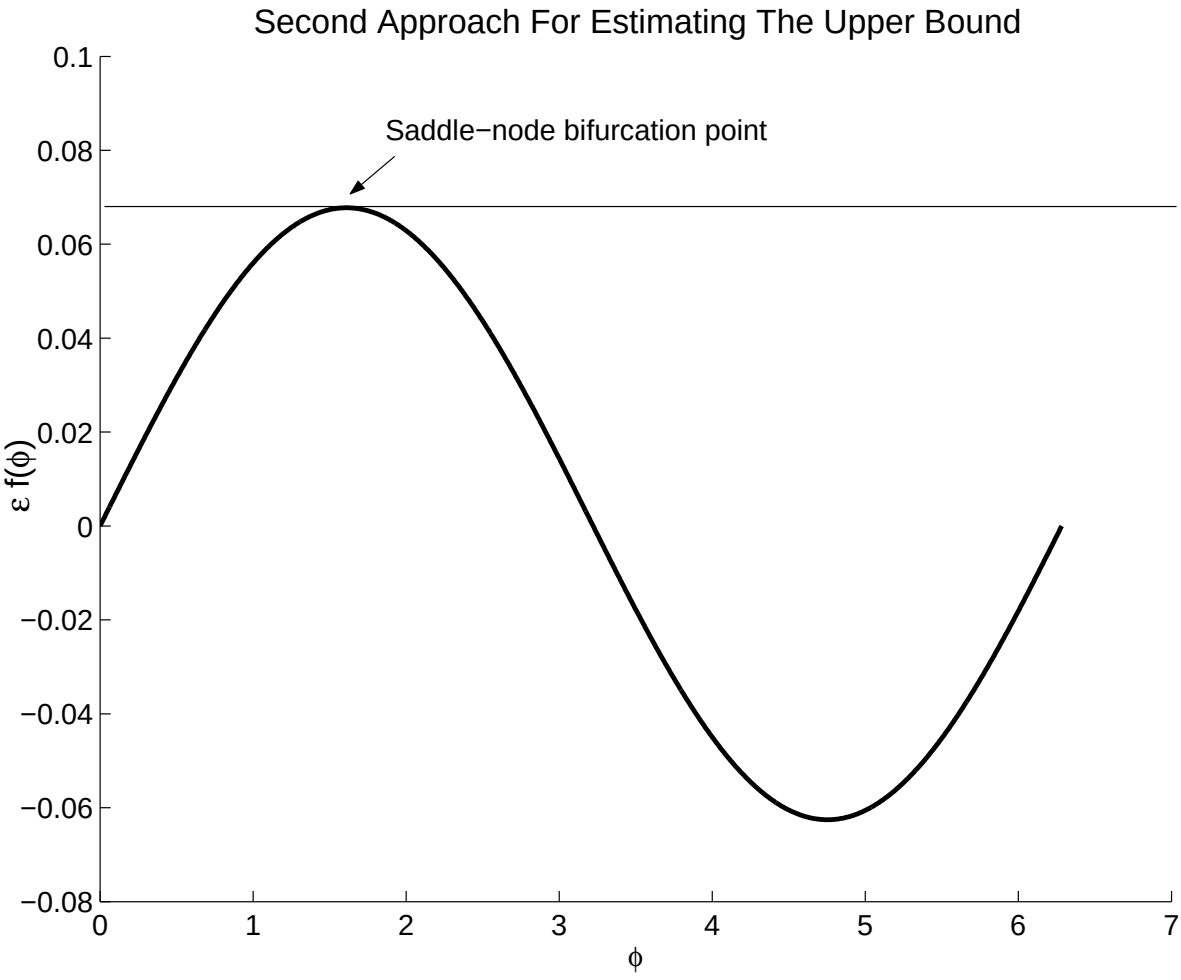

Figure 4.3: Graphical description of employing the second approach for estimating the upper bound (saddle-node bifurcation value) on the heterogeneity.

4.4.5 Interaction function for the hippocampal interneurons

Recall that the membrane potential dynamics for two mutually coupled hippocampal interneurons is governed by

$$\begin{aligned} C_m\frac{dV_1}{dt} &= I_{stim} + \mu - I_{ionic}(V_1) - g_{syn}s_{21}(V_1 - E_{syn}) \\ C_m\frac{dV_2}{dt} &= I_{stim} - \mu - I_{ionic}(V_2) - g_{syn}s_{12}(V_2 - E_{syn}) \\ \frac{ds_{21}}{dt} &= \alpha\frac{1}{1+\exp(-V_2/2)}(1-s_{21}) - \frac{s_{21}}{\tau_{syn}} \\ \frac{ds_{12}}{dt} &= \alpha\frac{1}{1+\exp(-V_1/2)}(1-s_{12}) - \frac{s_{12}}{\tau_{syn}} \end{aligned} \tag{4.51}$$

The interaction function is computed for $I_{stim} = 3\mu\text{A/cm}^2$, $\mu = 0\mu\text{A/cm}^2$, and $g_{syn} = 0.25$ (mS/cm^2). τ_{syn} is selected from 1 to 10 ms. These parameter values are consistent with the literature ([36], and [19]). The parameter μ characterizes the heterogeneity in the two cell network and is used as a bifurcation parameter.

To simplify the analysis the interaction function is expanded in the Fourier series. Figures 4.4 and 4.5 show the numerically computed interaction functions (and their odd parts) superimposed with the five term Fourier approximations. In the range of the values for the synaptic decay time constant (τ_{syn}), it is observed that the five term Fourier approximation is quite accurate in approximating the true interaction function in this case. The interaction function can thus be represented in the following truncated form

$$H(x) = a_0 + \sum_{n=1}^{4}[a_n\cos(nx) + b_n\sin(nx)] \tag{4.52}$$

Notice that $H'_{odd}(0) > 0$ for the biologically relevant range of the decay time constant ($1 - 10$ ms) and therefore the synchronous oscillations are always stable in a homogenous network of hippocampal interneurons. Additionally, for $\tau_{syn} = 1$ ms and $\tau_{syn} = 2$ ms, the slope of the odd part of the interaction function at $\phi = \pi$ is positive ($H'_{odd}(\pi) > 0$)) which implies that the anti-phase oscillations will be also stable in the N cell network. Bi-stability between the synchronous and anti-phase oscillations imply that in a homogenous network of N neurons, one can switch between the two solutions by varying τ_{syn}. For completeness, Tables 4.1 and 4.2 contain the coefficients of the five term Fourier series approximation of the interaction function for the hippocampal interneurons.

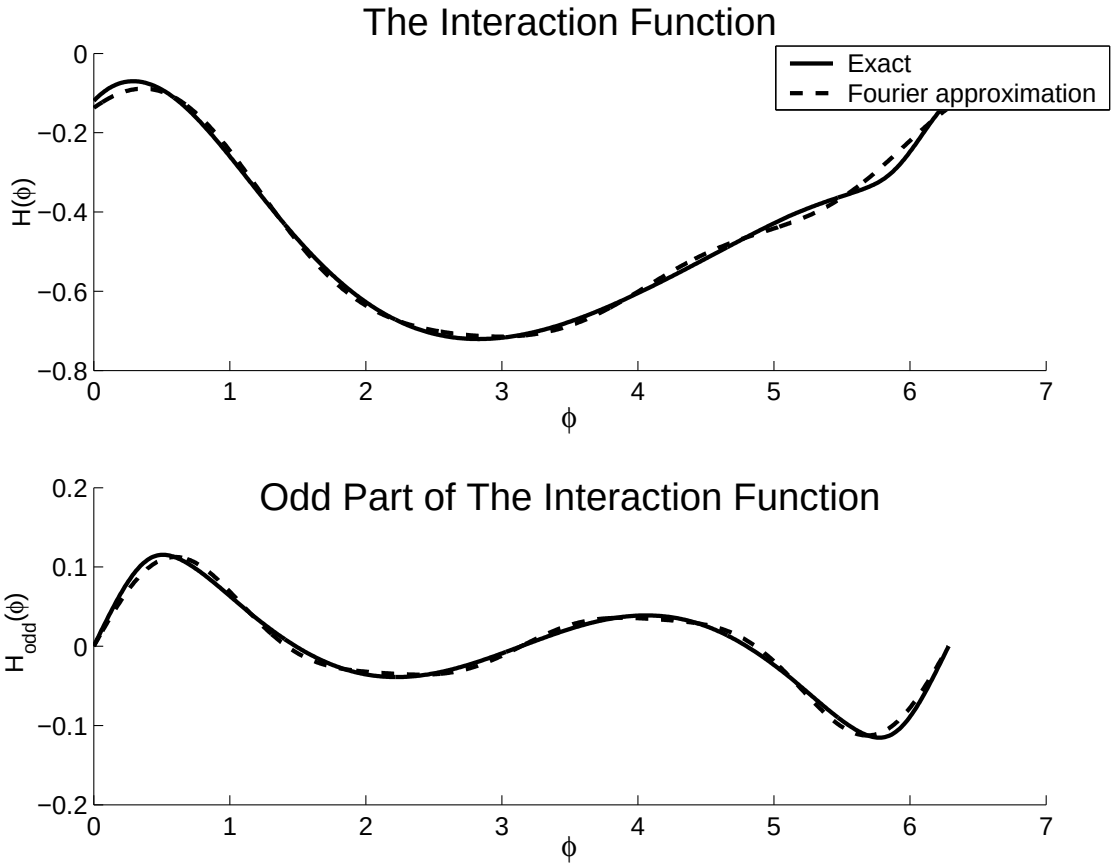

Figure 4.4: The interaction function and its odd part superimposed with the corresponding five term fourier approximation for $\tau_{syn} = 1$ ms.

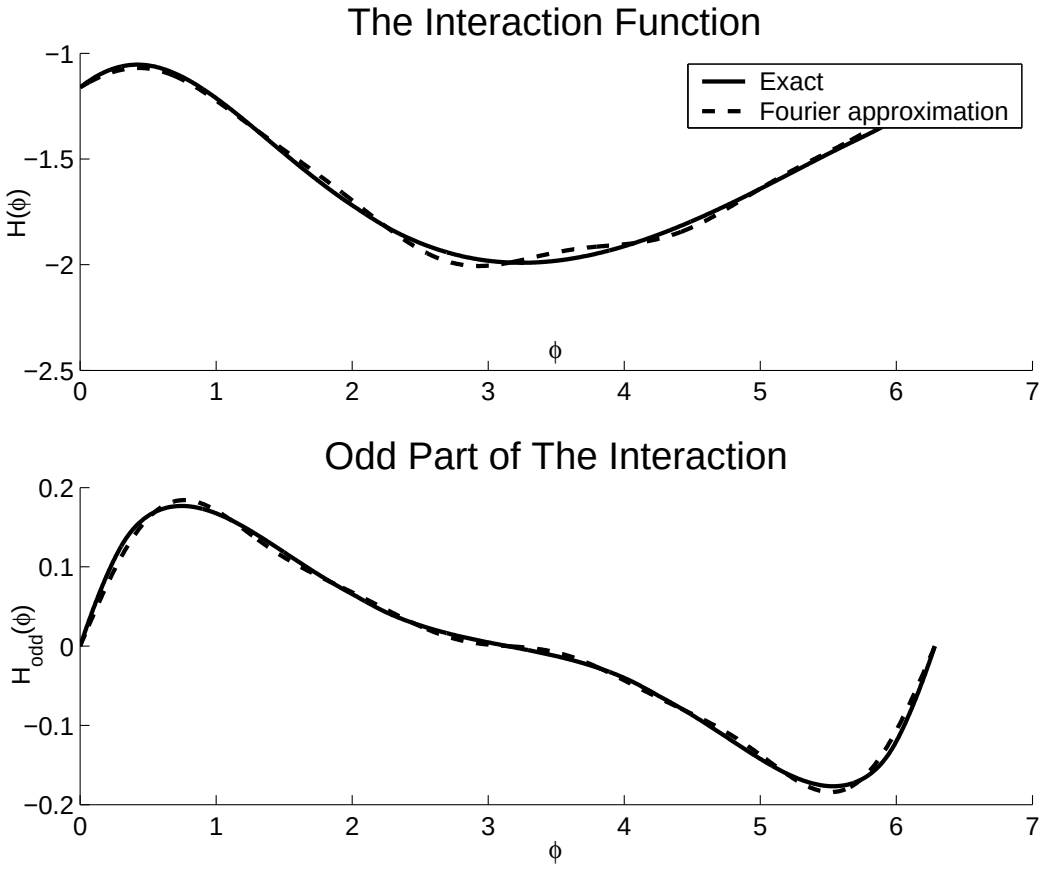

Figure 4.5: The interaction function and its odd part superimposed with the corresponding five term fourier approximation for $\tau_{syn} = 5$ ms.

Table 4.1: Computed values of a_n for the five term Fourier series approximation of the interaction function for the hippocampal interneurons.

τ_{syn} (ms)	a_0	a_1	a_2	a_3	a_4
1	-0.457	0.281	0.0324	0.0062	0.0049
2	-0.785	0.345	0.0222	2.91×10^{-5}	7.59×10^{-4}
3	-1.077	0.374	0.0208	-0.0013	-9.031×10^{-4}
4	-1.347	0.398	0.0214	-0.0019	-0.0012
5	-1.597	0.415	0.0221	-0.00170	-0.00160
6	-1.834	0.434	0.0233	-0.0017	-0.0017
7	-2.058	0.451	0.0258	-0.0017	-0.0021
8	-2.278	0.470	0.028	-0.0014	-0.00240
9	-2.484	0.486	0.0295	-0.00110	-0.0024
10	-2.680	0.503	0.0298	-0.00170	-0.00220

Table 4.2: Computed values of b_n for the five term Fourier series approximation of the interaction function for the hippocampal interneurons.

τ_{syn} (ms)	b_1	b_2	b_3	b_4
1	0.0156	0.0686	0.0309	0.0145
2	0.0775	0.0716	0.0296	0.0135
3	0.105	0.0717	0.0281	0.0127
4	0.119	0.0736	0.0262	0.0127
5	0.131	0.0736	0.0257	0.0122
6	0.137	0.0748	0.0255	0.0118
7	0.138	0.0762	0.0261	0.0113
8	0.140	0.0779	0.0265	0.0113
9	0.142	0.0793	0.0267	0.0113
10	0.145	0.0816	0.0263	0.0105

Table 4.3: Upper bound on the parameter μ and the intrinsic frequency difference for the two-cell network. Recall that the units are μ in $\mu\text{A/cm}^2$, and frequencies in kHz.

τ_{syn}(ms)	Max(μ)	Max$\lvert\Omega_1 - \Omega_2\rvert$	Phase equation prediction	Relative error (%)
1	0.134	0.0515	0.0577	12.0
2	0.190	0.0730	0.0732	0.274
3	0.231	0.0880	0.0802	8.86
4	0.254	0.0977	0.0846	13.4
5	0.267	0.103	0.0884	14.2
6	0.274	0.105	0.0913	13.0
7	0.278	0.107	0.0929	13.2
8	0.280	0.108	0.0949	12.1
9	0.280	0.108	0.0963	10.8
10	0.280	0.108	0.0980	9.26

4.4.6 Heterogenous two-cell network: Numerical solution versus the phase-coupled model

As mentioned earlier, the parameter μ (in units of $\mu\text{A/cm}^2$) determines the heterogeneity in the the neural network. The applied current $I_{stim} + \mu(\mu\text{A/cm}^2)$ determines the intrinsic frequencies and as discussed earlier there is an upper bound on μ above which the near-synchronous oscillations break down. In a previous work [36], the software XPPAUT [11] was used to numerically compute the frequency ($\frac{1}{\text{Oscillation period}}$) of a single neuron as a function of its applied current and a fourth order polynomial was then fitted to the points. The relationship between the frequency (kHz) and the applied current for a single neuron is therefore

$$\text{fr}(x) = -0.000112x^4 + 0.00188x^3 - 0.0131x^2 + 0.0705x + 0.000258. \tag{4.53}$$

The intrinsic frequency is given by $\Omega(\mu) = 2\pi\text{fr}(I_{stim} \pm \mu)$. In what follows, μ is taken as the bifurcation parameter and numerical continuation is used to follow the periodic solutions of (4.51) for $\mu > 0$ emanating. Referring to the figure of the heterogenous two-cell network, we see that the phase-locked oscillations are lost via saddle-node bifurcation. Table 4.3 shows the μ values for the occurrence of the saddle-node bifurcation. Note that there is a good correlation with the numerically computed values and the values predicted by the phase coupled model. Through the simulations we discovered that for $\tau_{syn} \geq 6$, the stability of the near-synchronous oscillations is lost via period doubling at a smaller values of μ, but the phase-coupled model is able only to capture the saddle-node bifurcations.

4.5 Three and four cell networks: Estimation of the maximum heterogeneity

In this section we present results of numerical bifurcation analysis for the three and four cell networks. As for the two-cell case, the stimulus current for the corresponding homogenous network is taken to be $I_{stim} = 3\ \mu\text{A/cm}^2$. The dynamics of the three-cell system is governed by

$$\begin{aligned}
C_m\frac{dV_1}{dt} &= I_{stim} + \mu_1 - I_{ionic}(V_1) - \frac{g_{syn}}{2}\sum_{\substack{j=1\\ j\neq 1}}^{3} s_{j1}(V_1 - E_{syn}) \\
C_m\frac{dV_2}{dt} &= I_{stim} + \mu_2 - I_{ionic}(V_2) - \frac{g_{syn}}{2}\sum_{\substack{j=1\\ j\neq 2}}^{3} s_{j2}(V_2 - E_{syn}) \\
C_m\frac{dV_3}{dt} &= I_{stim} + \mu_3 - I_{ionic}(V_3) - \frac{g_{syn}}{2}\sum_{\substack{j=1\\ j\neq 3}}^{3} s_{j2}(V_3 - E_{syn}) \\
\frac{ds_{jk}}{dt} &= \alpha'\frac{1}{1+\exp(-V_j/2)}(1-s_{jk}) - \frac{s_{jk}}{\tau_{syn}}, \quad j,k = 1,2,3.
\end{aligned} \tag{4.54}$$

Recall the two approaches derived in estimating the upper bound on the heterogeneity

1. The first approach:
$$|\Omega_1 - \Omega_N| > \frac{g_{syn}}{N-1}\text{Max}|U_N(\zeta)|,$$
and the function $U_N(\zeta)$ is given by
$$\begin{aligned}
U_N(\zeta) = &\sum_{n=1}^{M} R_N \frac{\cos(nN\zeta) - \cos(n(1+N)\zeta) + \cos(n\zeta) - 1}{2(1-\cos(n\zeta))} \\
&+ \sum_{n=1}^{M} L_N \frac{\sin(nN\zeta) - \sin(n(1+N)\zeta) + \sin(n\zeta)}{2(1-\cos(n\zeta))},
\end{aligned}$$
where

$$R_N = [a_n \cos(nN\zeta) - b_n \sin(nN\zeta) - a_n \cos(n\zeta) + b_n \sin(n\zeta)]$$
$$L_N = [a_n \sin(nN\zeta) + b_n \cos(nN\zeta) - a_n \sin(n\zeta) - b_n \cos(n\zeta)]\,.$$

2. The second approach:
$$\Omega_1 - \Omega_2 > \frac{g_{syn}}{N-1} f(\phi^*), \tag{4.55}$$
where ϕ^* denotes the bifurcation point (Figure 4.3) and
$$f(\phi) = 2(N_2 - N_1) \sum_{n=1}^{4} a_n \sin\left(\frac{n\phi}{2}\right)^2 + (N_1 + N_2) H_{odd}(\phi). \tag{4.56}$$
N_1 and N_2 are the numbers of the population clusters having the natural frequencies Ω_1 and Ω_2, respectively.

Heterogeneity in the network is characterized by the parameters μ_1, μ_2, and μ_3. Two sets of parameter values are used for comparison between the analytical and the numerical solutions. For the first set, $\mu_1 = \mu_2 = 0$ and μ_3 is used as the bifurcation parameter. Table 4.4 summarizes the results for four different values of the synaptic decay time constant τ_{syn}. Figures 4.6 and 4.7 demonstrate graphically a sample calculation of the upper bound employing the first and the second approaches respectively with the synaptic decay time constant, $\tau_{syn} = 1$ ms. According to the data in Table 4.4, the first approach correlates much better with the numerical results. Figure 4.8 shows the corresponding action potentials for the three cells with the heterogeneity parameters set to $\mu_1 = \mu_2 = 0, \mu_3 = 0.2$ and $\tau_{syn} = 1$ms. The cells are initially perfectly synchronized. By increasing the applied current to the third cell, the third cell begins to move away from the rest of the population, while the other cells remain perfectly synchronized together.

For the second set of simulations μ_1, μ_2 and μ_3 are chosen randomly from the range $(-\tilde{\mu}, \tilde{\mu})$ where $\tilde{\mu}$ is the corresponding saddle-node bifurcation value of the parameter μ for the two-cell network presented in Table 4.5 and are dependent on the synaptic decay time constant, τ_{syn} ([36], [37]). Once again, μ_3 is taken as the bifurcation parameter. Columns six and seven present the estimations from the first and second approaches similar to the previous case.

According to Table 4.4 the first method clearly correlates much better with the simulation results as can be seen from the relative error values. However; for the second simulation set, the first method has smaller relative error values for $\tau_{syn} = 1$ (ms) and $\tau_{syn} = 5$ (ms). For $\tau_{syn} = 2$ (ms) the second method has smaller relative error and for $\tau_{syn} = 10$ (ms) the errors are about the same for the two approaches. It can therefore be seen that when the heterogeneities are selected

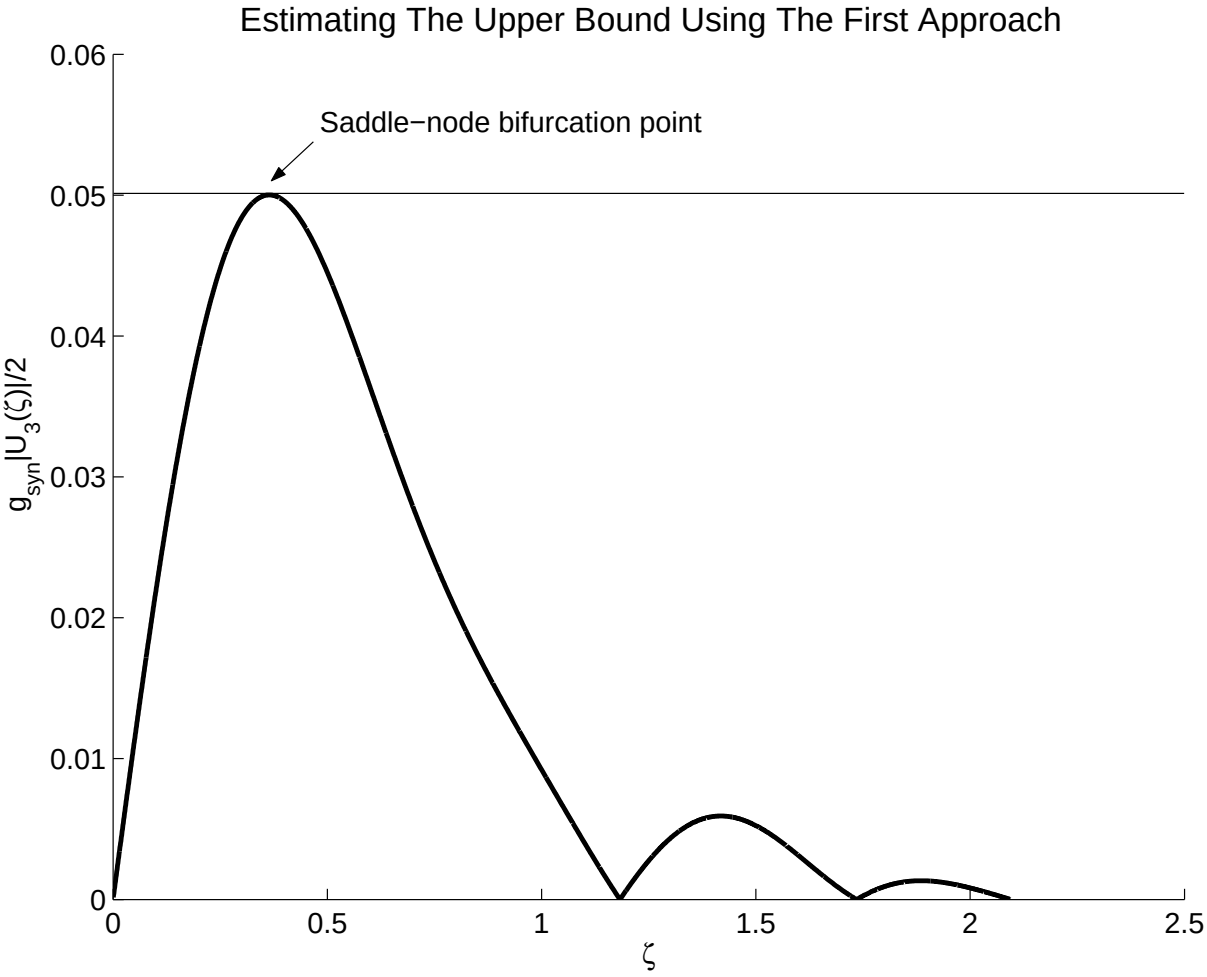

Figure 4.6: Calculating the upper bound for the loss of the near-synchronous solutions using the first approach when $\tau_{syn} = 1$ ms, $g_{syn} = 0.25$ mS/cm^2 in a 3-cell network.

Table 4.4: Upper bound on μ_3 and the natural frequency difference for the three-cell network for the first set of simulations. μ_3 is in units of μA/cm^2 and the frequencies are in kHz.

$\tau_{syn}(ms)$	Max(μ_3)	Max($\lvert\Omega_3 - \Omega_1\rvert$)	Approach 1 (% error)	Approach 2 (% error)
1	0.240	0.0453	10.4	26.7
2	0.368	0.0688	2.03	32.7
5	0.462	0.086	3.49	35.2
10	0.462	0.0861	6.04	31.7

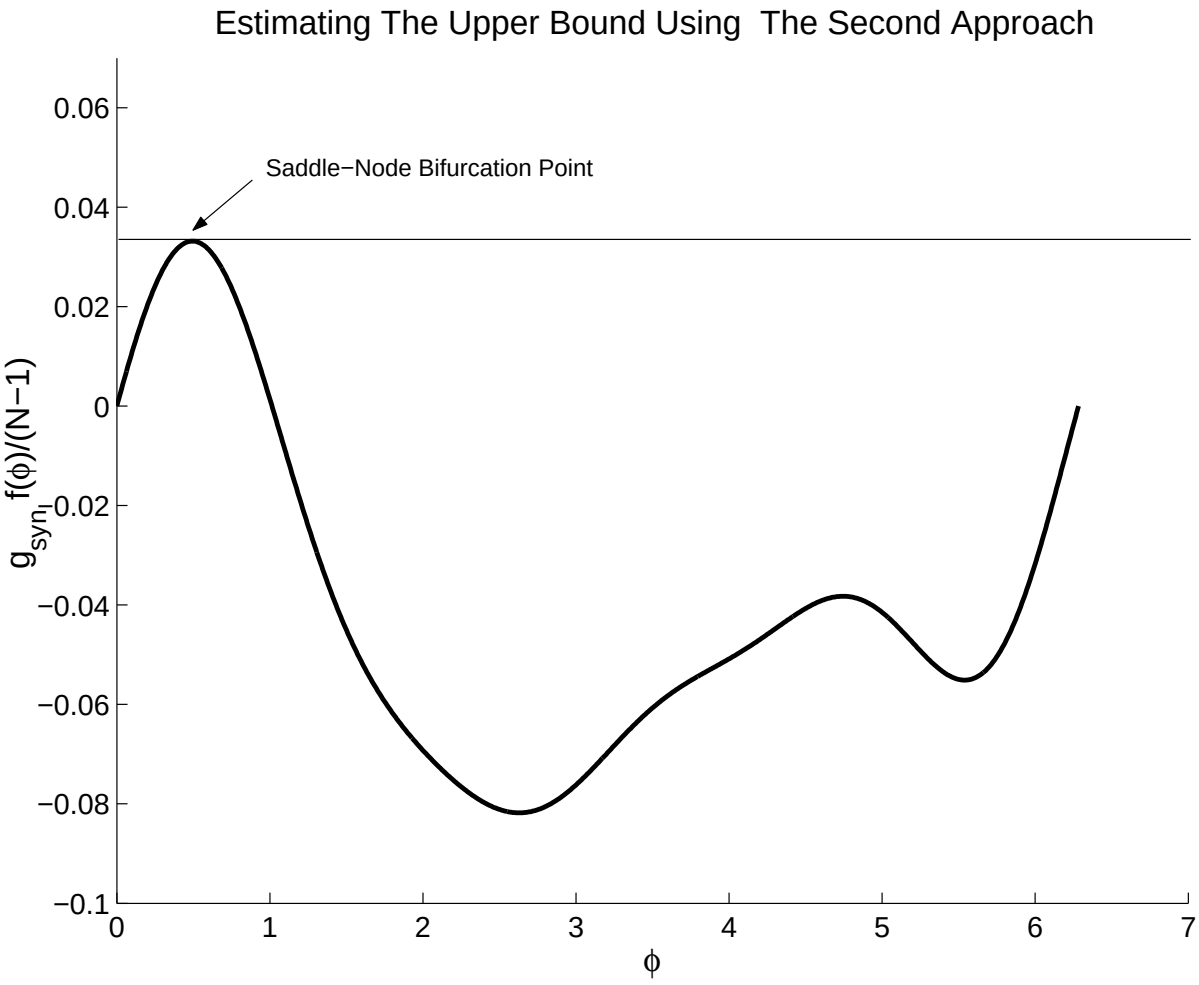

Figure 4.7: Calculating the upper bound for the loss of the near-synchronous solutions using the second approach for $\tau_{syn} = 1$ ms, $g_{syn} = 0.25$ mS/cm^2 and $N_1 = 1, N_2 = 2$ in a 3-cell network.

Table 4.5: Upper bound on μ_3 and the natural frequency differences for the three-cell network considering the second set of simulations. μ_3 is in units of μA/cm^2, and frequencies are in kHz.

τ_{syn} (ms)	μ_1	μ_2	Max(μ_3)	Approach 1 (%error)	Approach 2 (% error)
1	-0.023	0.052	0.238	1.21	32.8
2	-0.067	0.15	0.207	29.4	11.1
5	-0.0026	0.037	0.477	6.95	37.6
10	-0.13	0.057	0.268	20.4	22.4

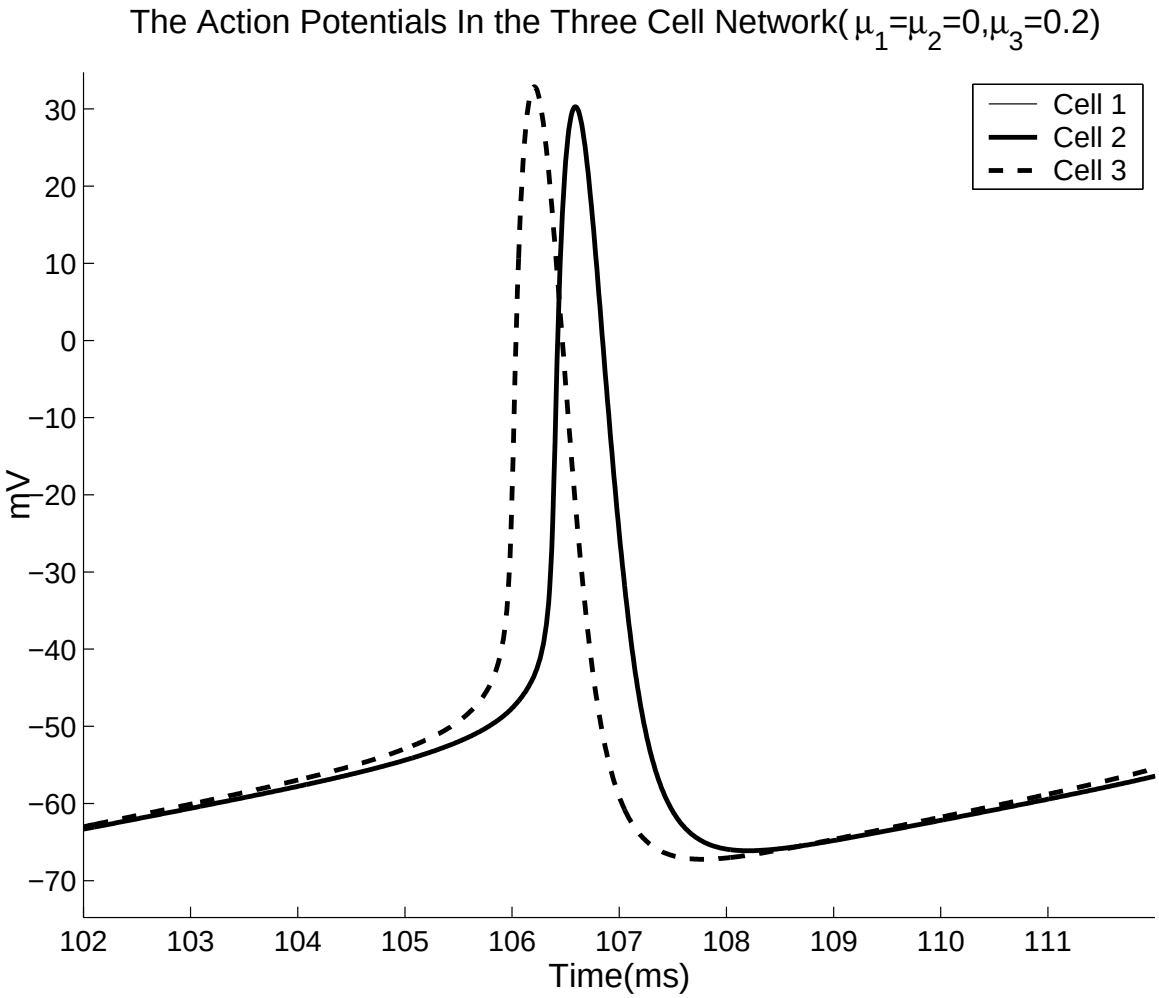

Figure 4.8: Sample Action potentials for the three cell network with heterogeneity parameters set to $\mu_1 = \mu_2 = 0, \mu_3 = 0.2$ (in μA/cm^2) and $\tau_{syn} = 1$ ms. The neurons 1 and 2 are completely synchronous and their action potentials are superimposed and can not be distinguished.

Table 4.6: The first set of numerical results for computing the upper bound on the heterogeneity for the four cell network. The parameter μ is in units of μA/cm^2 and the frequencies are in kHz.

τ_{syn} (ms)	Max(μ_3)	Max($\lvert\Omega_3 - \Omega_1\rvert$) (kHz)	First approach (%)	Second approach (%)
1	0.183	0.0348	36.5	7.76
2	0.238	0.0450	42.4	11.56
5	0.292	0.0549	44.3	11.84
10	0.2885	0.0543	60.2	24.1

randomly, non of the methods has clear advantage over the other one. Further simulations and theoretical investigations are necessary to reach definite conclusions regarding the two approaches. We repeat the same analysis for the four cell network. The dynamics of the four cell network is governed by

$$
\begin{aligned}
C_m\frac{dV_1}{dt} &= I_{stim} + \mu_1 - I_{ionic}(V_1) - \frac{g_{syn}}{3}\sum_{\substack{j=1\\ j\neq 1}}^{4} s_{j1}(V_1 - E_{syn}) \\
C_m\frac{dV_2}{dt} &= I_{stim} + \mu_2 - I_{ionic}(V_2) - \frac{g_{syn}}{3}\sum_{\substack{j=1\\ j\neq 2}}^{4} s_{j1}(V_2 - E_{syn}) \\
C_m\frac{dV_3}{dt} &= I_{stim} + \mu_3 - I_{ionic}(V_3) - \frac{g_{syn}}{3}\sum_{\substack{j=1\\ j\neq 3}}^{4} s_{j1}(V_3 - E_{syn}) \\
C_m\frac{dV_4}{dt} &= I_{stim} + \mu_4 - I_{ionic}(V_4) - \frac{g_{syn}}{3}\sum_{\substack{j=1\\ j\neq 4}}^{4} s_{j1}(V_4 - E_{syn}) \\
\frac{ds_{jk}}{dt} &= \alpha'\frac{1}{1+\exp(-V_j/2)}(1 - s_{jk}) - \frac{s_{jk}}{\tau_{syn}}, \quad j,k = 1,2,3,4.
\end{aligned}
\tag{4.57}
$$

As before, μ_1, μ_2, μ_3 and μ_4 characterize the heterogeneity in the network. We follow similar steps for carrying out simulations for the four cell network. The first set of the simulations assume that $\mu_1 = \mu_2 = 0$, $\mu_3 = \mu_4$ and μ_3 is then taken as the bifurcation parameter. Table 4.6 summarizes the results along with the analytical estimations. For the second set of simulations we chose the heterogeneity parameters of the neurons 1, 2, and 3 randomly and take μ_4 as the bifurcation parameter. Table 4.7 summarizes the results and Figure 4.9 shows the corresponding action potentials for $\tau_{syn} = 5$ ms and $\mu_1 = -0.13$ μA/cm^2, $\mu_2 = 0.07$ μA/cm^2, $\mu_3 = -0.1$ μA/cm^2, $\mu_4 = 0.23$ μA/cm^2.

The first approach has lower relative error when the heterogeneities are selected randomly and

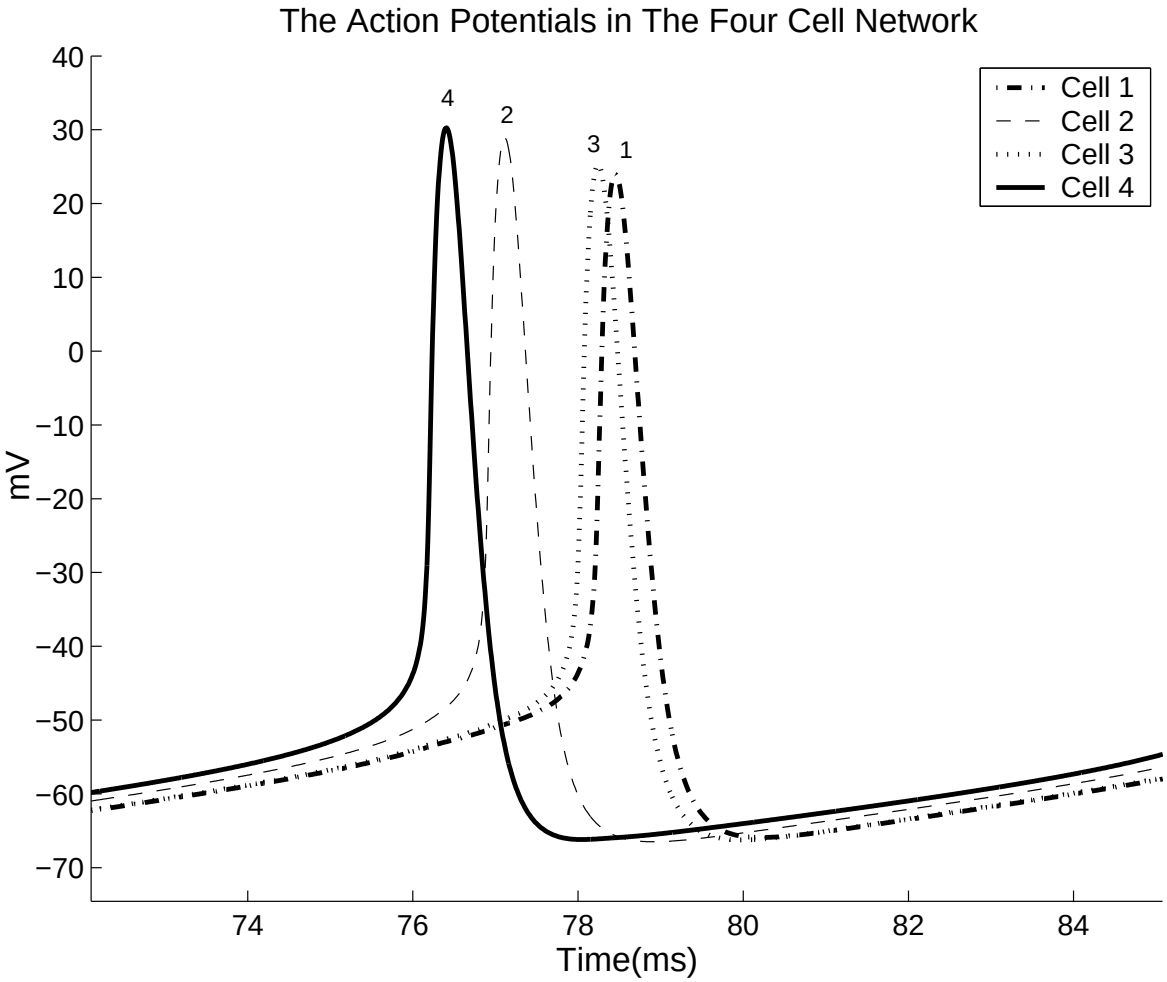

Figure 4.9: The action potentials in the four cell network with randomly chosen heterogeneities ($\mu_1 = -0.13$ μA/cm^2, $\mu_2 = 0.07$ μA/cm^2, $\mu_3 = -0.1$ μA/cm^2, $\mu_4 = 0.23$ μA/cm^2) and $\tau_{syn} = 5$ ms.

Table 4.7: The second set of numerical results for computing the upper bound on the heterogeneity for the four cell network. μ_1, μ_2, μ_3, μ_4 are in units of μA/cm^2.

τ_{syn} (ms)	μ_1	μ_2	μ_3	Max(μ_4)	Approach 1 (%)	Approach 2 (%)
1	-0.031	0.081	0.063	0.219	0.210	20.9
2	-0.05	0.061	0.11	0.291	0.470	22.1
5	-0.13	0.070	-0.10	0.252	8.94	15.5
10	0.01	0.1	0.05	0.553	13.0	32.5

higher error for the first simulation set where the heterogeneity selection is structured. As mentioned earlier, more simulations are necessary to reach a conclusive answer as which method is more accurate; however, based on the three and four cell network simulations, we conjecture that the first method better approximates the saddle node bifurcation values for the networks with randomly selected heterogeneities. This choice of random input heterogeneity is in accordance with larger network computer simulations (for example see [37], [36]). In the following we show that the predictions using the first approach developed in this thesis correlate with results obtained from a large scale computer simulation study. In particular, Skinner et al. [37] reported that as the synaptic decay time constant increases from $\tau_{syn} = 1$ ms to $\tau_{syn} = 5$ ms, the loss of the near-synchronous oscillations in a 10-cell network occurred at larger heterogeneities (see Table 4 in [37]). They observed the same pattern with the two cell simulations which showed that the two-cell network correctly reflected the modulation of the near-synchronous oscillations. Furthermore, the loss of the near-synchronous oscillations in their 10 cell network occurred at smaller heterogeneity than the two cell network for the values of τ_{syn} they considered. Table 4.8 shows the values of the upper-bound for heterogeneity calculated for networks with $N = 2$, $N = 10$, $N = 1000$ and $N = 1000000$ neurons using the first approach developed in this thesis. The calculation results are summarized as follows which is confirmed by simulations by Skinner et al. ([37], [36]):

1. Loss of the near-synchronous oscillations occurs at larger heterogeneity as the synaptic decay time constant, τ_{syn}, is increased and the pattern is preserved as we go from the two cell network to larger networks.

2. For a fixed τ_{syn}, loss of the near-synchronous oscillations occurs at smaller heterogeneity as the network size increases.

Furthermore, calculations predict that for a fixed τ_{syn}, there exists an asymptotical value that the upper bounds on heterogeneity approach as the network size increases. This is shown by the last column in Table 4.8 which is performed for a network with a million cells. This prediction remains to be confirmed by further computer simulations.

To better understand the implications of heterogeneity in neural networks, the next section deals with estimating the effect of the perturbations in the neural phases of the corresponding homogenous network.

Table 4.8: Calculating the upper bounds on the heterogeneity (maximum mutual neural frequency difference) using the first approach to show the modulation of the near-synchronous oscillations by τ_{syn} and more importantly, preservation of the pattern predicted by the two cell network in larger networks. The stimulus current is measured in $\mu\text{A/cm}^2$ and the percentage is computed by finding μ' such that $fr(3+\mu') - fr(3-\mu') =$ **(the frequency difference)** and then computing $\frac{\mu'}{I_{stim}} \times 100$.

τ_{syn} (ms)	$N = 2$	$N = 10$	$N = 1000$	Asymptotic value	Percentage of $I_{stim} = 3$
1	0.0562	0.0436	0.0414	0.0414	6.13
2	0.0753	0.0590	0.0561	0.0560	9.13
5	0.0921	0.0730	0.0694	0.0694	11.1
10	0.101	0.0802	0.0762	0.0762	13.0

4.6 Estimating phase separation in the heterogenous network

Assume that neurons in a homogenous network are oscillating synchronously. Adding heterogeneity to the network, perturbs the neural phases and separates the initially in-phase (zero phase difference) neurons. The added heterogeneity also perturbs the network frequency and our aim in this section is to predict this phase separation and network frequency alteration by applying the first order analysis. The analytical results will then be compared with numerical simulations for three and four cell networks.

First order analysis

Recall that in a synchronous network phases are given by

$$\theta_k = \Lambda t, \quad k = 1, \ldots, N.$$

We assume that adding heterogeneity perturbs the above phases by δ_k such that $|\delta_k| << 1$

$$\theta_k = \Lambda t + \delta_k, \quad k = 1, \ldots, N. \tag{4.58}$$

The above equation is substituted in the phase equations and it is assumed that linear approximation to the interaction function holds true

$$\begin{aligned}\frac{d\theta_k}{dt} = \Lambda' &= \Omega_k + \epsilon \sum_{j=1}^{N} H(\theta_j - \theta_k) - \epsilon H(0) \\ &= \Omega_k + \epsilon \sum_{j=1}^{N} H(\delta_j - \delta_k) - \epsilon H(0) \\ &\approx \Omega_k + \epsilon \sum_{j=1}^{N} [H(0) + H'(0)(\delta_j - \delta_k)] - \epsilon H(0) \\ &= \Omega_k + \epsilon N H(0) + \epsilon H'(0) \sum_{j=1}^{N} (\delta_j - \delta_k) - \epsilon H(0).\end{aligned}$$

Similar expression holds for the $k+1$st neuron and the equation for the phase difference, $\phi_k = \theta_k - \theta_{k+1}$ becomes

$$\Omega_k - \Omega_{k+1} - \epsilon N H'(0)(\delta_k - \delta_{k+1}) \approx 0. \tag{4.59}$$

Thus the perturbed phase difference, $\delta_k - \delta_{k+1}$ is approximated by

$$\delta_k - \delta_{k+1} \approx \frac{N-1}{N} \frac{\Omega_k - \Omega_{k+1}}{g_{syn} H'(0)}. \tag{4.60}$$

We take the first neuron as the reference point ($\delta_1 = 0$), and the phase-shifts can easily be found

$$\delta_1 = 0 \tag{4.61}$$
$$\delta_2 = -\frac{N-1}{N} \frac{\Omega_1 - \Omega_2}{g_{syn} H'(0)} \tag{4.62}$$
$$\delta_3 = -\frac{N-1}{N} \frac{\Omega_1 - \Omega_3}{g_{syn} H'(0)} \tag{4.63}$$
$$\vdots \tag{4.64}$$
$$\delta_k = -\frac{N-1}{N} \frac{\Omega_1 - \Omega_k}{g_{syn} H'(0)}. \tag{4.65}$$

Let Λ' be the new network frequency. Then

$$\Lambda' = \Omega_k + \epsilon \sum_{j=1}^{N} H(\delta_j - \delta_k) - \epsilon H(0)$$

$$\approx \Omega_k + \epsilon N H(0) + \epsilon H'(0) \sum_{j=1}^{N} (\delta_j - \delta_k) - \epsilon H(0)$$

$$= \Omega_k + \epsilon(N-1)H(0) + \epsilon H'(0) \sum_{j=1}^{N} \frac{\Omega_j - \Omega_k}{\epsilon N H'(0)} \tag{4.66}$$

$$= \Omega_k + \epsilon(N-1)H(0) + \frac{1}{N} \sum_{j=1}^{N} (\Omega_j - \Omega_k) \tag{4.67}$$

$$= \frac{\sum_{j=1}^{N} \Omega_j}{N} + g_{syn} H(0) \tag{4.68}$$

$$= \bar{\Omega} + g_{syn} H(0), \tag{4.69}$$

where $\bar{\Omega} = \frac{\sum_{j=1}^{N} \Omega_j}{N}$ denotes the mean intrinsic frequency of the neurons. It is interesting to notice that the form of the network frequency is exactly the same as that of the homogeneous network having the intrinsic frequency of $\bar{\Omega}$. Further, notice that for neurons with odd interaction function, the network frequency of the heterogeneous network is equal to the mean intrinsic frequencies (since $H(0) = 0$ for an odd interaction function). Therefore, to estimate the network frequency in a heterogenous network, it suffices to compute the mean intrinsic frequency and add $g_{syn}H(0)$.

4.6.1 Comparison of the first order analysis with numerical solutions

To test the analytical results, consider a network of four neurons initially in perfect synchrony. The effect of adding heterogeneity results in temporal separation of the neural action potentials (the peak action potentials move away from each other) as depicted in Figure 4.10. We compare the analytical results with numerical simulations for the cases with $\tau_{syn} = 1$ ms and $\tau_{syn} = 5$ ms. The heterogeneity parameters are: $I_{stim} = 3\mu\text{A/cm}^2$, $\mu_1 = -0.05$, $\mu_2 = 0.08$, $\mu_3 = 0.1$, $\mu_4 = -0.1$ all in units of $\mu\text{A/cm}^2$. The perturbation in the phases for $N = 4$ is given by

$$|\delta_k - \delta_{k+1}| = \frac{3}{4} \frac{|\Omega_k - \Omega_{k+1}|}{g_{syn} H'(0)}. \tag{4.70}$$

The intrinsic frequencies are given by

$$\Omega_1 = 0.846 \text{ kHz}$$
$$\Omega_2 = 0.867 \text{ kHz}$$
$$\Omega_3 = 0.864 \text{ kHz}$$
$$\Omega_4 = 0.871. \text{ kHz}$$

We provide the detailed calculations for the case of $\tau_{syn} = 1$ ms. In this case, $H'(0) = 0.303$. The phase differences are then calculated using equation 4.70

$$|\delta_1 - \delta_2| = 0.208$$
$$|\delta_2 - \delta_3| = 0.0297$$
$$|\delta_3 - \delta_4| = 0.0693.$$

Knowing the oscillation period, $T = 7.70$ms, the temporal separations (the time separation between the peak action potentials) can also be calculated

$$|\Delta t_{12}| = |\delta_1 - \delta_2|\frac{T}{2\pi} = 0.255 \text{ ms}$$
$$|\Delta t_{23}| = |\delta_2 - \delta_3|\frac{T}{2\pi} = 0.0364 \text{ ms}$$
$$|\Delta t_{34}| = |\delta_3 - \delta_4|\frac{T}{2\pi} = 0.0849 \text{ ms}.$$

The temporal differences are computed from the numerical simulations by calculating the time difference between the two action potential peaks (Figure 4.10). The numerical values of the temporal differences are as follows

$$|\Delta t_{12}|_{numeric} = 0.25 \text{ ms}$$
$$|\Delta t_{23}|_{numeric} = 0.040 \text{ ms}$$
$$|\Delta t_{34}|_{numeric} = 0.070 \text{ ms}.$$

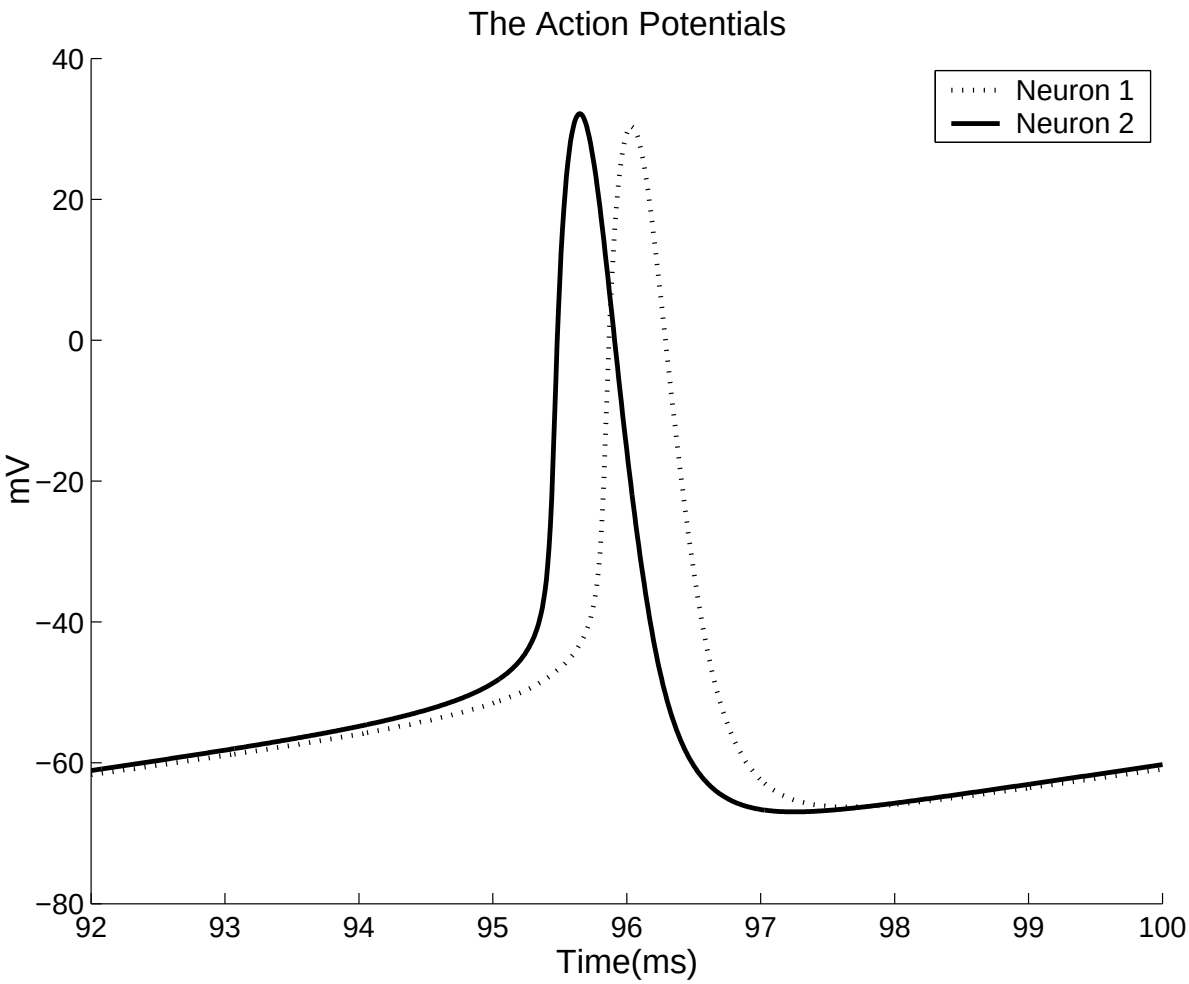

Figure 4.10: The action potentials for neurons 1 and 2 in the four cell network with $\tau_{syn} = 1$ ms.

Table 4.9: The relative error between the analytical and computed values of the temporal separation of the action potentials in the four-cell network.

τ_{syn} (ms)	Δt_{12} error (%)	Δt_{23} error (%)	Δt_{34} error (%)
1	1.96	9.00	21.3
5	21.5	26.8	13.8

For $\tau_{syn} = 5$ ms, similar calculations are carried out to yield

$$|\Delta t_{12}| = 0.259 \text{ ms}$$
$$|\Delta t_{23}| = 0.0366 \text{ ms}$$
$$|\Delta t_{34}| = 0.0862 \text{ ms},$$

and the corresponding numerical results

$$|\Delta t_{12}|_{numerical} = 0.33 \text{ ms}$$
$$|\Delta t_{23}|_{numerical} = 0.05 \text{ ms}$$
$$|\Delta t_{34}|_{numerical} = 0.1 \text{ ms}.$$

Table 4.9 summarizes the relative error between the analytical and numerical results. Notice that for smaller value of the synaptic decay time constant the errors are smaller.

The change in network frequency (as an indicator of the input heterogeneity) can also be compared. Recall the expression for the network frequency in a heterogeneous network

$$\Lambda = \bar{\Omega} + g_{syn} H(0), \tag{4.71}$$

where $\bar{\Omega}$ is the mean intrinsic frequency. Table 4.10 summarizes the network frequencies for four different choices of τ_{syn} values and for the $N = 3$ cell network. As can be seen from Table 4.10, there is a good correlation between the numerically computed values and the analytical estimations for $\tau_{syn} < 5$ ms and the prediction gets worse as the synaptic decay time constant is increased. The above approximations for calculating the phase shifts and network frequency along with the previously described approaches to estimate the upper bounds on the input heterogeneity,

Table 4.10: Comparison of the numerically computed network frequency versus the analytical results.

τ_{syn}(ms)	$\Lambda_{numerical}$(kH)	$\Lambda_{analytical}$(kH)	Relative error (%)
1	0.816	0.829	1.59
2	0.753	0.758	0.660
5	0.604	0.571	5.46
10	0.468	0.324	10.77

provide useful approaches in understanding implications of the heterogeneity on the existence and stability of the synchronous oscillations.

Chapter 5

Conclusion

We began by considering the general phase model for a network of all-to-all coupled neurons. We provided conditions for the stability of the synchronous and anti-phase oscillations in a homogenous network consisting of N neurons. The phase reduction method was then applied to the model of hippocampal interneurons [43] to gain a better understanding of the stability and existence of the synchronous oscillations in the heterogeneous network of hippocampal interneurons. The results confirmed the notion that the heterogeneity of inputs (thus the intrinsic frequencies) strongly affect the ability of the neurons to synchronize ([41], [43]) and reduces the basin of attraction of the stable synchronous oscillations. An interesting finding from the above analysis is that in a synchronous network of N neurons, if the intrinsic frequency difference of any two neurons goes beyond a critical value, the synchronous oscillation will be destroyed. In pathological rhythms such as epilepsy [9] which is generated in hippocampus, this finding suggests a method for using focused high frequency stimulation of a local region of a synchronized network, for alleviating and controlling the synchronous oscillations. The local high frequency stimulation has been applied for annihilating oscillations in biological neural networks. Kiss et al [24] showed suppression of rhythms in rat thalamus and related their findings to oscillations in Parkinson patients. Benabib et al [4] found symptom alleviation (tremor, rigidity) after the application of high frequency stimulation of the brains (thalamus) of Parkinson patients. From their data the extent of the localization of the stimulating field is not clear. The symptom alleviation can either result from oscillation suppression where the neurons in the population fail to oscillate altogether, or it may result from the loss of synchronous oscillations. Although, our results do not deal with suppressing the oscillations, they support the idea that local high frequency stimulation can annihilate synchrony in neural networks. Assuming that Parkinsonian tremors in patients result from synchronization in an appropriate controlling neural network, the findings support the use of local electrical fields to increase the input heterogeneity above critical value and alleviate the

synchronous oscillations (and thus the tremors).

There has been only few serious analytical studies of heterogeneous networks. Ermentrout [10] studied the existence and stability of phase-locked solutions in network of oscillators and the theorem proved in his article was used here to establish the stability of the solutions resulting from the perturbation of the corresponding homogenous solutions. Another work containing significant analytical insight, carried out by Chow[8], who used a simplified model to establish that there exists a a critical heterogeneity level above which phase-locked solutions do not exist and that, if the homogenous solutions are stable, the corresponding heterogeneous solutions will be stable for sufficiently weak heterogeneities. The above two results were confirmed by the numerical and analytical approaches of this thesis. A result not mentioned in the literature, was application of the first order analysis to derive a formula for the network frequency and thus establish a direct correspondence between the input heterogeneity and frequency of the rhythms. This result becomes intriguing when one contemplates the possibility of using input heterogeneity by the brain to switch between different frequency regimes. Finally, as mentioned earlier, synchronous oscillations are believed to be involved in different cognitive functions and brain might switch between different cognitive states by changing patterns of input currents to neural networks involved in modulating the rhythms. Additionally, the results of this thesis are derived for general interaction functions and can therefore be applied to other types of neurons not considered here.

5.1 Future directions

Heterogeneity seems to play an important role in modulating the brain rhythms and specifically in the interneuronal population considered here. One immediate future step is to attempt to perform bifurcation analysis of the networks with 5 to 10 cells and compare the numerical values of the maximum heterogeneity with the analytical results obtained here. Another project would be aimed at comparing validity of the network frequency formula developed here, with frequencies computed numerically for large scale networks ($N > 10$) and confirming the hypothesis that heterogeneity has a significant controlling effect on the network frequency. A long term future project, may involve application of time dependent stochastic stimulating current to interneuronal phase model, and determining its role in altering the stability of synchronous oscillations.

Bibliography

[1] M. Bartos, I. Vida, M. Frotscher, J. R. P. Geiger, and P. Jonas, *Rapid signaling at inhibitory synapses in a dentate gyrus interneuron network*, J. Neurosci. **21** (2001), 2687–2698.

[2] M. Bartos, I. Vida, M. Frotscher, A. Meyer, H. Monyer, J. R. P. Geiger, and P. Jonas, *Fast synaptic inhibition promotes synchronized gamma oscillations in hippocampal interneuron network*, Proc. Natl. Acad. Sci. **99(20)** (2002), 13222–13227.

[3] M. F. Bear, M.A Paradiso, and B. W. Connars, *Neuroscience: Exploring the Brain*, 2nd ed., Lippincott Williams and Wilkins, Baltimore, 2001.

[4] A. L. Benabib, A. Khoudsi, A. Benazzouz, V. Fraix, A. Ashraf, J. F. Le Base, S. Chapardes, and P. Pollak, *Subthalamic stimulation for Parkison's disease.*, Archives of medical research **31** (2000), 282–289.

[5] A. Bragin, G. Jandó, Z. Nádasdy, J. Hetke, K. Wise, and G. Buzsáki, *Gamma [40-100Hz] oscillation in the hippocampus of the behaving rat*, J. Neurosci **15** (1995), 47–60.

[6] G. Buzsáki, *Theta oscillations in the hippocampus*, Neuron **33** (2002), 325–340.

[7] G. Buzsáki and J. Chrobak, *Temporal structure in spatially organized neuronal ensembles: A role for interneuronal networks.*, Curr. Opin. Neurobiol. **5** (1995), 504–510.

[8] C. C. Chow, *Phase locking in weakly heterogenous networks.*, Physica D **118** (1998), 343–370.

[9] P. Érdi and K. Szalisznyó, *Hippocampal rhythm generation*, In: M. Arbib, ed., The Handbook of Brain Theory and Neural Networks, The MIT Press, Cambridge, Massachusetts, USA, 2nd edition, 2003.

[10] G. B. Ermentrout, *Stable periodic solutions to discrete and continuum array of weakly coupled nonlinear oscillators.*, SIAM J. Appl. Math. **52** (1992), 1665–1687.

[11] _____, *Simulating, analyzing, and animating dynamical systems: A guide to XPPAUT for researchers and students*, SIAM, Philadelphia, 2002, http://www.math.pitt.edu/∼bard/xpp/xpp.html.

[12] G. B. Ermentrout and N. Kopell, *Mechanisms of phase-locking and frequency control in pairs of coupled neural oscillators*, In: B. Fiedler ed., Handbook of Dynamical Systems, Vol.2, Elsevier Science B.V., Amsterdam.

[13] T. F. Freund, *Interneuron diversity series: Rhythm and mood in persomatic inhibition.*, Trends Neurosci. **26(9)** (2003), 489–495.

[14] D. Golomb and J. Rinzel, *Clustering in globally coupled inhibitory neurons*, Physica D **72** (1994), 259–282.

[15] D. Golomband, D. Hansel, and G. Mao, *Mechanisms of synchrony of neural activity in large networks.*, In: S. Gielen, M. Moss, eds., Handbook of Biological Physics, Vol. 4, Elsevier Science B.V., Amsterdam, pp.887-968., 2001.

[16] C. M. Gray, *Synchronous oscillations in neuronal systems:mechanisms and functions*, J. Comput. Neurosci. **1** (1994), 11–38.

[17] M. R. Guevara, *Dynamics of excitable cells*, In: A. Beuter, L. Glass, M. C. Mackay, and M. S. Titcombe, eds., Nonlinear Dynamics in Physiology and Medicine (Interdisciplinary Applied Mathematics), Vol. 25, Springer-Verlag, New York.

[18] B. Hille, *Ion Channels of Excitable Membranes*, 3rd ed., Sinauer Associates, Sunderland, Massachusetts, 2001.

[19] A. L. Hodgkin and A. F. Huxley, *A quantitative description of membrane current and its application to conduction and excitationi in nerve.*, J. Physiol.(Lond.) **117** (1952), 500–544.

[20] F. C. Hoppensteadt and E. M. Izhikevich, *Weakly Connected Neural Networks*, Springer-Verlag, New York, 1997.

[21] E. M. Izhikevich, *Phase equations for relaxation oscillators*, SIAM J. Appl. Math. **60** (2000), no. 5, 1789–1805.

[22] ———, *Dynamical Systems in Neuroscience: The Geometry of Excitability and Bursting*, Springer-Verlag, New York, 2004.

[23] J. Keener and J. Sneyd, *Mathematical Physiology (Interdisciplinart Applied Mathematics)*, vol. 8, Springer-Verlag, New York, 1998.

[24] Z. H. T. Kiss, D. M. Mooney, L. Renaud, and B. Hu, *Neuronal response to local electrical stimulation in rat thalamus:physiological implications for mechanisms of deep brain stimulation.*, J. Neurosci. **113** (2002), no. 1, 137–143.

[25] Y. Kuramoto, *Chemical Oscillations, Waves, and Turbulence*, Springer-Verlag, New York, 1984.

[26] ———, *Collective synchronization of pulse-coupled oscillators and excitable units.*, Physica D **40** (1991), 15–30.

[27] P. Lancaster, *Theory of Matrices*, Academic Press, Orlando, US, 1969.

[28] Y. X. Li, *Clustering in neural networks with heterogeneous and asymmetrical coupling strengths*, Physica D **180** (2003), 210–234.

[29] C. McBain and A. Fisahn, *Interneurons unbound*, Nature Rev. Neurosci. **2** (2001), 11–23.

[30] K. Okuda, *Variety and generality of clustering in globally coupled oscillators.*, Physica D **63** (1993), 424–436.

[31] P. F. Pinsky and J. Rinzel, *Intrinsic and network rhythmogenesis in a reduced traub model for CA3 neurons.*, J. Comput. Neurosci. **1** (1994), 39–60.

[32] G. Pocock and C. D. Richards, *Human physiology*, Oxford University Press, Oxford, 1999.

[33] J. Rinzel, *Intercellular communication*, In: C. Fall, E. Marland, J. Wangner, and J.Tyson eds., Computational Cell Biology (Interdisciplinary Applied Mathematics), Vol.20, Springer-Verlag, New York, 2002.

[34] J. A. Sanchez, J. A. Dani, D. Siemen, and B. Hille, *Slow permeation of organic cations in acetylcholin receptor channels*, J. Gen. Physiol **87** (1986), 985–1001.

[35] W. Singer, *Synchronization of cortical activity and its putative role in information processing and learning.*, Ann. Rev. Physiol. **55** (1993), 11–38.

[36] F. K. Skinner, H. Bazzazi, and S. A. Campbell, *Two-cell to n-cell heterogenous inhibitory networks:precise linking of multistable and coherent properties*, J. Comput. Neurosci. **18** (2005), 343–352.

[37] F. K. Skinner, J. Y. J. Chung, I. Ncube, P. A. Murray, and S. A. Campbell, *Using heterogeneity to predict inhibitory network model characteristics.*, J. Neurophysiol. **93** (2005), 1898–1907.

[38] F. K. Skinner, N. Kopell, and E. Marder, *Mechanisms for oscillation and frequency control in reciprocally inhibitory model neural networks*, J. Comput. Neurosci. **1** (1994), 69–87.

[39] R. D. Traub, G. R. Jeffreys, and M. A. Whittington, *Simulation of gamma rhythms in networks of interneurons and pyramidal cells.*, J. Comput. Neurosci. **4** (1997), 141–150.

[40] R. D. Traub, J. G. R. Jeffreys, and M. A. Wittington, *Fast oscillations in cortical circuits*, MIT Press, Cambridge, MA, 1999.

[41] P. H. E. Triesinga and J. V. Jose, *Robust gamma oscillations in networks of inhibitory hippocampal interneurons.*, Network: Comput. Neural Syst. **11** (2000), 1–23.

[42] C. van VreesWvijk, L. F. Abbott, and G. B. Ermentrout, *When inhibition not excitation synchronizes neural firing*, J. Comput. Neurosci. **1** (1994), 313–332.

[43] X. J. Wang and G. Buzsàki, *Gamma oscillation by synaptic inhibition in a hippocampal interneuronal network model*, J. Neurosci. **16** (1996), 6402–6413.

[44] X. J. Wang and J. Rinzel, *Alternating and synchronous rhythms in reciprocally inhibitory model neurons*, Neural Comput. **4** (1992), 84–97.

[45] J. A. White, C. C. Chow, J. Ritt, C. Soto-Tre no, and N. Kopell, *Synchronization and oscillatory dynamics in heterogenous mutually inhibited neurons*, J. Comput. Neurosci. **5** (1998), 5–16.

[46] T. Williams and G. Bowtell, *The calculation of the frequency-shift functions for chains of coupled oscillators with application to a network model of the lamprey locomotor pattern generator*, J. Comput. Neurosci. **4** (1997), 47–55.

[47] M. A. Wittington, R. D. Traub, and J. G. R. Jeffreys, *Synchronized oscillations in interneuron networks driven by metabotropic glutamate receptor activation*, Nature **373** (1995), 612–615.

[48] C. Wu, H. Shen, W. P. Luk, and L. Zhang, *A fundamental oscillatory state of isolated rodent hippocampus*, J. Physiol. (Lond.) **540.2** (2002), 509–527.